University of Kentucky
UKnowledge

Theses and Dissertations--Mechanical Engineering

Mechanical Engineering

2012

SIMULATION AND EXPERIMENTAL VALIDATION OF AIRBORNE AND STRUCTURE-BORNE NOISE TRANSMISSION IN HVAC PLENUMS

Srinivasan Ramalingam
University of Kentucky, srinivaspdy@gmail.com

Right click to open a feedback form in a new tab to let us know how this document benefits you.

Recommended Citation

Ramalingam, Srinivasan, "SIMULATION AND EXPERIMENTAL VALIDATION OF AIRBORNE AND STRUCTURE-BORNE NOISE TRANSMISSION IN HVAC PLENUMS" (2012). *Theses and Dissertations--Mechanical Engineering*. 6.
https://uknowledge.uky.edu/me_etds/6

This Master's Thesis is brought to you for free and open access by the Mechanical Engineering at UKnowledge. It has been accepted for inclusion in Theses and Dissertations--Mechanical Engineering by an authorized administrator of UKnowledge. For more information, please contact UKnowledge@lsv.uky.edu.

STUDENT AGREEMENT:

I represent that my thesis or dissertation and abstract are my original work. Proper attribution has been given to all outside sources. I understand that I am solely responsible for obtaining any needed copyright permissions. I have obtained and attached hereto needed written permission statements(s) from the owner(s) of each third-party copyrighted matter to be included in my work, allowing electronic distribution (if such use is not permitted by the fair use doctrine).

I hereby grant to The University of Kentucky and its agents the non-exclusive license to archive and make accessible my work in whole or in part in all forms of media, now or hereafter known. I agree that the document mentioned above may be made available immediately for worldwide access unless a preapproved embargo applies.

I retain all other ownership rights to the copyright of my work. I also retain the right to use in future works (such as articles or books) all or part of my work. I understand that I am free to register the copyright to my work.

REVIEW, APPROVAL AND ACCEPTANCE

The document mentioned above has been reviewed and accepted by the student's advisor, on behalf of the advisory committee, and by the Director of Graduate Studies (DGS), on behalf of the program; we verify that this is the final, approved version of the student's dissertation including all changes required by the advisory committee. The undersigned agree to abide by the statements above.

Srinivasan Ramalingam, Student

Dr. David W. Herrin, Major Professor

Dr. James M. McDonough, Director of Graduate Studies

SIMULATION AND EXPERIMENTAL VALIDATION OF AIRBORNE AND STRUCTURE-BORNE NOISE TRANSMISSION IN HVAC PLENUMS

THESIS

A thesis submitted in partial fulfillment of the
requirements for the degree of Master of Science in
Mechanical Engineering in the College of Engineering
at the University of Kentucky

By

Srinivasan Ramalingam

Lexington, Kentucky

Director: Dr. David W. Herrin, Associate Professor of Mechanical Engineering

Co-Director: Dr. Tingwen Wu, Professor of Mechanical Engineering

Lexington, Kentucky

2012

Copyright © Srinivasan Ramalingam 2012

ABSTRACT OF THESIS

SIMULATION AND EXPERIMENTAL VALIDATION OF AIRBORNE AND STRUCTURE-BORNE NOISE TRANSMISSION IN HVAC PLENUMS

This research demonstrates the usage of numerical acoustics to model sound and vibrational energy propagation in HVAC ducts and plenums. Noise and vibration in HVAC systems propagates along three primary paths that can be classified as airborne direct, airborne indirect and structure-borne. The airborne direct path was simulated using acoustic FEM with special boundary conditions to handle the diffuse acoustic field loading and the baffled termination. The insertion loss for a number of different plenum geometries was compared to published measurement results. Results were in good agreement both below and above the cutoff frequency. Additionally, the airborne indirect path, often termed breakout noise by the HVAC community, was assessed using Statistical Energy Analysis (SEA). This path was examined experimentally by placing a loudspeaker inside the air handler and measuring the sound power transmitted through the walls. SEA results compared favorably with the measured results in one-third octave bands even at low frequencies. Finally, the structure-borne path was considered by exciting the walls of the aforementioned air handler using an electromagnetic shaker. The panel vibration and the sound power radiated from the panels were measured. Results were compared with the SEA with good agreement provided that SEA loss factors were determined experimentally.

KEYWORDS: HVAC, Acoustic FEM, Statistical Energy Analysis (SEA), Airborne, Structure-Borne, Breakout Noise

Srinivasan Ramalingam

April 6, 2012

SIMULATION AND EXPERIMENTAL VALIDATION OF AIRBORNE AND STRUCTURE-BORNE NOISE TRANSMISSION IN HVAC PLENUMS

By

Srinivasan Ramalingam

Dr. David W. Herrin
Director of Thesis

Dr. James M. McDonough
Director of Graduate Studies

April 6, 2012
Date

To my dad for his support and encouragement all through my life

ACKNOWLEDGEMENTS

I would like to take this as an opportunity in expressing sincere gratitude for my advisor, Dr. David Herrin. All the research skills which I gained during this master's study should be credited to my advisor, to say the least. His patience and his efforts to motivate me were truly commendable. I am grateful for his support and his constant guidance without which this work would not have been possible.

I would like to thank my co-director Dr. Tingwen Wu and Dr. Andrew Seybert for their support and insightful suggestions which are invaluable. I also thank Dr. John Baker for his support in completing this thesis. I also extend my appreciation to Dr. John Baker for serving on my committee

My sincere appreciation also goes to students that I worked with, Jinghao Liu, Xin Hua, Limin Zhou, Jiawei Liu, Yitian Zhang, Wanlu Li, Rui He, Wentao Zhuo who all have made my stay enjoyable.

Most of all, I would like to thank my family for their unconditional love and encouragement. I am truly grateful to my cousin Dr. Balasubramanian Datchanamourty and my uncle Mr. Selvamani L. for their support and motivation to pursue my education. Finally I want to thank my dad for his sacrifices. I am indebted to my dad for being by my side throughout my life, without whose support I would not have achieved anything in my education.

TABLE OF CONTENTS

ACKNOWLEDGEMENTS iii

LIST OF TABLES vii

LIST OF FIGURES viii

CHAPTER 1 1

INTRODUCTION 1

1.1 Introduction 1

CHAPTER 2 7

CALCULATION OF AIRBORNE ATTENUATION IN PLENUMS 7

2.1 Analysis above the Plane Wave Cutoff 7

2.2 Typical Methods to Simulate Plenums and Ducts 10

2.2.1 Wells Energy Model 11

2.2.2 Mouratidis and Becker Empirical Model: 12

2.2.3 Statistical Energy Analysis (SEA) 14

2.2.4 Acoustic Boundary Element (BEM) Analysis 16

2.2.5 Acoustic Finite Element (FEM) Analysis 19

2.3 Summary 20

CHAPTER 3 21

APPLICATION OF ACOUSTIC FEM TO PLENUM SIMULATION 21

3.1 Acoustic FEM with Special Boundary Condition: 21

3.2 Experimental work by Mouratidis and Becker (2003) 24

3.3 Comparison of Measurement and Simulation 28

3.4 Summary 38

CHAPTER 4 39

BREAKOUT NOISE IN DUCT SYSTEMS 39

4.1 Theoretical Background 39

4.2 Determination Wall Transmission Loss Using Energy Methods 42

4.2.1 Simple Plate model 43

4.2.2 Sound transmission between two rooms separated by a wall 45

4.3 Determination of Insertion loss of an Air Handler using Energy Methods 50

4.3.1 Procedure to Determine the Insertion Loss of an Air Handler Experimentally ... 50

4.3.2 Validation Study 52

4.4 Summary 57

CHAPTER 5 58

MACHINERY NOISE 58

5.1 Background 58

5.2 Statistical Energy Analysis Background 59

5.2.1 Statistical Energy Analysis of Two Coupled Subsystems 61

5.3 Application of Experimental SEA to an Air Handler to determine the Structure-Borne Noise 64

5.3.1 Procedure to determine the input power at the point of excitation 66

5.3.2 Procedure to determine the Vibration Velocity and Sound Power 67

5.4 Validation Study 69

5.4.1 Single Structural Source 71

5.4.2 Multiple Structural Sources 74

5.5 Summary 79

CHAPTER 6 80

NOTES ON EXPERIMENTAL SEA 80

6.1 Experimental SEA Background 80

6.2 Modal Energy 80

6.3 Equivalent Mass 82

6.4 Coupling Loss Factor 87

6.4.1 Inverse Matrix Method 87

6.4.2 Two-Subsystem Method 94

6.5 Damping Loss Factor 101

6.5.1 Decay Rate Method 101

6.5.2 Energy Matrix Method 101

6.6 Summary 106

CHAPTER 7 107

CONCLUSIONS 107

7.1 Summary and Conclusions 107

7.2 Airborne Attenuation in Plenums 107

7.3 Breakout Noise in Duct Systems 109

7.4 Machinery Noise in HVAC Plenums 109

7.4.1 Determination of Loss Factors 110

7.5 Future Work 111

REFERENCES 113

VITA 120

LIST OF TABLES

Table 3.1 Plenum cases considered for analysis 31

LIST OF FIGURES

Figure 1.1 Typical paths of noise and vibration propagation in HVAC systems (ASHRAE Handbook, 2007[2]) 2

Figure 1.2 Frequency spectrums in which different HVAC equipment propagates noise (ASHRAE Handbook, 2011[3]) 3

Figure 1.3 Comparison of Insertion loss of the duct system. 4

Figure 2.1 SEA model of a simple expansion chamber 16

Figure 2.2 Schematic diagram of a simple expansion chamber illustrating the transfer matrix approach. 18

Figure 3.1 Side View of the straight duct with and without the HVAC plenum 21

Figure 3.2 Hybrid FE-SEA model of the HVAC plenum with inlet/outlet ducts. 22

Figure 3.3 Schematic diagrams representing the calculation of insertion loss of a plenum 25

Figure 3.4 Types of mufflers used for analysis (Mouratidis and Becker, 2003[6]) 26

Figure 3.5 Two models used for Noise Reduction Calculation 27

Figure 3.6 SEA model of a HVAC Plenum with an input power and semi-infinite fluid termination 29

Figure 3.7 Acoustic FEM mesh of right angle duct configuration 30

Figure 3.8 Insertion loss comparison for a 1.22 x1.22 x 0.91 m^3 plenum with inlet and outlet ducts in line. The plenum is unlined. 34

Figure 3.9 Insertion loss comparison for a 1.22 x 1.22 x 0.91 m^3 plenum with inlet and outlet ducts in line. The plenum is lined with 10.2 cm fiber 34

Figure 3.10 Insertion loss comparison for a 1.22x1.83x1.52 m^3 plenum with inlet and outlet ducts in line. The plenum is unlined 35

Figure 3.11 Insertion loss comparison for a 1.22x1.83x1.52 m^3 plenum with inlet and outlet ducts in line. The plenum is lined with 10.2 cm fiber 35

Figure 3.12 Insertion loss comparison for a 1.22x1.83x3.05 m^3 plenum with inlet and outlet ducts in line. The plenum is unlined 36

Figure 3.13 Insertion loss comparison for a 1.22x1.83x3.05 m^3 plenum with inlet and outlet ducts in line. The plenum is lined with 10.2 cm fiber 36

Figure 3.14 Insertion loss comparison for a 1.22x1.83x1.52 m^3 plenum with inlet and outlet ducts……37

Figure 3.15 Insertion loss comparison for a 1.22x1.83x3.05 m^3 plenum with inlet and outlet ducts offset by 90 degrees. The plenum is lined with 20.3 cm fiber 37

Figure 4.1 Power balance for a sound field incident upon an insulated plate..... 43

Figure 4.2 Sound Transmission between two rooms. 45

Figure 4.3 Air handler utilized for acoustic measurement..... 51

Figure 4.4 Fiberglass embedded into a perforated panel……. 51

Figure 4.5 Insertion loss measurement setup for an air handler 52

Figure 4.6 SEA model of the air handler 53

Figure 4.7 Original and SEA model of the air handler with an opening 53

Figure 4.8 Enclosure fully sealed with fiberglass 55

Figure 4.9 Enclosure fully sealed without fiberglass 56

Figure 4.10 Enclosure with an opening with fiberglass 56

Figure 4.11 Enclosure with an opening without fiberglass 57

Figure 5.1 Two Subsystem SEA model 63

Figure 5.2 Air handler used in this research work 65

Figure 5.3 Panels of the air handler fastened to the frames 65

Figure 5.4 Power input measurement setup 67

Figure 5.5 Setup to determine the vibration velocity 68

Figure 5.6 Sound power measurement setup 69

Figure 5.7 SEA model of the Air Handler. 70

Figure 5.8 Air handler excited by single source (electromagnetic shaker) 72

Figure 5.9 Excitation (rear) panel velocity 73

Figure 5.10 Opposite (front) panel velocity 73

Figure 5.11 Sound power radiated from the adjacent (left side) panel 74

Figure 5.12 Air handler excited by two shakers 76

Figure 5.13 Power input from the two electromagnetic shakers shown in figure 5.9 76

Figure 5.14 Comparison of measured and predicted front panel velocity 77

Figure 5.15 Comparison of measured and predicted top panel velocity 77

F**igure 5.16** Comparison of measured and predicted sound power radiated from the front panel 78

Figure 5.17 Comparison of measured and predicted sound power radiated from the top panel 78

Figure 6.1 Decay Test conducted on the top panel of the air handler 86

Figure 6.2 Transient response of the top panel 86

Figure 6.3 Air handler used for coupling loss factors measurement 88

Figure 6.4 Condition number of the inverse matrix. 89

Figure 6.5 Comparison of the coupling loss factors 90

Figure 6.6 Representation of the coupling loss factors between the panels 91

Figure 6.7 Comparison between the coupling loss factors between all the panels of the air handler as the top panel is excited. 92

Figure 6.8 Comparison between the coupling loss factors between all the panels of the air handler as the left side panel is excited. 93

Figure 6.9 Comparison between the coupling loss factors between all the panels of the air handler as the front panel is excited. 93

Figure 6.10 Two Subsystem Method 94

Figure 6.11 SEA model of a two subsystem system with a secondary path 95

Figure 6.12 Comparison of the energy flow in the response panel 96

Figure 6.13 Panels heavily damped using sand bags 96

Figure 6.14 Damping Loss Factor of the right side panel of the air handler 97

Figure 6.15 Damping Loss Factor of the left side panel of the air handler 97

Figure 6.16 Comparison of the coupling loss factors between the left side panel and the rear panel of the air handler 105

Figure 6.17 Comparison of the coupling loss factors between the rear panel and the top panel of the air 99

Figure 6.18 Comparison of the coupling loss factors between the right side panel and the top panel of the air handler 100

Figure 6.19 Damping loss factor of the front panel of the air handler 103

Figure 6.20 Damping loss factor of the right side panel of the air handler 103

Figure 6.21 Damping loss factor of the rear panel of the air handler 104

Figure 6.22 Damping loss factor of the left side panel of the air handler..... 104

Figure 6.23 Damping loss factor of the top panel of the air handler 105

Figure 6.24 Damping loss factor of the bottom panel of the air handler 105

CHAPTER 1

INTRODUCTION

1.1 Introduction

Noise in the buildings affects occupants most of the time. Sound from heating, ventilation, and air conditioning (HVAC) equipment normally exceeds the American National Standards Institute (ANSI) sound pressure level for desired human living (Technology for a Quieter America (2010)[1]). Nevertheless, noise is normally secondary to other design concerns, and the best design, simulation, and analysis tools are not presently used in the building industry.

Building noise is primarily caused by power generating equipment in HVAC systems. Chillers, boilers, furnaces, fans and pumps are all sources of noise. Energy can propagate through the duct airspace (airborne) or through the duct structure (structure-borne) itself. Airborne noise is mostly due to fan or flow noise (i.e. turbulence or vortex shedding caused by flow over a cavity or sharp edge). Airborne noise propagates through the duct airspace to the rooms. Airborne noise is typically reduced by using sound absorbing material like fiber or foam, adding silencers or plenums, or by extending the length of the ducts.

Structure-borne noise is propagated through ductwork, piping, and mounts and transmitted to other parts of the building. Sound then radiates from vibrating walls, floors and ceilings. Additionally, sound can be radiated from the ductwork or plenum itself. This is typically referred to as breakout noise. The structure borne noise in the

duct system can be attenuated by using proper isolation or adding additional damping to the structure.

Figure 1.1 illustrates the different noise transmission paths to a receiving room from an air-handling unit. In the figure, structure-borne paths are indicated in red and include propagation through the wall, floor, roof, HVAC Plenum, mounts and ductwork. Duct breakout noise in the inlet duct is indicated in green. Airborne paths are indicated in blue and include propagation through the duct airspace. Figure 1.2 shows the frequency ranges at which different types of equipment contribute to the sound spectra.

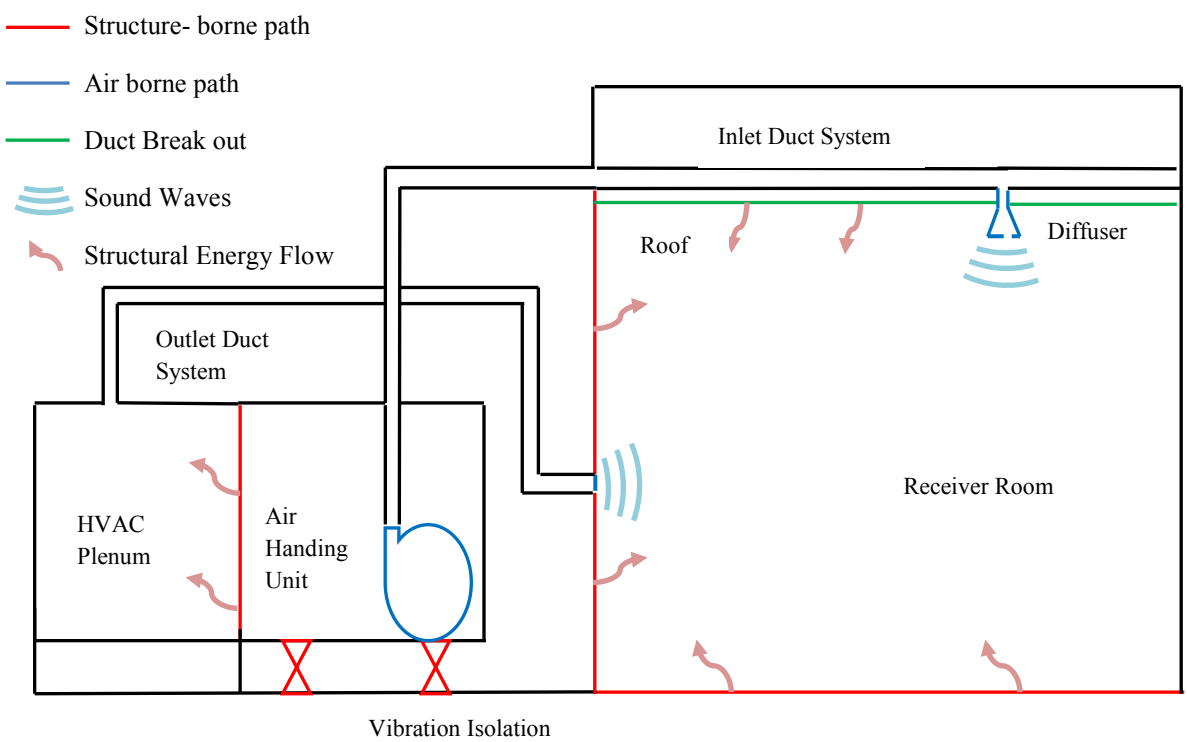

Figure 1.1 Typical paths of noise and vibration propagation in HVAC systems (ASHRAE Handbook (2007)[2])

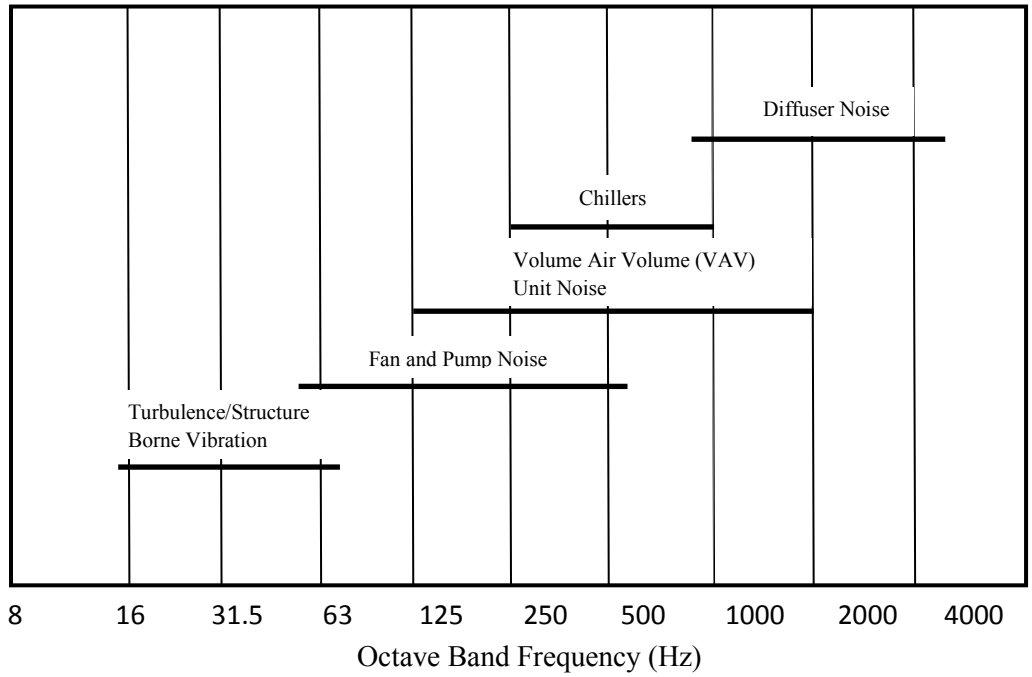

Figure 1.2 Frequency spectrums of noise for different HVAC equipment propagates noise (ASHRAE Handbook (2011)[3]).

Building noise can be reduced by a) reducing the noise level at the source, b) modifying the energy transmission path, or c) reducing the noise level to the occupant by adding sound absorption or by enclosing the occupant. Noise and vibration at the source can be reduced by operating fan and power equipment at lower speeds and eliminating imbalances. Alternatively, the transmission path can be modified utilizing silencers (i.e. plenums), and introducing sound absorbing materials like fiber and foam to the HVAC ducting. Structure-borne noise can be reduced by using isolators, and by adding damping to the HVAC ductwork. While not desirable, the noise level at the receiver can be reduced by building an enclosure around the applicant, using hearing protection, or by adding sound absorption to the room (Crocker (2007)[4]; ASHRAE Handbook (2007)[2]).

This thesis will focus on the problem of sound propagation through ductwork and plenums. This can include propagation through the air space (airborne noise) or through the ductwork (structure-borne). For the most part, building designers and engineers utilize the ASHRAE Handbook (2007)[2] equations in order to predict the acoustic attenuation associated with HVAC ductwork.

The most commonly used model for predicting the airborne attenuation of HVAC plenums is an energy-based formula first developed by Wells (1958)[5]. However, Wells' formula is approximate and does not fully account for the wide variety of HVAC plenum geometries. For instance, the Wells' model does not fully account for effects like inlet and outlet duct orientation, multiple inlet and outlet ducts, or even the first few acoustic modes of the plenum. Figure 1.3 compares the measured insertion loss to the Wells' prediction for a plenum. Notice that the Wells' model is within 3 dB at higher frequencies where energy models are more appropriate. However, it is clear that the Wells' model does not agree with measurement at low frequencies.

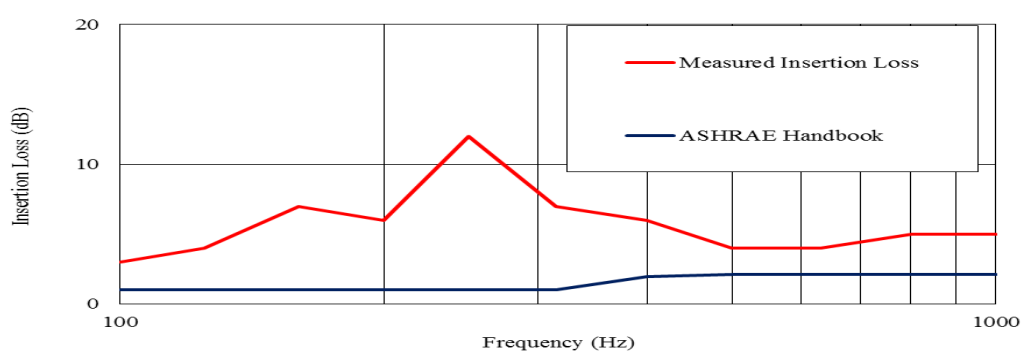

Figure 1.3 Comparison of Insertion loss of the duct system.

This research work details numerical simulation approaches which includes acoustic FEM and SEA. The Acoustic FEM is utilized to determine airborne noise

whereas SEA is utilized for structure-borne noise in plenums. The numerical approaches can be extended beyond the cutoff frequency for inlet and outlet ducts as well as plenums. The acoustic FEM approach meets an important need in predicting the airborne noise since the plane wave cutoff frequency is quite low in frequency for duct and plenum systems. For instance, the cutoff frequency for a 0.61 m x 0.61 m (2 ft x 2 ft) square duct is only 280 Hz. The suggested technique is a modal approach where modes are first determined using a finite element (FE) model. Stochastic boundary conditions at the source and termination are then applied in modal coordinates. The boundary conditions include a diffuse acoustic field at the inlet and radiation impedance (baffled termination) at the termination.

Duct breakout or rumble is a common problem for ductwork that extends into a receiver room. The duct breakout noise is defined as the sound radiated from the duct walls into the receiver room. Sometimes this noise is caused by sources in the duct like turbulence in the airflow or by strong noise sources upstream such as fans. The ASHRAE Handbook includes several tables, which catalog the wall transmission loss for a number of different wall types. However, models of the source itself are not included. Moreover, structure-borne energy propagation along the length of the duct is not considered in the model.

In each case, simulation is compared to measurement. The primary objectives of the current research effort are to

1. Model the airborne sound transmission using acoustic FEM with special boundary conditions at the inlet and the outlet ducts. The suggested approach is

advantageous over ASHRAE Handbook because the simulation agrees very well with the measured insertion loss both above and below plane wave cutoff frequency. The other important advantage is the simulation can account for wide variety of HVAC plenum geometries. It also includes the effect of first several acoustic modes of the plenum in the analysis.

2. Apply SEA to model the insertion loss of both sealed and partial enclosures. This approach should be suitable for modeling breakout noise.

3. Apply experimental SEA to simulate structure borne noise for a typical air handler. This approach will be especially beneficial in modeling structure borne energy propagation from machinery. Application of experimental SEA in a HVAC plenum is novel to HVAC industry.

CHAPTER 2

CALCULATION OF AIRBORNE ATTENUATION IN PLENUMS

2.1 Analysis above the Plane Wave Cutoff

Sound waves propagating through small ducts possess wavelengths that are much larger than the duct itself. This simplifies the analysis since the sound pressure across the duct cross-section can be assumed to be constant. If such is the case, transfer matrix theory (also known as four-pole theory) pioneered by Munjal (1982)[6] can be used to determine the transmission loss. The transfer matrix uses the acoustic wave equation to relate the sound pressure and particle velocity on one side of a muffler or silencer element to the other side. The approach is general enough to consider elements with three-dimensional wave behavior. However, the wave behavior at the inlet duct and outlet must be plane wave.

The plane wave cutoff frequency for duct sections can be determined based on the speed of sound (c) and characteristic duct dimension (d). The plane wave cutoff frequency for a square duct is equal to $c/2d$. Ericsson (1980)[7] determined that the cut-off frequency for circular ducts (for non-axisymmetric waves) was equal to $c/1.71d$ whereas the cut off frequency equals $c/0.82d$ for axi-symmetric modes.

It should be noted that there are two classic models for analyzing HVAC plena above the cutoff frequency. The first is Wells' (1958) [5] model based on room acoustics theory, and the second is by Cummings (1978)[8] who extended the Wells model to include directivity between the inlet and outlet ducts and included baffles in the expansion chamber or plenum. Neither approach accounted for the acoustic modes in the inlet and outlet ducts, or the plenum itself. Later, Mouratidis and Becker (2003) [9]

documented two separate empirical models of HVAC plenums for frequencies above and below the cutoff. However, the developed models were only applicable for inline plenums. Detailed descriptions about Wells' and Mouratidis and Becker's models are documented in Sections 2.2.1 and 2.2.2 respectively.

There have been numerous investigations where transfer matrix theory is extended beyond the cutoff frequency to include three-dimensional effects. Most of these investigations assume plane wave behavior in the inlet and outlet ducts (Ih, Lee (1985)[10]; Ih, Lee (1987)[11]; Yi and Lee (1986)[12]; Yi and Lee (1987)[13]; Ih (1992)[14]; Munjal (1987)[15]; Selamet and Radavich (1997)[16] and Selamet and Ji (1998)[17]). For example, Ih and Lee (1985) [10] investigated the effect of higher order modes in a circular expansion chamber with mean flow. The effect of higher order modes was included using a Fourier Bessel expansion to express the four pole parameters. The developed model also considered cases in which the inlet and outlet ducts were not centered. Likewise, Ih and Lee (1987) [11] developed a mathematical model for the transmission loss of a reversing chamber muffler with circular cross section. By reversing chamber, it is meant that both the inlet and the outlet of the muffler are located on the same side of the chamber. Also the relative offset location of the inlet and outlet and the length to diameter ratio of the inlet and the outlet is considered.

Similarly Yi and Lee (1986[12], 1987[13]) determined the transmission loss for cylindrical expansion chambers for side-in / side-out and side-in / end-out configurations. Munjal (1997)[18] concluded that the side in / side out configuration behaved in essence like an extended inlet and outlet plenum configuration especially for acoustically long chambers i.e. length of the chamber is greater than or equal to two times the diameter of

the inlet and the outlet. In similar work, Selamet and Radavich (1998) [16] analyzed circular expansion chambers with extended inlet and outlet ducts. Their work examined the effect of length of the chamber on the acoustical attenuation performance by using a 2D analytical approach and a 3D computational solution based on the boundary element method (BEM). The models were experimentally validated using an extended impedance tube setup.

Ih (1992) [14] also developed a theoretical method to investigate the effect of the higher order modes using a three dimensional analysis (Ih (1992)[14]). The model developed was valid for rectangular shaped plenums. More recently, Venkatesham et al (2009) [19] used Green's functions expressed in terms of the rectangular cavity modes to model rectangular expansion chambers assuming plane wave behavior with no mean flow and no acoustic source inside the chamber.

The aforementioned papers (Cummings (1978)[8]; Ih and Lee (1985)[10]; Ih and Lee (1987)[11]; Yi and Lee (1986)[12]; Yi and Lee (1987)[13]; Ih (1992)[14]; Munjal (1987)[15]; Selamet and Radavich (1997) [16] and Venkatesham et al (2009)[19]) document useful models for extending plane wave based transfer matrix theory to include muffler components (expansion chambers) which exhibit three dimensional wave behaviors. However, plane wave behavior was assumed in the inlet and outlet ducts to the muffler components in each case.

In the same way, deterministic approaches like the finite element method and boundary element method have been used. Craggs (1976[20], 1977[21]) utilized axisymmetric finite element models for reactive and dissipative mufflers. Subsequently,

Peat (1982)[22] and Sasrabudhe et al (1991)[23] used three-dimensional finite element models to determine the transfer matrices for muffler components.

Wu et al. (1998)[24] first used the improved four-pole to determine the transmission loss of plenums. More recently, Barbieri et al. (2004)[25] has used the improved four-pole method to determine the four-pole parameters and thereby the transmission loss and compared with FEM and experiment. Similarly, Herrin et al. (2007)[26] have used similar approaches to determine the transmission loss for plenums. Wang et al. (1993)[27] used the 3-D boundary element method to determine the four-pole and the transmission loss. In all the aforementioned finite element and boundary element studies, results were reported at frequencies such that plane wave behavior was present in both inlet and outlet ducts. In most of the studies, the four-pole parameters were determined as a precursor to determining transmission loss.

2.2 Typical Methods to Simulate Plenums and Ducts

Five different methods have been used to determine the attenuation (transmission or insertion loss) of HVAC plenums. These include:

- Wells' (1958) energy model
- Mouratidis and Becker's (2003) empirical model
- Statistical energy analysis (SEA)
- Boundary element (BEM) analysis
- Finite element (FEM) analysis.

The limitations of the aforementioned methods and their applicability towards determining the airborne sound transmission of HVAC duct systems are discussed in the following sections.

2.2.1 Wells Energy Model

At the present, the equation in the ASHRAE Handbook (ASHRAE, 2011[3]) is the primary tool used by designers to estimate the insertion loss of plenums in the design stage. This equation developed by Wells (1958) [5] over 50 years ago is based on room acoustics theory.

Wells (1958) [5] developed an expression to estimate plenum attenuation based on conservation of energy. The total sound energy density at the outlet is assumed to be the summation of the direct and reverberant field energy densities (Wells (1958)[5]). The plenum attenuation was defined as the difference between the sound power entering the plenum and the sound power exiting the plenum. This definition of attenuation is broad and is strictly speaking neither a transmission or insertion loss. However, insertion loss will be less sensitive to the boundary conditions at the source and termination at high frequencies and should be roughly the same as the attenuation defined in this manner. The ASHRAE Handbook equation for attenuation is given as

$$IL = 10\log\left[S_e\left(\frac{Q\cos\theta}{4\pi d^2} + \frac{1-\alpha}{\alpha S_w}\right)\right]^{-1} \tag{2.1}$$

Where IL is insertion loss or attenuation, S_e is the plenum exit area, d is the slant distance between the entrance and exit, θ is the angle of incidence for the direct sound field at

exit, S_w is the total wall surface area, and α is the average sound absorption coefficient for the walls. Q is a directivity factor which is equal to 2, 4, or 8 depending on whether the opening is at the center of the wall, a bihedral corner, or a trihedral corner respectively. The average sound absorption coefficient can be determined from

$$\alpha S_w = \sum_{i=1}^{n} \alpha_i S_i \tag{2.2}$$

Where α_i and S_i are the absorption coefficient and area for each plenum wall.

In order to verify his numerical model, Wells built a plenum of dimension 0.8483 x 0.635 x 0.31242 m^3 with 0.0127 m fiberglass lining. Measurements were conducted for a single plenum and for two or three plenums in series. The net attenuation prediction also included the effect of the end corrections for each chamber considered for measurement.

Wells' (1958) [5] concluded that at low frequencies (below the cutoff frequency) where the wavelength exceeds the plenum dimensions, the mathematical prediction underestimates the measurement by 5 to 10 dB because of the chamber end corrections and acoustic resonances. Moreover, factors such as inlet area, location of the outlet opening, and the presence of airflow were not considered for predicting the acoustic performance of the plenum.

2.2.2 Mouratidis and Becker Empirical Model:

Mouratidis and Becker (2003) [9] conducted numerous experiments on HVAC plenums with various inlet/outlet duct configurations to determine the insertion loss. The HVAC plenum configurations include inlet and outlet ducts being inline, offset by 90

degrees, with elbow, side in/end out, end in/side out, and multiple outlets. The detailed discussion about the measurements carried out by Mouratidis and Becker is documented in Chapter 3. From the measured insertion loss, they performed a curve fit and developed empirical equations for the insertion loss of the HVAC plenums. One equation corresponds to the insertion loss below the plane wave cut off and the other equation corresponds to the insertion loss above the plane wave cutoff. However, the equations were limited to inline plenums and results were only compared for a few cases. Below the cutoff frequency insertion loss was expressed as

$$IL = A \cdot S_w + W_e \tag{2.3}$$

where A and W_e were empirically determined for different wall constructions. Above the cutoff frequency, insertion loss was expressed as

$$IL = bS_e \left[\frac{Q}{4\pi r^2} + \frac{(1-\alpha)}{S_w \alpha} \right]^n \tag{2.4}$$

where b and n were determined empirically and were respectively 3.505 and-0.359.

Above the plane wave cut off frequency, the insertion loss is similar to Wells' model (eq. 2.1) with the logarithm of the total sound energy density at the outlet being replaced by empirically derived proportionality constants. Below the plane wave cut off frequency, a regression analysis between the low frequency test data and the geometry of the plenums was conducted. Factors such as plenum surface area produced strong correlation with low error residuals.

In contrast, the regression analysis between the expansion ratio, which is used to characterize sound attenuation in Wells' model, and the test data showed weak

correlation. Further, a trend analysis on the wall effects (effect of surface absorption in plenums) results in a standard deviation between 1 to 6 dB below the cutoff and is independent of expansion ratio.

Therefore, Mouratidis and Becker concluded that the direct correlation with the magnitude of the plenum surface area and corresponding surface absorption characteristics (wall effect) were the key factors for sound attenuation in plenums for frequency less than the plane wave cut off frequency. Hence, direct application of the expansion ratio to characterize sound attenuation below cutoff is incorrect. This enables the Mouratidis and Becker prediction (Mouratidis and Becker, 2003[9]) to be more accurate when compared to Wells model (1958) [5] especially at frequencies below the cutoff frequency.

2.2.3 Statistical Energy Analysis (SEA)

The foundation for statistical energy analysis (SEA) was laid in the 1960's. Since that time, a number of authors have documented the background of SEA and also its applicability in noise and vibration analysis of mechanical structures. (Burroughs et al. (1997)[28]; Lyon, DeJong (1995)[29]; Langley (1981)[30]; Woodhouse (1981)[31] ; Fahy (1994)[32]; Lalor (1989)[33]; De Langhe and Sas (1996)[34]). SEA has been successfully applied in building structures to determine the structure borne noise transmission (Craik (1982)[35]; Stimpson (1986)[35]), and for both the airborne (Cimmerman et al (1997)[36]) and structure-borne (Yamazaki et al (2003)[37]) sound transmission in automobiles.

SEA is a power and energy balance approach. The basic assumption of SEA is that the total energy in each subsystem, which is the sum of the energies of each mode in the subsystem, resides only in the resonant frequencies that are uniformly distributed within each of the frequency bands in the analysis. Since SEA assumes only resonant modes, the total assumed degrees of freedom in the SEA analysis is greatly reduced for complicated structures. Accordingly, SEA is computationally inexpensive compared to finite element and boundary element analyses.

For SEA, the system is normally divided up into a number of subsystems and an energy balance equation is constructed for each subsystem. A global energy balance equation is formed for the entire system, and the average energy density can be calculated for each subsystem. For example, a simple expansion chamber considered for analysis is showed in Figure 2.1. The panels of the inlet, outlet ducts and the expansion chamber are assumed to be individual structural subsystems. But the air cavity in the simple expansion chamber is modeled as a single acoustic subsystem. Each subsystem is assumed to contain groups of resonant modes with energy equally distributed among the modes. Input forces or acoustic sources are modeled as an input power, and the damping for each subsystem is an energy sink. Upon solving the energy balance equation, the energy density in each subsystem can be obtained which can be directly related to the spatially averaged vibration velocity or sound pressure.

Oldham and Hillarby (1991) [38, 39] applied SEA for high and low frequency problems for the airborne path in enclosures. Two separate expressions were developed based on SEA to predict the insertion loss for close fitting enclosures. One equation corresponds to low frequency noise problem and the other equation corresponds to high

frequency noise problem (Oldham and Hillarby (1) (1991)[38]).The aforementioned mathematical equations developed by Oldham and Hillarby (1) were compared to the measured insertion loss of close fitting enclosures (Oldham and Hillarby (2) (1991)[39]). From the measurements, it was concluded that the high frequency model agreed well with the measured results. The low frequency model agreed with the measured results only when the sound source vibrates in (1, 1) mode shape. If the source vibrates in other mode shapes, then the agreement between the low frequency model and the measured data is affected because of strong coupling between the source mode shapes and the resonant mode shapes of the panels of the enclosure.

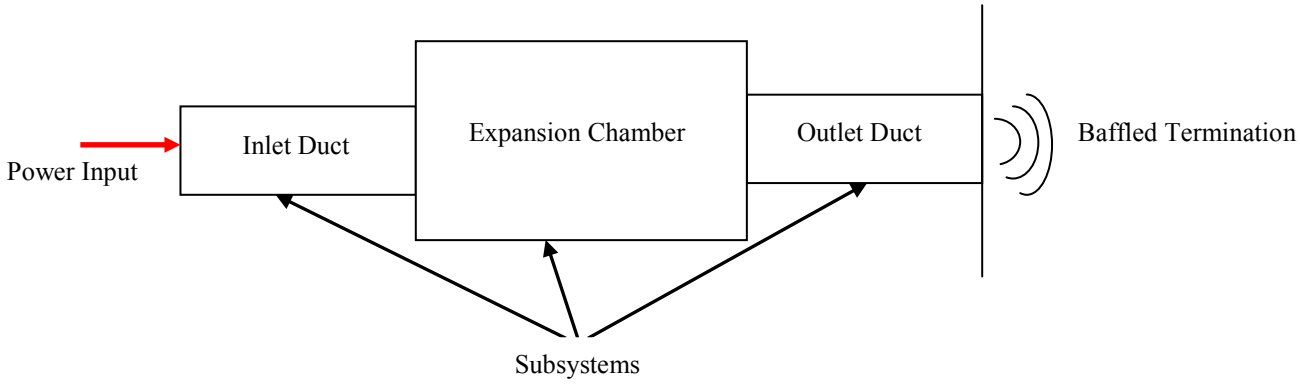

Figure 2.1 SEA model of a simple expansion chamber

2.2.4 Acoustic Boundary Element (BEM) Analysis

The boundary element method (BEM) is a deterministic approach used to solve the acoustic wave equation. The advantage of BEM over other deterministic approaches is the numerical solution of the boundary integral equation can be achieved by discretizing only the boundary surface of the domain into a finite number of elements using collocation techniques. (Seybert et al (1985)[40]; Seybert and Wu (1997)[41]; Selamet and Ji (1999)[42]; Zhang et al (2003)[43]; .Ji (2010)[44]).

Boundary element methods have been successfully used in the determining sound transmission in applications such as the interior cabin noise with complicated boundary conditions (Bernhard et al (1987)[45]; Suzuki et al. (1988)[46]), noise reduction using bulk reacting sound absorbing materials (Utsuno et al. (1990)[47]), scattering problems (Demkowicz et al. (1990)[48]; Desanto (2010)[49]) and flow problems (Mushtaq et al. (2010)[50]). The BEM may also be coupled with structural finite element modes for solving coupled problems (.Felippa (1981)[51]; Vlahopoulos et al. (1999)[52]). Since the current research work deals with airborne sound attenuation in plenums, emphasis is placed on the application of BEM to simulate the airborne path in HVAC plenums.

Herrin et al. (2007)[26] utilized the BEM to determine the transmission loss of HVAC plenums. Plane wave behavior was assumed in the inlet and the outlet ducts so that the transmission loss could be determined using four-pole theory.

The four pole parameters are expressed in the form of matrix equation.

$$\begin{bmatrix} P_1 \\ V_1 \end{bmatrix} = \begin{bmatrix} A & B \\ C & D \end{bmatrix} \begin{bmatrix} P_2 \\ V_2 \end{bmatrix} \tag{2.5}$$

where P_1 and P_2 are the sound pressures, V_1 and V_2 are the particle velocities at the locations shown in Figure 2.2. A, B, C and D are the four pole parameters.

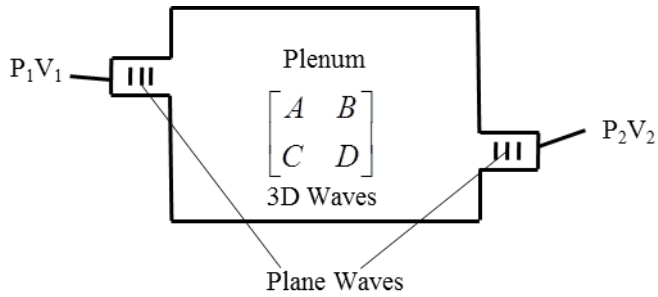

Figure 2.2 Schematic diagram of a simple expansion chamber illustrating the transfer matrix approach.

Herrin et al. (2007) [26] used two BEM analyses to determine the transfer matrix. A unit velocity boundary condition is applied first to the inlet and the BEM analysis is conducted to determine the modified four pole parameters A^* and C^*. Similarly a unit velocity boundary condition is applied to the outlet and a BEM analysis is performed to determine the modified four pole parameters B^* and D^*. From the modified four pole parameters, the original four pole parameters are expressed as

$$A = A^* / C^* \qquad B = B^* - A^* D^* / C^*$$

$$C = 1 / C^* \qquad D = -D^* / C^* \tag{2.6}$$

Once the four-pole parameters (A, B, C, and D) are obtained, the transmission loss can be determined using (Munjal, 1987) [15]

$$TL = 20\log_{10}\left(\frac{1}{2}\left[A + \frac{B}{\rho c} + C\rho c + D\right]\right) + 10\log_{10}\left(\frac{S_{in}}{S_{out}}\right) \tag{2.7}$$

where S_{in} is the inlet duct cross sectional area, S_{out} is the outlet duct cross sectional area, ρ is the fluid density, and c is the fluid speed of sound.

2.2.5 Acoustic Finite Element (FEM) Analysis

The finite element method is a deterministic approach, which is used extensively to predict the structural vibration response of mechanical components. FEM approximates the exact solution to the governing differential equation using standard techniques such as the Galerkin or Ritz methods over several small regions called elements. Thus the system is divided into a finite number of degrees of freedom. Then the matrix equation of each element is assembled in the form of a global matrix satisfying the continuity conditions between the elements and the boundary conditions so that the unknown field variables can be solved at each degree of freedom.

The acoustic FEM can be used to determine the acoustic attenuation of silencers or HVAC plenums (Craggs (1976)[20]; Craggs (1977)[21]; Peat (1982)[22]; Sahasrabudhe et al. (1991)[23]). Several authors have used acoustic FEM to solve the acoustic wave equation including interior and exterior problems and scattering problems (Cook et al. (1989)[53]; Nefske at al. (1982)[54]).

Craggs (1976)[20] developed a finite element model to determine the transmission loss for reactive mufflers. The transmission loss of a muffler with extended inlet and outlet was compared to a one-dimensional mathematical model developed by Davis (1975)[55] with good agreement at low frequencies. At high frequencies, the agreement was not as good because of the error due to discretization and the difficulty in correlating high frequency modes. This problem can be overcome in part by refining the mesh, but with more computational time. Craggs (1977)[21] also investigated dissipative mufflers including absorbing lining. He observed that the lining improves the

transmission loss of the muffler at high frequencies whereas negligibly affecting the transmission loss at low frequencies.

Similarly, Sahasrabudhe et al. (1991)[23] developed a 3-D finite element model to determine the acoustic behavior of a simple expansion chamber with an extended inlet and outlet. Plane wave behavior was assumed in the inlet and outlet ducts so that the transfer matrix approach could be utilized to determine the transmission loss.

2.3 Summary

A literature survey about analysis above the plane wave cutoff frequency in duct systems was discussed. The chapter also includes a discussion about the theoretical background of the various methods to determine the airborne sound attenuation in HVAC plenums. The different methods discussed in this chapter include the Wells' energy model, Mouratidis and Becker empirical model, statistical energy analysis, boundary element analysis and finite element analysis.

In this research work, the insertion loss is used as a metric to characterize noise attenuation in HVAC plenums. Further, the application of acoustic FEM with special boundary conditions on HVAC plenums to determine the insertion loss is discussed in Chapter 3. Plane wave behavior in the inlet and the outlet ducts is not assumed for the analysis.

CHAPTER 3

APPLICATION OF ACOUSTIC FEM TO PLENUM SIMULATION

3.1 Acoustic FEM with Special Boundary Condition:

The discussion, which follows, details the methodology used to apply acoustic FEM to determine the insertion loss. The strategy to determine insertion loss is illustrated in Figure 3.1. Two models are compared. In the first model, the output power at the termination is predicted without the plenum in place. Notice that the straight duct has the same length and cross-sectional dimensions as the duct and plenum combined. The second model includes the plenum. The same input power is used for the second model as was used for the first model, and the insertion loss is calculated directly by subtracting the output power from the second model from that of the first. Results are computed first in narrowband, and then are converted to one-third octave band before computing insertion loss.

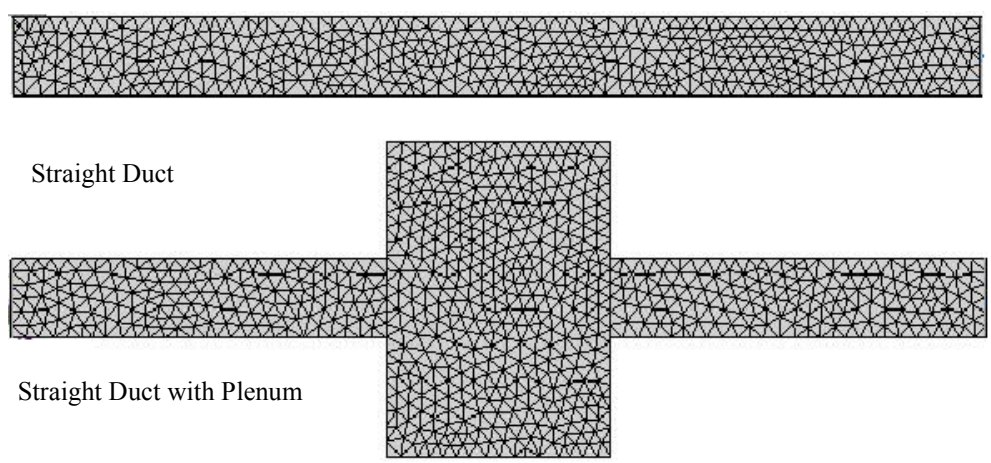

Figure 3.1 Side View of the straight duct with and without the HVAC plenum

The mesh of the plenum and the boundary conditions are shown in Figure 3.2. The acoustic FEM model consists of the HVAC plenum and inlet and outlet ducts. The input is a diffuse acoustic field or reverberant field. The termination is assumed to be a baffled termination. These boundary conditions are now considered in more detail. Also, observe that an absorptive lining can be added to the plenum FEM model via an impedance boundary condition.

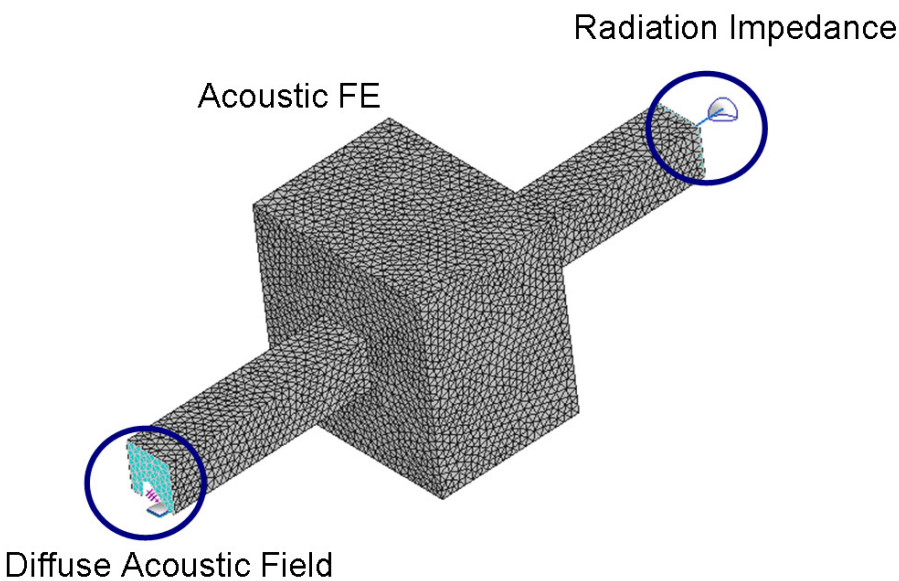

Figure 3.2 FEM model of the HVAC plenum with inlet/outlet ducts.

The diffuse acoustic field loading is applied via a reciprocity relationship between direct field radiation and diffuse reverberant loading developed by Shorter and Langley (2005)[56]. The most notable application of this relationship has been the development of hybrid junctions (Shorter and Langley (2005)[57]) between FEM and SEA subsystems. However, there are other important applications of the reciprocity relationship besides the development of hybrid junctions. For example, the reciprocity relationship also provides a mechanism for applying a diffuse field loading to a FE model. Shorter and Langley

(2005) [57] concluded that the cross-spectral matrix of the force or sound pressure is proportional to the imaginary part of the direct field dynamic stiffness matrix. The input to the model is expressed mathematically as a cross-spectral force matrix. Shorter and Langley (2005) [57], Langley (2007)[58, 59], and Shorter and Mueller (2008)[60] expressed the cross-spectral force matrix (S_{ff}) as

$$\mathbf{S}_{ff} = p_{DAF,RMS}^{2} \frac{8\pi c}{\rho\omega^{3}} \mathrm{Im}\left\{\mathbf{D}_{a}\right\} \tag{3.1}$$

where $p_{DAF,\ RMS}$ is the RMS Sound pressure of the diffuse acoustic field (DAF), c is the speed of the sound, ρ is the density of the fluid, and ω is the frequency spectrum. $\mathbf{D_a}$ is the direct field stiffness dynamic matrix of the loaded boundary. The cross-spectral force matrix ($\mathbf{S}_{ff}$) describes the reverberant loading on the FEM.

The radiation impedance at the outlet is determined using a wavelet approach developed by Lanley (2007)[59] in which jinc functions are selected as the wavelet basis. The dynamic stiffness matrix at the outlet (radiation boundary) is found by multiplying the radiation impedance by $1/i\omega$ (Langley (2007) [59]).

The plenum modeling is carried out using a deterministic approach for the plenum itself whereas the source and the termination boundary conditions are modeled in a statistical sense. The ensemble average acoustic pressure response $<\mathbf{S}_{qq}>$ of the FEM model is expressed as

$$\left\langle \mathbf{S_{qq}} \right\rangle = \mathbf{D_{tot}^{-1} S_{ff} D_{tot}^{-H}} \tag{3.2}$$

where $\mathbf{D_{tot}}$ is the summation of the dynamic stiffness for the finite element model and the direct field dynamic stiffness at the inlet ($\mathbf{D_a}$), Termination ($\mathbf{D_{rad}}$) and for any impedance boundary condition ($\mathbf{D_{imp}}$). The time and ensemble averaged sound power radiated ($\mathbf{P_{rad}}$) at the termination can be expressed as

$$\langle P_{rad} \rangle = \frac{\omega}{2} \sum_{jk} \mathrm{Im}\{D_a\}\{S_{qq}\}. \tag{3.3}$$

The time and spatially averaged sound pressure can be related to the sound pressure radiated. Additionally, absorption can be added to the models in one of two ways. For fiberglass lining, the absorption is modeled using a complex impedance matrix expressed in modal coordinates that describes the impedance of the lining on the acoustic cavity. For unlined plenums, the procedure suggested by Lyon and DeJong (1995)[29] Herrin et al. (2007)[26] was adopted to determine an appropriate loss factor (η) and is expressed as

$$\eta = \frac{cS_w}{4\pi f V} \frac{\alpha_w}{2 - \alpha_w} \tag{3.4}$$

where f is the frequency in Hertz, V is the plenum volume, and α_w is the absorption coefficient of the lining, S_w is the total surface area of the absorption lining in the plenum and c is the speed of sound in air. The sound absorbing coefficient for the plenum walls (α_w) was chosen using the ASHRAE Handbook (2011)[3].

3.2 Experimental work by Mouratidis and Becker (2003)

The simulation results in this work were compared to insertion loss measurements for HVAC plena made by Mouratidis and Becker (2003)[9]. As mentioned in the earlier

chapter, the measurements were made in accordance with ASTM-E477 (2006)[61]. A loudspeaker array was located in the noise source room and produced pink noise. The source room was connected to a receiving room (a 12.5 m x 8.5 m x 5.2 m reverberation room) via an unlined duct in which plenums could be inserted. The concrete reverberation room used in the measurement of insertion loss was qualified in accordance to ANSI S12.31 procedure for third octave band measurements. The distance between the source chamber and reverberant room was 38 m. The plenum was constructed such that the base was open and rested on concrete.

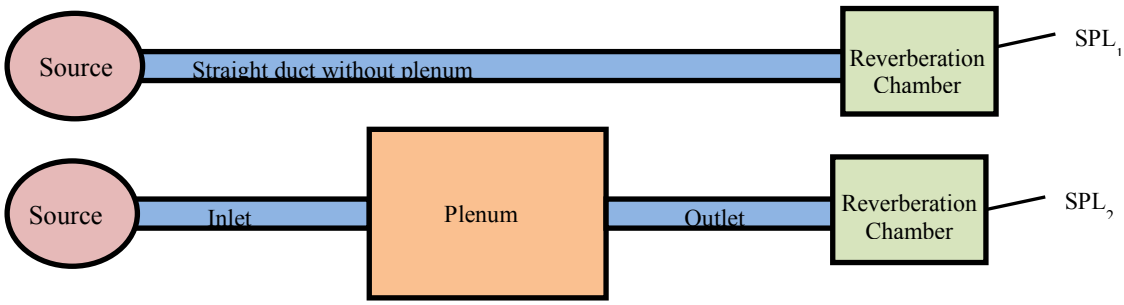

Figure 3.3 Schematic diagrams illustrating the calculation of insertion loss of a plenum

Insertion loss (*IL*) was determined by measuring the sound pressure level in one-third octave bands in the receiving room with and without the plenum inserted into the duct connecting source and receiving rooms and is expressed as

$$IL = SPL_1 - SPL_2 \tag{3.5}$$

where SPL_1 is the sound pressure level in dB in the empty duct and SPL_2 is the sound pressure level in dB in the duct with plenum as shown in figure 3.3.

Several different plenum configurations were measured. These included examples with the inlet and outlet ducts inline, offset, and at right angles to one another. The inlet and outlet ducts were unlined for each case, and fiber lining was placed on all sides of the

plenum except the base. The experimental investigation also examined the effect of inlet and outlet duct areas, and multi-outlet plenums. Figure 3.4 shows different types of silencers considered for analysis.

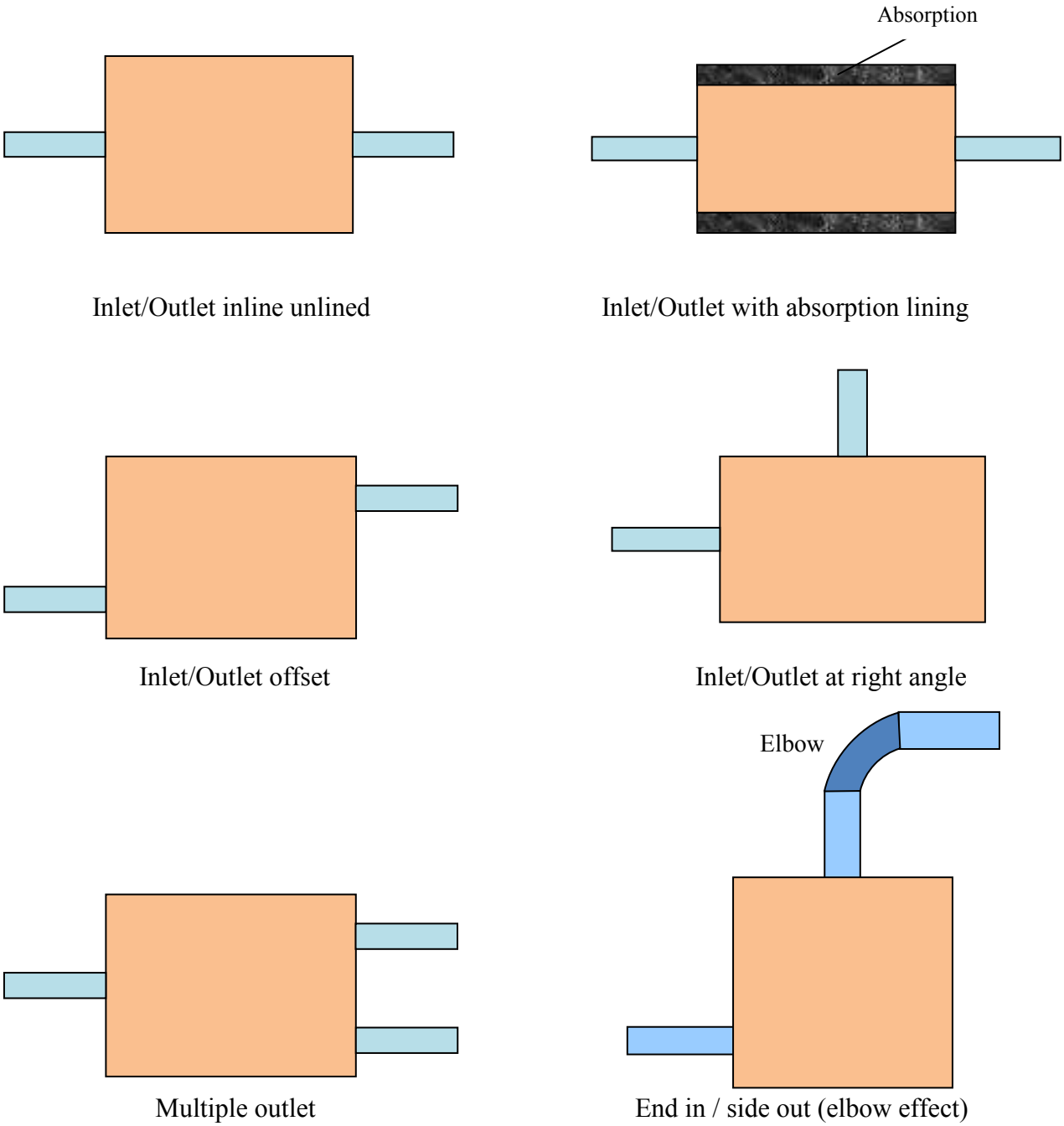

Figure 3.4 Types of mufflers measured by Mouratidis and Becker, 2003[9]

For the inlet and outlet ducts at right angles, Mouratidis and Becker (2003) [9] measured the noise reduction instead of insertion loss. Measuring insertion loss, while preferable, requires acoustic facilities with reverberation rooms positioned appropriately. Instead, a type of noise reduction was determined by comparing the sound power of the inlet duct without the plenum installed to the sound power at the outlet of the plenum. The sound power was measured using sound intensity scanning according to ISO 9614-2[62]. Noise reduction in this research work is defined as the difference in sound power at the inlet duct without the plenum installed to the sound power at the outlet opening of the plenum. The noise reduction of a simple expansion chamber is shown in figure 3.5 and is expressed as

$$NR = L_{W1} - L_{W2} \tag{3.6}$$

where NR is the noise reduction, L_{W1} is the sound power level without the plenum in dB, and L_{W2} is the sound power level with the plenum in dB

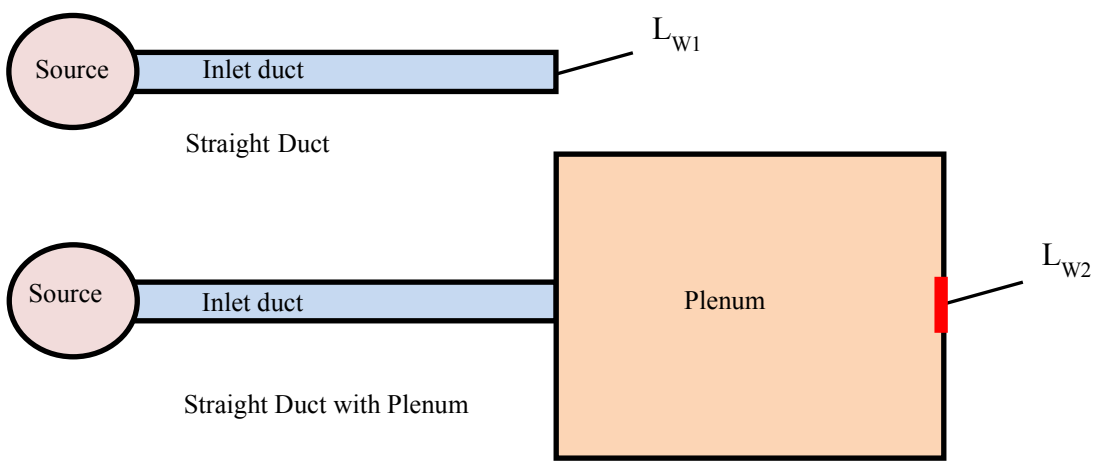

Figure 3.5 Two models used for Noise Reduction Calculation

The measured noise reduction was comparable to the measured insertion loss above the cutoff frequency for cases where both measurement techniques were applied. In fact, Mouratidis and Becker (2003)[9] compared over 40 cases and found both metrics to be in good agreement above the plane wave cutoff. However, there were significant variations below the cutoff frequency.

3.3 Comparison of Measurement and Simulation

The acoustic FEM analysis was compared with the measured insertion loss and noise reduction. Additionally, insertion loss was compared with the classical theory for plenum attenuation developed by Wells (1958)[5], the empirical models developed by Mouratidis and Becker (2003) [9], and statistical energy analysis (SEA).

For the Acoustic FEM simulation, linear tetrahedral acoustic finite elements are used. The mesh resolution was selected to allow at least four elements per acoustic wavelength up to 1150 Hz. ESI (VA-One, 2010[63]) conducted a study on mesh convergence for a rectangular cavity, and the error between predicted and analytical natural frequencies was below 10% for 4 elements per wavelength and was below 4% with 6 elements per wavelength. The accuracy at frequencies above the plane wave cutoff frequency should be sufficient since the excitation is broadband and the respective sound powers are summed in one-third octave bands. Moreover, the length of the inlet and the outlet ducts are reduced from 38 m to 1.524 m for the analysis because of the computational difficulties.

For the SEA analysis, the inlet and outlet ducts, and the plenum are modeled as single acoustic subsystem. The input boundary condition to the SEA model is a diffuse acoustic field and the termination is connected to a semi-infinite fluid (an energy sink) as shown in Figure 3.6. The absorption of the plenum is simulated by an appropriate loss factor. Additionally, a damping of 0.1% is applied to the plates of the plenum.

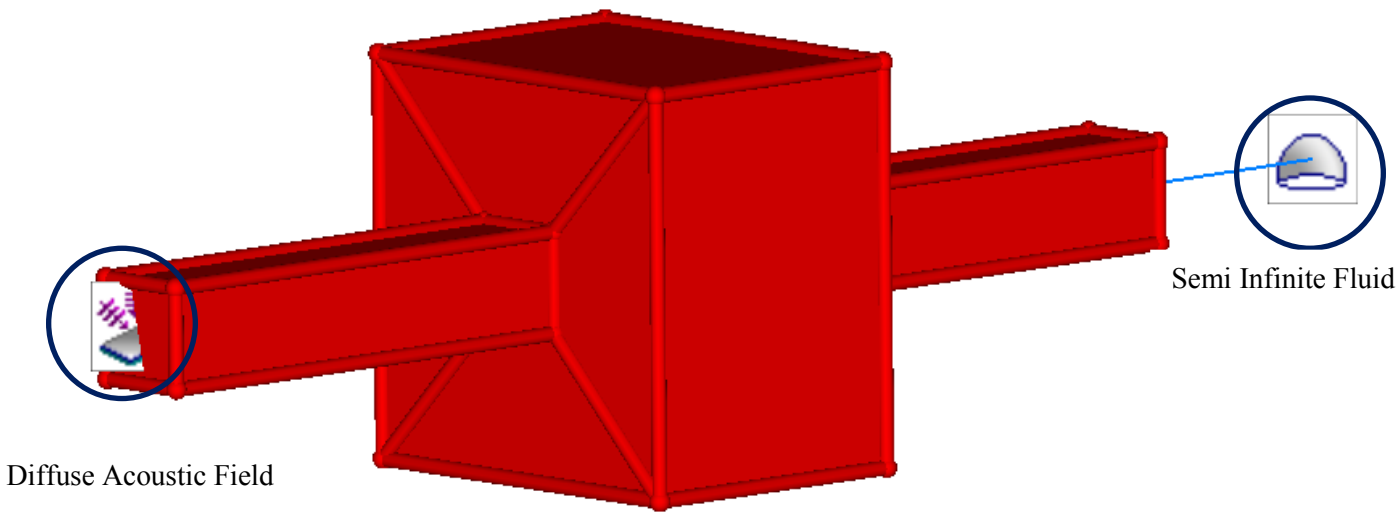

Figure 3.6 SEA model of a HVAC Plenum with an input power and semi-infinite fluid termination.

The eight different plenum cases considered are summarized in Table 3.1. The first six cases are for the inlet and outlet ducts inline while the last two are for inlet and outlet ducts perpendicular to one another (Figure 3.7). Three different plenum sizes and two different inlet/outlet duct cross-sectional areas were considered.

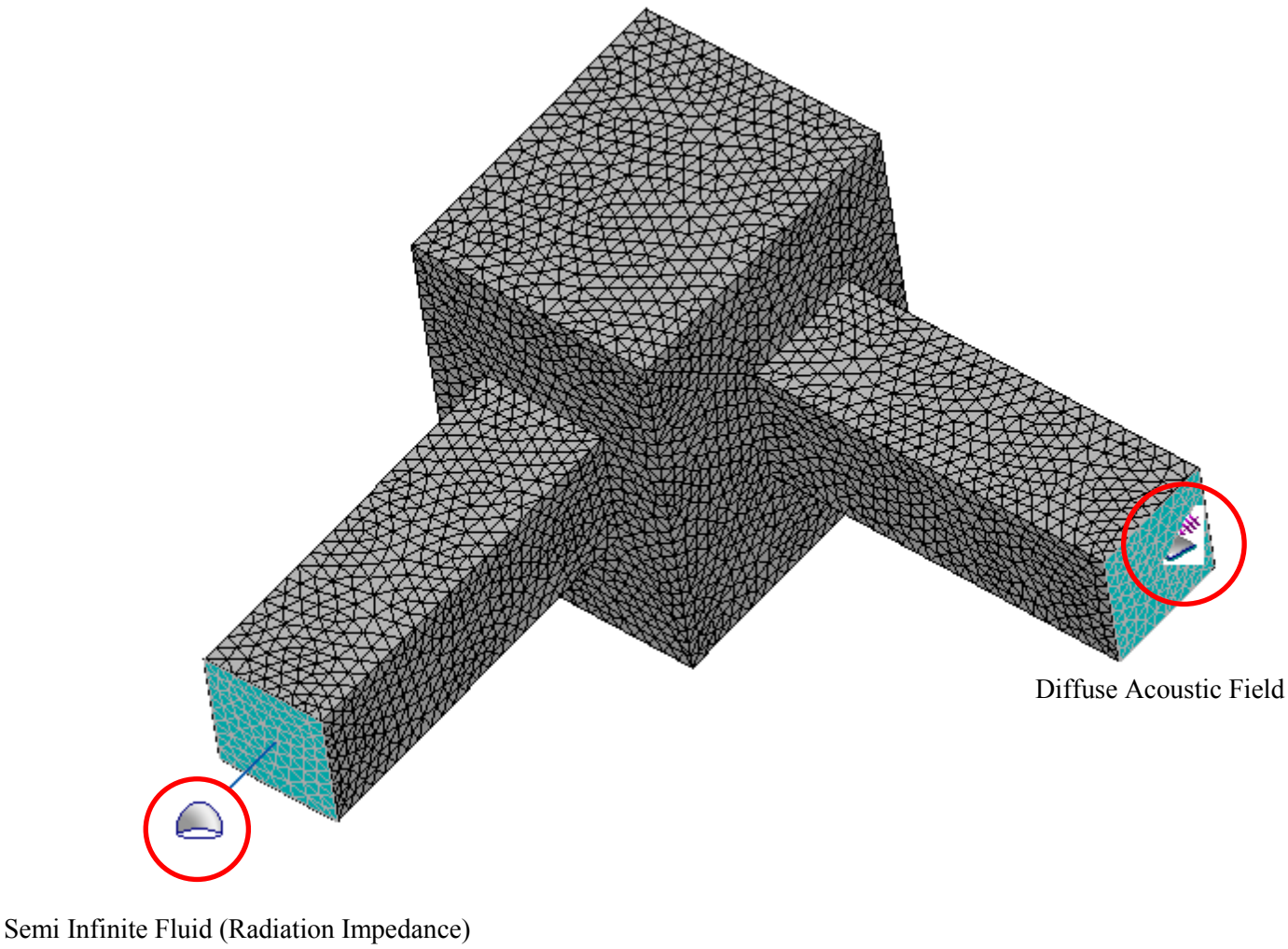

Figure 3.7 Acoustic FEM mesh of right angle duct configuration

TABLE 3.1 PLENUM CASES CONSIDERED FOR ANALYSIS

Case	Plenum Description			Inlet/Outlet Dimensions Duct cross section (m^2)	Absorptive Lining	Inlet/Outlet duct orientation
	Plenum dimensions (in meters)					
	Width	Height	Length			
1	1.22	1.22	0.91	0.31x0.31	Unlined	Inline
2	1.22	1.22	0.91	0.31x0.31	0.102 m Fiber	Inline
3	1.22	1.83	1.52	0.61x0.61	Unlined	Inline
4	1.22	1.83	1.52	0.61x0.61	0.102 m Fiber	Inline
5	1.22	1.83	3.05	0.61x0.61	Unlined	Inline
6	1.22	1.83	3.05	0.61x0.61	0.102 m Fiber	Inline
7	1.22	1.83	1.52	0.61x0.61	0.203 m Fiber	Right Angle
8	1.22	1.83	3.05	0.61x0.61	0.203 m Fiber	Right Angle

The results are shown in Figures 3.8 to 3.15 for Cases 1 through 8 respectively. In the plots the FEM refers to analysis utilizing special boundary conditions, and ASHRAE Handbook refers to the mathematical model for plenum attenuation developed by Wells (1958)[5]. Notice that the cutoff frequency (which is related to the cross-sectional dimensions) of inlet and outlet ducts is 570 Hz for Cases 1 and 2, and 285 Hz for Cases 3 through 8.

One important difference between the simulation and the measurement is the length of inlet and outlet duct. The combined 38 m length of inlet and outlet ducts was not modeled in FEM and SEA. Instead, the inlet and outlet duct lengths were shortened to

1.52 m to decrease the model size. Below the plane wave cutoff frequency, the modal frequencies are highly sensitive to the inlet and outlet duct lengths. However, it should be borne in mind that the insertion loss below the cutoff frequency is less important for most HVAC components. Additionally, measurements are difficult at low frequencies and signal to noise ratio is often low because of the low source strength and also environmental noise.

The following conclusions can be made based upon the comparisons.

- Above the cutoff frequency the acoustic FEM simulation is within 3 dB compared to the measurement. Additionally, the acoustic FEM agrees well with measured insertion loss even below the cutoff frequency except the 125 Hz band of Case 8 (Figure 3.14). In Figure 3.14, the insertion loss calculated from acoustic FEM is compared to the measured noise reduction. Even though the noise reduction is close to the insertion loss above the cut off frequency, there were significant variations below the cutoff frequency. Additionally, the measured data is suspect below the plane wave cutoff frequency due to background noise. From Figures 3.8 to 3.15, it is evident that the acoustic FEM can be used to determine the insertion loss of HVAC plenums both below and above the cutoff frequency.

- SEA compares well (within 3 dB) with the measured insertion loss above the cutoff frequency. Below the cutoff frequency, SEA does not compare well because the insertion loss depends on individual plenum modes. At frequencies below the cutoff, SEA under predicts the insertion loss by 10 dB because SEA assumes that total energy in each subsystem resides only in the resonant

frequencies. In other words, the total energy in each subsystem is uniformly distributed within each of the frequency bands in the analysis.

- The ASHRAE Handbook (2007)[2] or Wells' model (1958) [5] is nearly the same as the SEA model. This is expected since both approaches are energy based. Additionally, at low frequencies, insertion loss will be more sensitive to the boundary conditions at the source and termination.
- The empirical model developed by Mouratidis and Becker (2003) [9] is inferior to the Wells' model in most of the cases, especially above the cutoff. Below the cutoff frequency, Mouratidis and Becker model has better agreement with the measured insertion loss compared to the Wells' model.

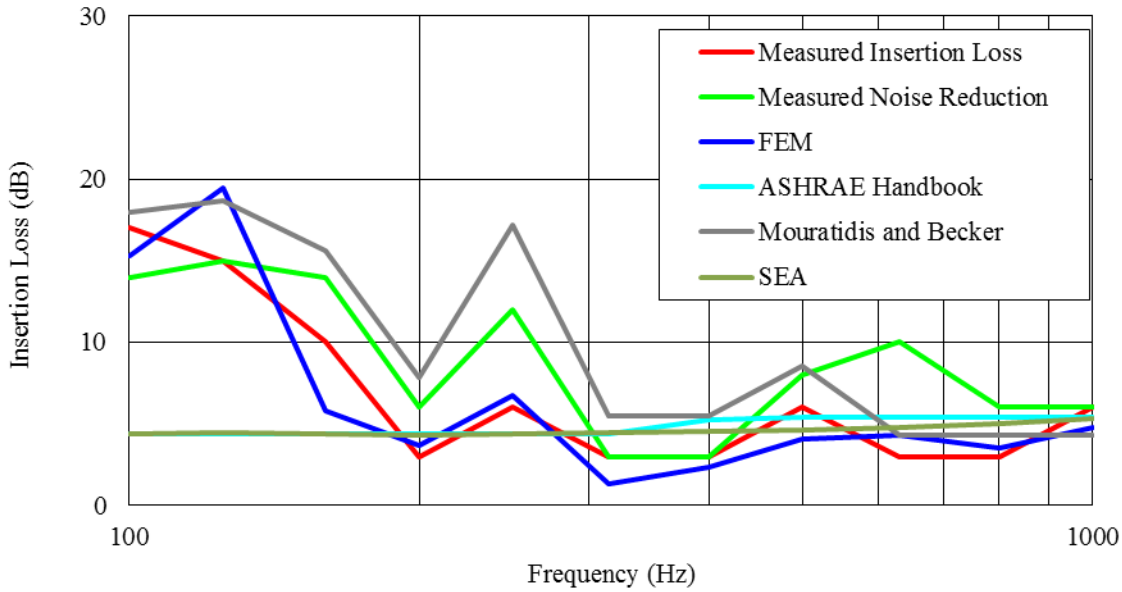

Figure 3.8 Insertion loss comparison for a 1.22 x1.22 x 0.91 m^3 plenum with inlet and outlet ducts in line. The plenum is unlined.

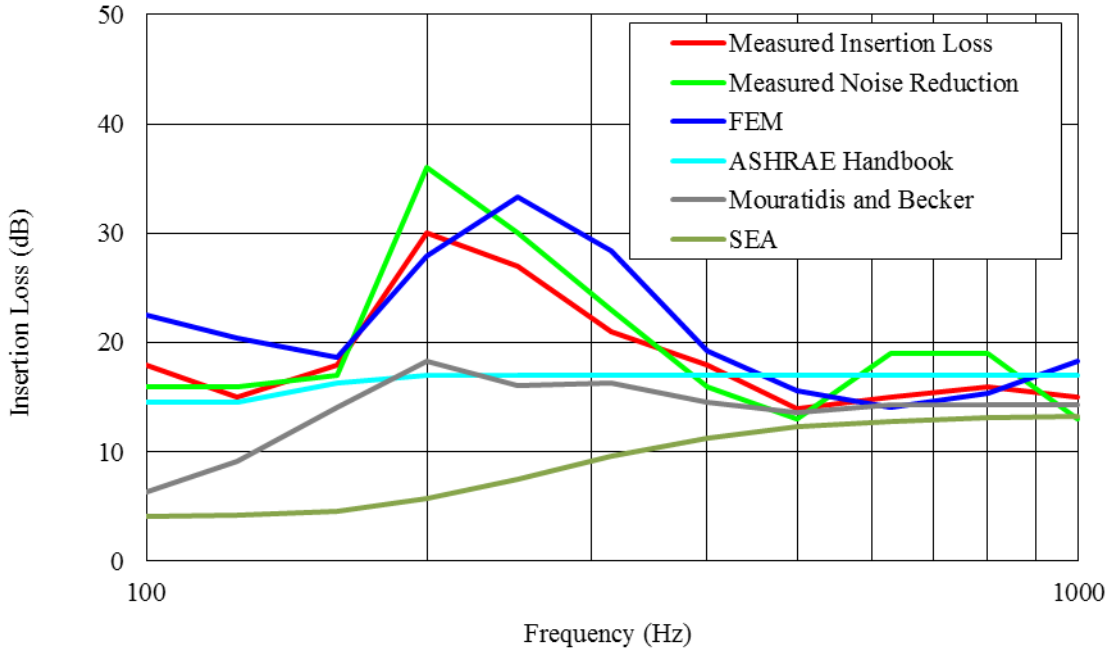

Figure 3.9 Insertion loss comparison for a 1.22 x 1.22 x 0.91 m^3 plenum with inlet and outlet ducts in line. The plenum is lined with 10.2 cm fiber.

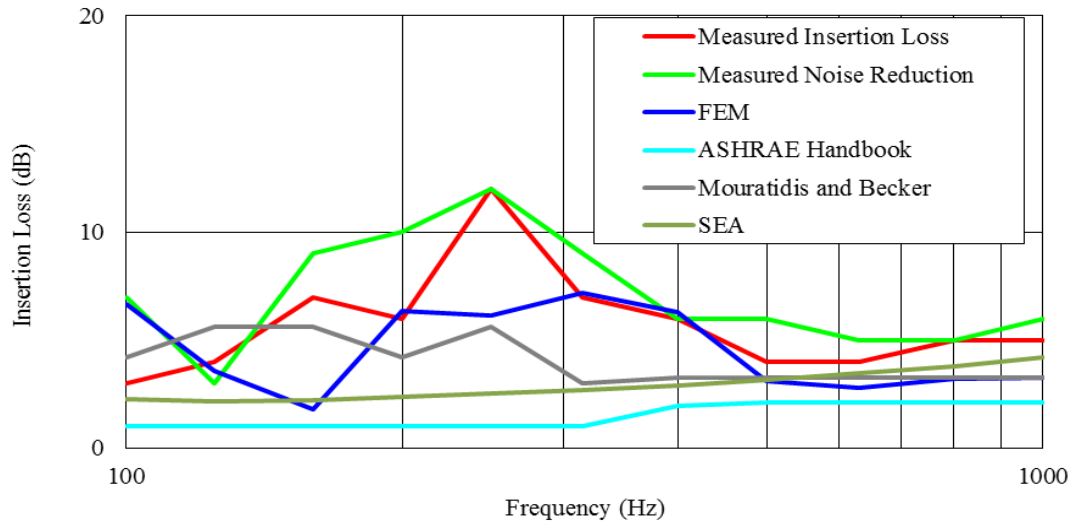

Figure 3.10 Insertion loss comparison for a 1.22 x 1.83 x 1.52 m^3 plenum with inlet and outlet ducts in line. The plenum is unlined.

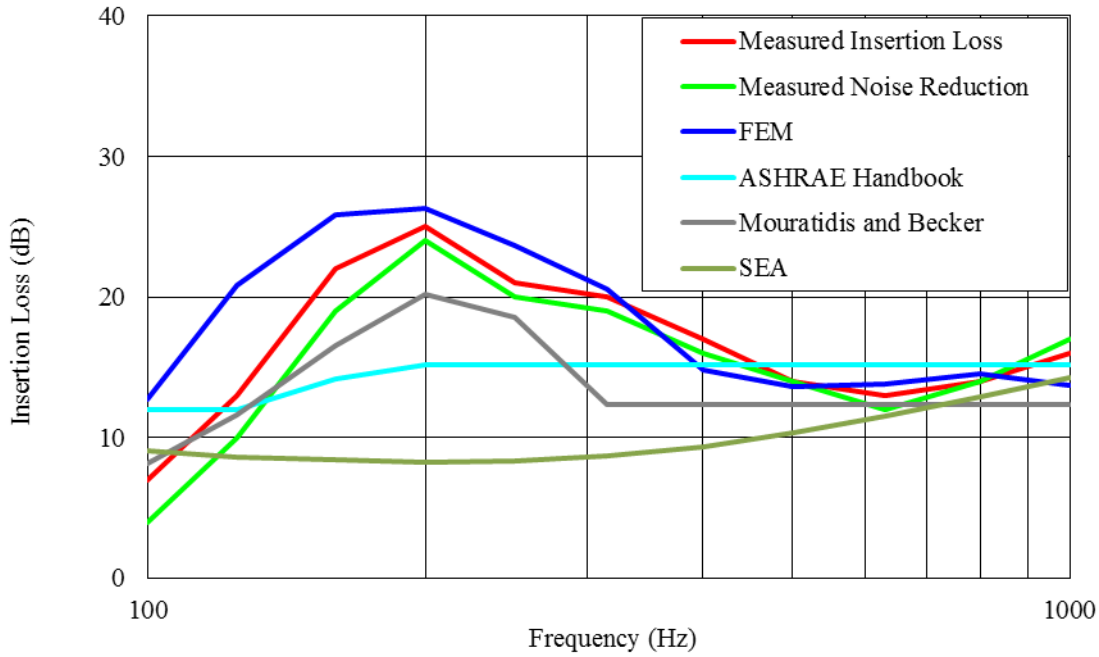

Figure 3.11 Insertion loss comparison for a 1.22 x 1.83 x 1.52 m^3 plenum with inlet and outlet ducts in line. The plenum is lined with 10.2 cm fiber.

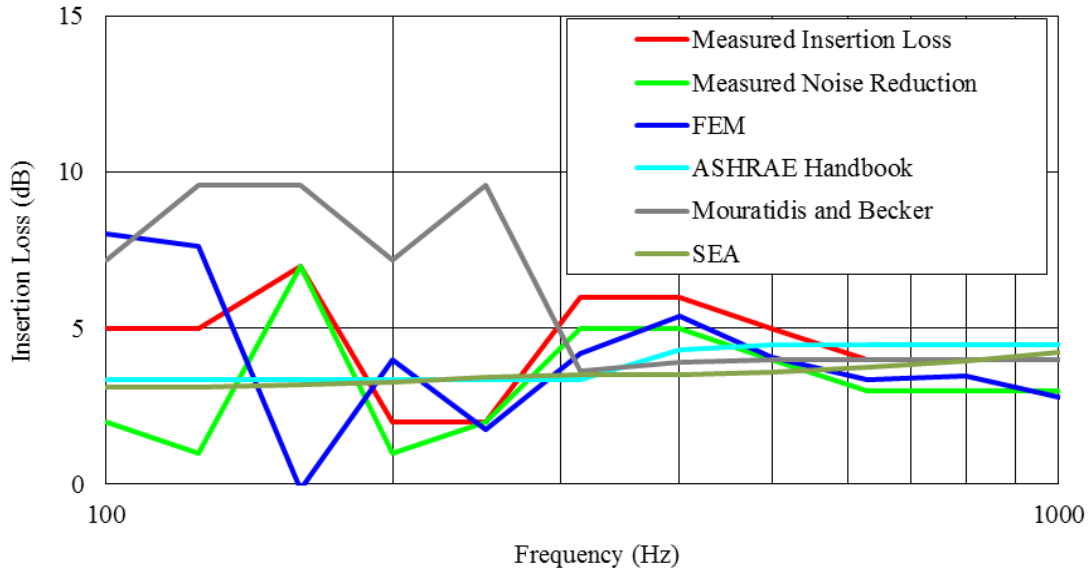

Figure 3.12 Insertion loss comparison for a 1.22 x 1.83 x 3.05 m^3 plenum with inlet and outlet ducts in line. The plenum is unlined.

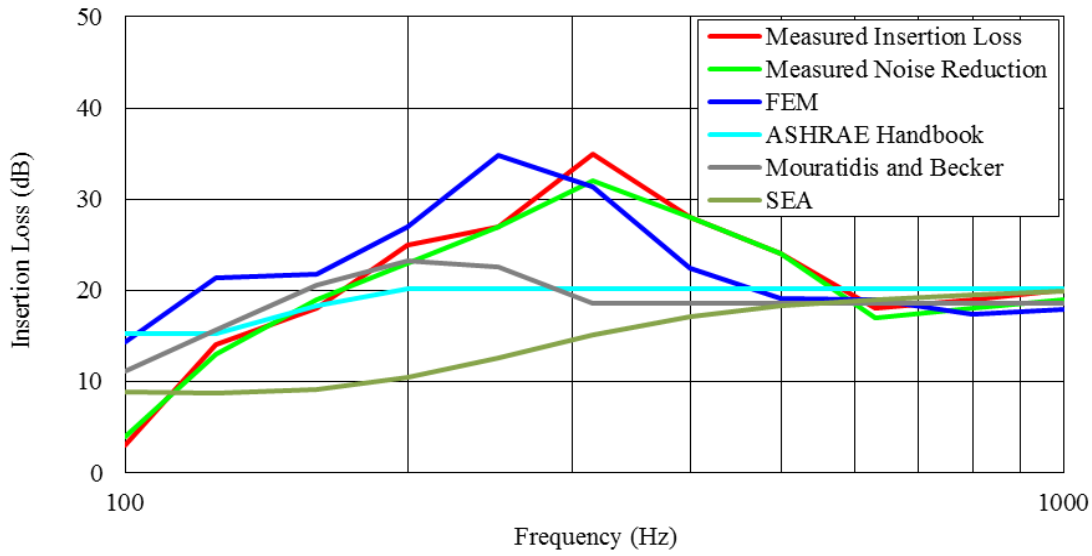

Figure 3.13 Insertion loss comparison for a 1.22 x 1.83 x 3.05 m^3 plenum with inlet and outlet ducts in line. The plenum is lined with 10.2 cm fiber.

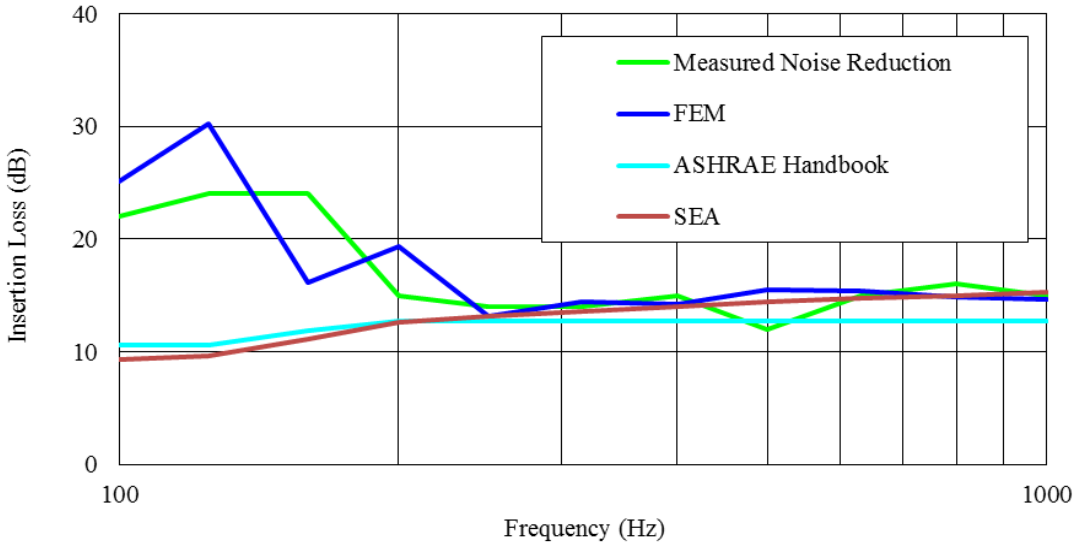

Figure 3.14 Insertion loss comparison for a 1.22 x 1.83 x 1.52 m^3 plenum with inlet and outlet ducts offset by 90 degrees. The plenum is lined with 20.3 cm fiber.

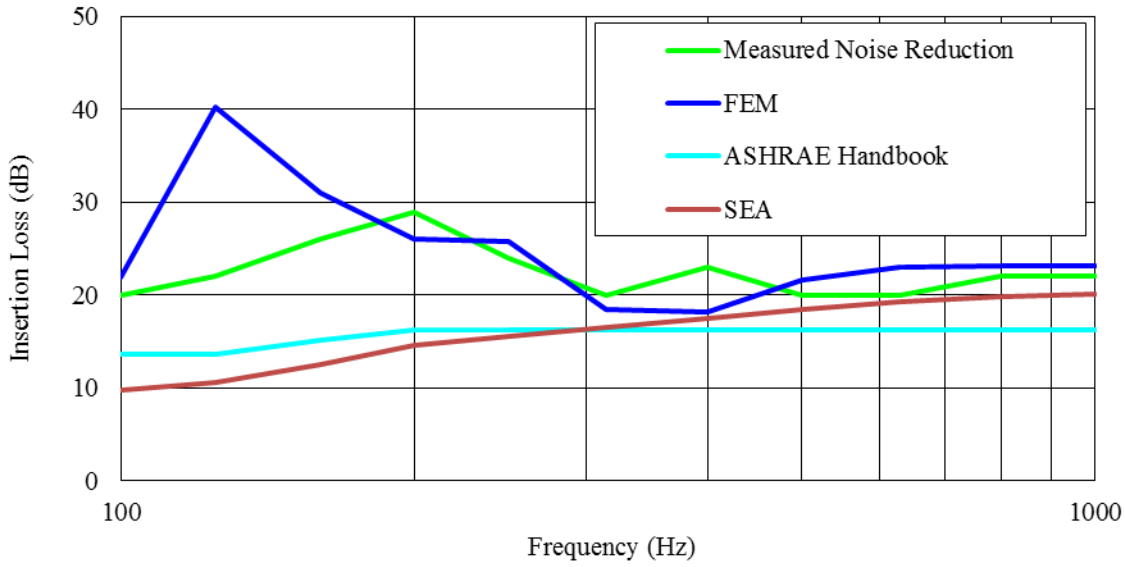

Figure 3.15 Insertion loss comparison for a 1.22 x 1.83 x 3.05 m^3 plenum with inlet and outlet ducts offset by 90 degrees. The plenum is lined with 20.3 cm fiber.

3.4 Summary

The measured insertion loss and measured noise reduction of the HVAC plenums with different geometries are compared with the acoustic FEM and SEA models of the HVAC plenums. Additionally, the ASHRAE Handbook (2007)[2] or Wells model (1958)[5] and the empirical model developed by Mouratidis and Becker (2003) [9] are also compared with the measurements.

From the comparisons, the Acoustic FEM with special boundary conditions has the best agreement with the measurements over the entire frequency band (below and above the cutoff frequency) when compared to the other models. Most importantly, the analysis does not assume plane wave behavior in the inlet and the outlet ducts.

The SEA and the ASHRAE handbook models are similar to each other as both the models are energy based. Furthermore, both the SEA and the ASHRAE handbook models differ by as much as 10 dB, below the cutoff frequency with the measured insertion loss. Above cut off frequency, both the approaches compare better. Additionally, the ASHRAE Handbook model is superior to the Mouratidis and Becker model above cut off frequency. However, the Mouratidis and Becker model has better agreement with measurement when compared to the Wells' or the ASHRAE handbook model below the cutoff. Moreover, the Mouratidis and Becker model was developed for HVAC Plenums with inlet/outlet ducts inline.

Therefore it can be concluded that Acoustic FEM can be used to determine the airborne noise transmission in HVAC Plenums in place of extensive and costly measurements.

CHAPTER 4

BREAKOUT NOISE IN DUCT SYSTEMS

4.1 Theoretical Background

Structure-borne noise in heating, ventilating, and air conditioning (HVAC) duct systems can be separated into two primary categories: (1) vibration caused by rotating machinery and (2) acoustic breakout. In the first case, rotating machinery transmits energy through the connected HVAC ductwork into building spaces. Machinery will excite the floor, wall or ceiling of a source room transmitting energy to other parts of a building (ASHRAE Handbook (2007)[2]). Most vibrational problems are at low frequencies and are best treated by isolation mounts or damping.

The second mechanism is known as acoustic breakout. Energy is transmitted from the HVAC duct air space to the surrounding duct walls, which in turn radiate energy into building spaces. This noise transmission through the duct wall is commonly referred to as breakout noise. Breakout noise is primarily a low frequency problem since fans and other equipment are dominated by lower frequency tones (Cummings (1978)[8]).

For breakout noise, energy is primarily transmitted through the HVAC duct wall. Accordingly, the sound attenuation through the duct wall, also known as the wall transmission loss, is the primary metric for assessing duct breakout noise. Duct breakout noise is documented in this chapter and the machinery noise is considered in Chapter 5.

There are several studies that discuss the determination of wall transmission loss of duct systems. Cummings (1978) [8] assumed plane wave behavior in the duct and coupled the structural and acoustic wave solutions together. The duct was assumed to be a line source radiating sound. In follow-on work, Cummings (1983)[64] determined the

duct breakout for higher order acoustic mode propagation through rectangular duct walls. Subsequently, Astley and Cummings (1984)[65] determined the wall transmission loss of rectangular duct system using FEM by including the coupling between the duct vibration and the external sound field in the FEM model.

Cummings and Chang (1986)[66] developed two mathematical models to predict wall transmission loss for oval ducts. The first model was based on forced wave theory assuming an infinite panel. The model accounts for the sound transmission through both flat and curved duct walls. The second model utilizes finite difference methods to solve the Reissner-Naghdi-Berry equations of motion for an arbitrarily shaped cylindrical shell in order to predict the wall transmission loss assuming only the plane acoustic modes within the duct. Cummings and Chang (1986) [66] concluded that the acoustic radiation that emanates from the flat wall of the duct results in higher transmission loss than the normal rectangular duct especially at low frequencies .

Later, Cummings (2001)[67] documented an excellent review on the sound transmission through duct walls where he discussed the effect of cross sectional geometry of the ducts on wall transmission loss and reciprocity relations between breakout and break-in noise. He also documented the method of stiffening the duct walls to reduce breakout noise.

Venkatesham et al. (2008) [68] predicted the breakout noise of rectangular cavities assuming one compliant wall when all the other walls of the plenum are rigid. Flexural vibration caused by compliant plenum walls due to the internal acoustic excitation radiates noise as breakout noise.

Venkatesham et al. (2008) [68] assumed a strong coupling between the compliant plate and the inside cavity and a weak coupling between the compliant plate and the exterior radiated acoustic field for a rectangular cross-section. An impedance mobility approach is used to calculate the inside sound pressure of the cavity and normal cavity wall vibration, from which the radiated sound power is calculated. Then, the transverse transmission loss is determined from the incident sound power inside the cavity and the radiated sound power. The incident sound power, radiated sound power and the transverse transmission loss of the rectangular cavity were expressed as

$$W_{in} = \frac{|A|^2}{2Y} \tag{4.1}$$

$$W_{rad} = \frac{1}{2} b^H \operatorname{Re}[\mathbf{Z}]\, b \tag{4.2}$$

$$TL_{transverse} = 10 \log\left(\frac{W_{in}}{W_{rad}}\right) \tag{4.3}$$

where W_{in} is the incident sound power, A is the amplitude of the incident sound power, Y is the characteristic impedance of the cavity plane waves, W_{rad} is the radiated sound power, b is the amplitude of the vibration velocity mode, H is the Hermitian of a matrix, Z is the radiation impedance of the un-baffled plate and $TL_{transverse}$ is the transverse transmission loss of the rectangular cavity.

Venkatesham et al. (2010)[69] extended his previous work by developing a 3D approach to predict breakout noise from rectangular plenums with four compliant walls. The mathematical model is expressed in terms of the acoustic impedance and the

mobility, for the acoustic pressure inside the plenum chamber and the displacement caused by the flexible wall vibration respectively. Venkatesham et al. (2010) [69] compared the mathematical model to FEM models with good agreement. Alternatively, the acoustic pressure inside the rectangular cavity and the vibration displacement of the compliant wall can also be expressed using a Green's function (Venkatesham et al. 2011)[70]. The advantage of using a Green's function to express vibrational displacement and acoustic pressure is that this method permits different end conditions and irregular geometries.

4.2 Determination Wall Transmission Loss Using Energy Methods

Energy methods have various applications in acoustics. One such application is the determination of wall transmission loss of panels. As mentioned earlier in Section 4.1, wall transmission loss can be used as a primary metric to assess the breakout noise. Additionally, wall transmission loss is also used to characterize the ability of an insulated partition to attenuate sound.

In order to explain the application of energy methods in determining the wall transmission loss, two case studies are considered. Firstly, the energy method is applied to a simple insulated plate and a mathematical model is developed to determine the wall transmission loss. Secondly, the energy method is used to develop a mathematical model to determine the sound transmission between two rooms separated by an insulated partition (wall).

4.2.1 Simple Plate model

The energy method is applied to a simple plate model. It is assumed that the plate is insulated with an absorption lining. Figure 4.1 shows a power balance for a sound field incident upon an insulated plate. The sound reduction index, R is expressed as

$$R = 10\log\left(\frac{1}{\tau}\right) \tag{4.4}$$

with

$$\tau = \frac{W_t}{W_i} \tag{4.5}$$

where W_i is the incident sound power, W_t is the transmitted sound power and τ is the transmission factor.

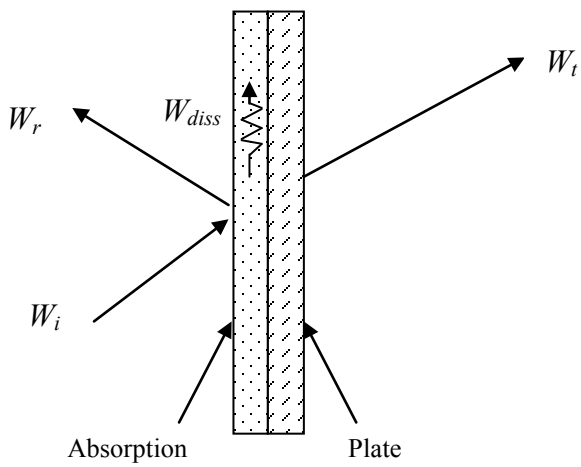

Figure 4.1 Power balance for a sound field incident upon an insulated plate

The power balance equation for a sound field incident on the panel is developed based on balancing the energy. The power balance equation is expressed as

$$W_i = W_r + W_t + W_{diss} \tag{4.6}$$

where W_r is the reflected sound power and W_{diss} is the sound power dissipated by damping due to the sound absorption applied to the panel. Upon dividing Eqn. 4.6 by W_i,

$$1 = \frac{W_r}{W_i} + \frac{W_t}{W_i} + \frac{W_{diss}}{W_i} \tag{4.7}$$

$$1 - \frac{W_r}{W_i} = \frac{W_t}{W_i} + \frac{W_{diss}}{W_i} \tag{4.8}$$

and

$$\alpha = \tau + \delta \tag{4.9}$$

where $\alpha = 1 - \frac{W_r}{W_i}$ is the absorption coefficient, $\tau = \frac{W_t}{W_i}$ is the transmission coefficient and $\delta = \frac{W_{diss}}{W_i}$ is the dissipation factor.

For an absorbent mounted on a plate, τ is always less than δ ($\tau << \delta$) (HP Wallin (2011)[71]). In other words, the power transmitted from the wall is always less when compared to the power dissipated due to the damping except in the mid-frequency range where there are only a few modes that dominate the plate behavior. Therefore, it can be concluded from Eq. (4.9) that the absorption factor (α) is significantly influenced by the power dissipated due to the damping. Therefore, the wall transmission loss can be increased significantly by using insulation with the absorbent factor close to 1.Additionally, the transmission loss for an incident sound field on a plate is expressed as

$$TL_{panel} = 10\log\left(\frac{W_i}{W_t}\right) \tag{4.10}$$

where W_i is the incident sound power, W_t is the transmitted sound power, and TL_{panel} is the plate transmission loss. From the Eqns. 4.5 and 4.10, the transmission factor and the transmission loss of a plate are related directly to each other. Therefore, the transmission loss of a panel can be directly determined using energy methods by calculating the transmission factor of the panel.

4.2.2 Sound transmission between two rooms separated by a wall

The energy method is applied to determine the sound transmission between the two rooms (H P Wallin et al (2011) [71]; Ver and Beranek (2006)[72]). Figure 4.2 shows two rooms separated by a partition. From Figure 4.2, it is also noted that the sound source is placed in room 1. The sound field is incident on the partition and transmits to room 2. Again, the sound is reflected back from the walls back into room 1 through the partition.

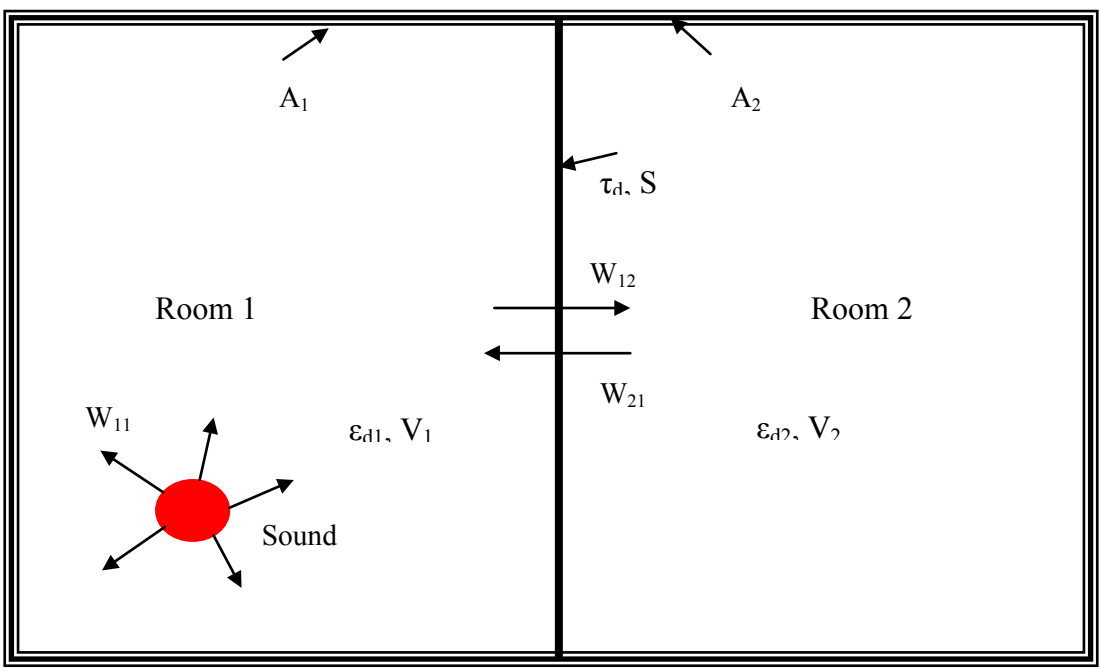

Figure 4.2 Sound Transmission between two rooms.

An energy balance equation is applied for room 1 and room 2 separately and expressed as

$$\frac{dE_1}{dt} = W_{1,in} - W_{1,diss} \tag{4.11}$$

$$\frac{dE_2}{dt} = W_{2,in} - W_{2,diss} \tag{4.12}$$

For the case of room 1,

$$W_{1,in} = W_{11} + W_{21} \tag{4.13}$$

$$W_{1,diss} = \eta_1 \omega E_1 + W_{12} \tag{4.14}$$

where $W_{1,in}$ is the net power input into room 1, W_{11} is the power input into room 1 from sound source, W_{21} is the power input into room 1 from room 2, $W_{1,diss}$ is the power dissipated from room 1, E_1 is the total energy in room 1, η_1 is the loss factor of room 1 and ω is the angular frequency.

Similar expressions for room 2 can be developed. These are expressed as

$$W_{2,in} = W_{12} \tag{4.15}$$

$$W_{2,diss} = \eta_2 \omega E_2 + W_{21} \tag{4.16}$$

where $W_{2,in}$ is the net power input into room 2, W_{12} is the power input into room 2 from room 1, $W_{2,diss}$ is the power dissipated from room 2, E_2 is the total energy in room 2 and η_2 is the loss factor of room 2

Substituting Eqns. 4.13 to 4.16 in Eqns. 4.11 and 4.12, one obtains

$$\frac{dE_1}{dt} + \eta_1 \omega E_1 + W_{12} = W_{11} + W_{21} \tag{4.17}$$

and

$$\frac{dE_2}{dt} + \eta_2 \omega E_2 + W_{21} = W_{12} \tag{4.18}$$

Eqns. 4.16 and 4.17 represents the energy balance equations for the two coupled systems (rooms). The equations are valid only for sound sources placed in both the rooms (i.e. the equations do not include vibratory sources or energy flow). If the sound field that is emitted by the sound source is stationery, then the Eqns. 4.17 and 4.18 are reduced to

$$\eta_1 \omega E_1 + W_{12} = W_{11} + W_{21} \tag{4.19}$$

and

$$\eta_2 \omega E_2 + W_{21} = W_{12} \tag{4.20}$$

From the power balance equations, Eqns. 4.19 and 4.20, the wall transmission loss of the wall that separates the two rooms can be determined. To predict the power transmission between the rooms, it is assumed that the diffuse fields are incident upon the wall separating the rooms. From Eqn. 4.5, the transmission factor of the wall can be determined. The transmission factor from room 1 to 2 (τ_d) can be expressed as

$$\tau_d = \frac{W_{12}}{W_{d1}} \tag{4.21}$$

with

$$W_{d1} = I_{d,1} S \tag{4.22}$$

where $I_{d,1}$ is the sound intensity in room 1 and S is the cross-sectional area of the wall.

Similarly, the transmission factor from room 2 to room 1 is expressed as

$$\tau_d = \frac{W_{21}}{W_{d2}} \tag{4.23}$$

with

$$W_{d2} = I_{d,2} S \tag{4.24}$$

where τ_d is the transmission factor of the wall and $I_{d,2}$ is the sound intensity.

It should be noted that the transmission factor from room 1 to room 2 is the same as the transmission factor from room 2 to room 1 because the partition between the rooms remains the same. Further, the field energy and the sound intensity are expressed as

$$E = \varepsilon V \tag{4.25}$$

$$I_d = \frac{\varepsilon_d c}{4} \tag{4.26}$$

$$\varepsilon_d = \frac{\widetilde{p}^2{}_d}{\rho_0 c^2} \tag{4.27}$$

where E is the field energy, ε is the energy density, I_d is the diffuse field intensity, c is the speed of sound, V is the volume of the room, ε_d is the energy density of the diffuse field, $\widetilde{p}_d$ is the diffuse sound pressure and ρ_0 is the air density. Eqns. 4.25-4.27 are also

utilized in the Sabine room acoustic model (Wallin et al (2011) [71]; Ver and Beranek (2006) [72]; Kinsler and Frey[73]).

Substituting Eqn. 4.26 into Eqns. 4.21 and 4.23

$$W_{12} = \frac{\tau_d \varepsilon_{d1} c S}{4} \tag{4.28}$$

$$W_{21} = \frac{\tau_d \varepsilon_{d2} c S}{4} \tag{4.29}$$

Substituting Eqns. 4.28 and 4.29 in Eqn. 4.20

$$\eta_2 \omega E_2 + \varepsilon_{d,2} \tau_d \frac{c}{4} S = \varepsilon_{d,1} \tau_d \frac{c}{4} S \tag{4.30}$$

Dividing Eqn. 4.30 by $\varepsilon_{d,2} \tau_d \frac{c}{4} S$ and substituting $\eta_2 = \frac{CA_2}{4\omega V_2}$ (Lyon and DeJong (1995)[29])

$$\frac{\varepsilon_{d,1}}{\varepsilon_{d,2}} = 1 + \frac{A_2}{S\tau_d} \tag{4.31}$$

Substituting 4.27 in 4.31, one obtains

$$\frac{p_{d,1}^2}{p_{d,2}^2} = 1 + \frac{A_2}{S\tau_d} \tag{4.32}$$

Taking the log on both sides of Eqn. 4.32, one obtains

$$L_{p,1} - L_{p,2} = 10 \log\left(1 + \frac{A_2}{S\tau_d}\right) \tag{4.33}$$

where $L_{p,1}$ is the sound pressure level at room 1 and $L_{p,2}$ sound pressure level at room 2 and A_2 is the equivalent absorption areas in room 2.

Thus Eqn. 4.33 can be used to determine the wall transmission loss, which is developed using energy methods. Furthermore, the wall transmission loss can also be determined experimentally from Eqn. 4.33 by assuming the rooms to be reverberant and by placing a sound source in one of the reverberant rooms.

4.3 Determination of Insertion loss of an Air Handler using Energy Methods

The insertion loss of an air handler was determined experimentally. Then, a SEA model was created using the commercial software VA-One. The theory used is similar to that described in the prior section. This section discusses the procedure to determine the insertion loss of an air handler experimentally. Then, the different test cases that are considered to validate the experimental results with simulation are documented.

4.3.1 Procedure to Determine the Insertion Loss of an Air Handler Experimentally

The air handler that is used for the measurement is shown in Figure 4.3. The air handler is built with panels made of galvanized steel. Each panel of the air handler is treated with absorption. Figure 4.4 shows two-inch fiber inserted into a high porosity perforated panel and attached to the panels of the air handler.

In the case of an enclosure (air handler), it is more appropriate to consider the insertion loss as the primary metric instead of the transmission loss, due to measurement ease. Moreover, for an enclosure

$$TL \approx IL \tag{4.34}$$

if the external sound field is anechoic and TL and IL are wide frequency band averages (at least one-third octave band) (Crocker (2007)[4]).

Figure 4.3 Air handler utilized for acoustic measurement

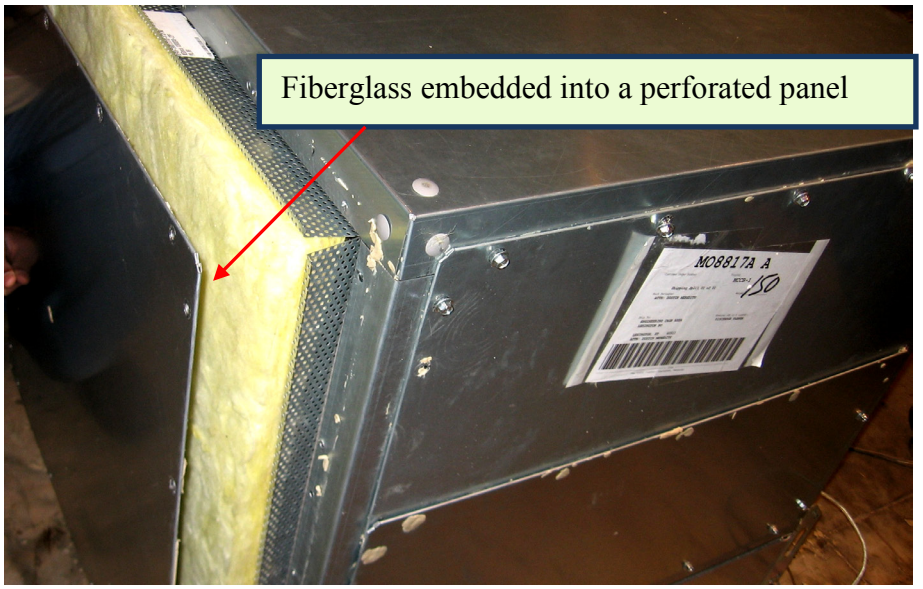

Figure 4.4 Fiberglass embedded into a perforated panel

The insertion loss of the air handler can be determined by placing the air handler inside an anechoic chamber. First, the sound power level of the source is measured without the

air handler. Then, the sound source is placed inside the air handler and the sound power is measured

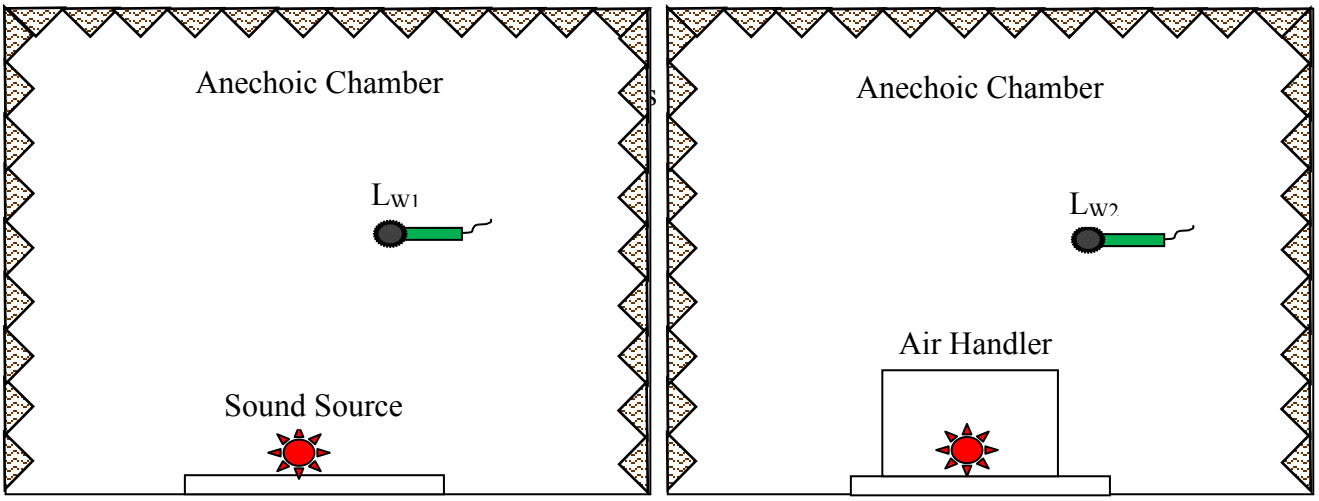

Figure 4.5 Insertion loss measurement setup for an air handler

The insertion loss of the air handler (*IL*) is determined as

$$IL = L_{W1} - L_{W2} \tag{4.35}$$

where L_{W1} is the sound power level of the source alone in dB, and L_{W2} is the sound power level of the source with the enclosure in dB. The sound power is measured in accordance with ISO 9614-2 standard which is discussed in detail in Chapter 5.

4.3.2 Validation Study

In this section, the air handler shown in Figure 4.3 is considered for the validation study. The insertion loss of the air handler is measured as explained in Section 4.3.1. Then, the SEA model of the air handler is developed using VA-One (2010)[63] and is shown in figure 4.6. Additionally, Figure 4.7 shows the air handler with an opening.

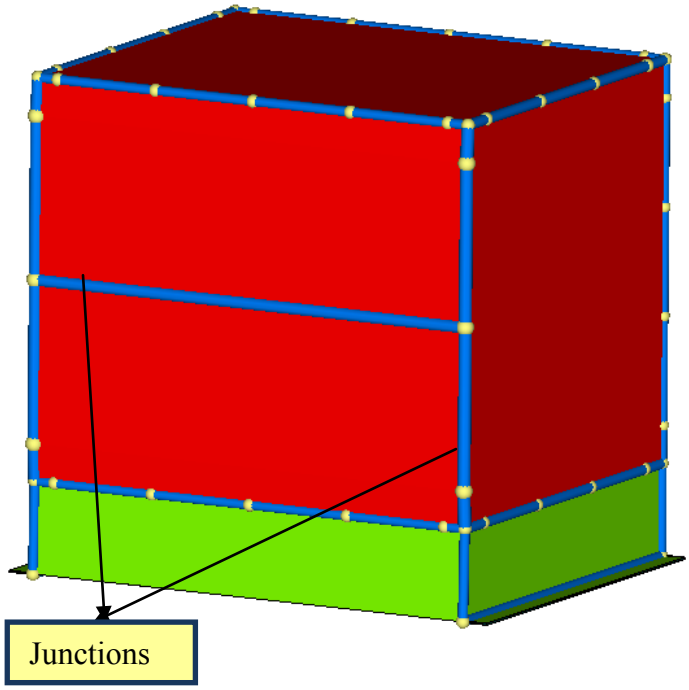

Figure 4.6 SEA model of the air handler

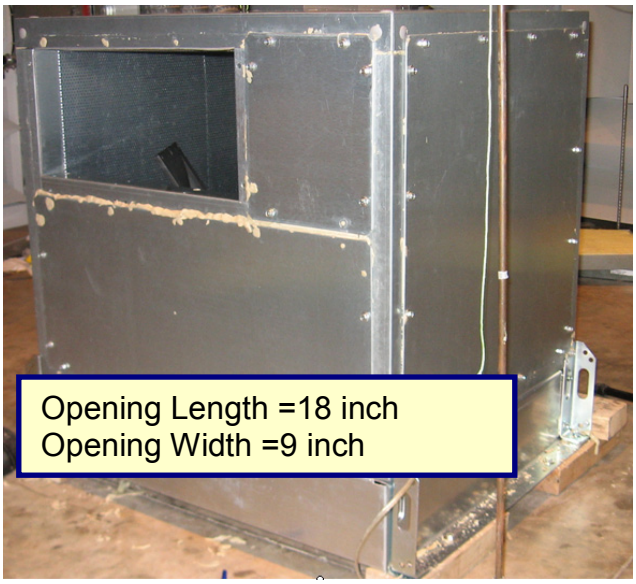

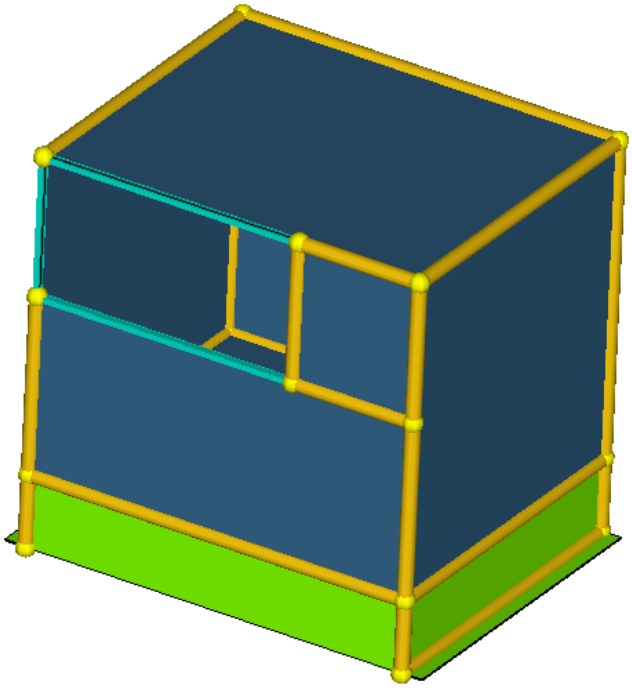

Figure 4.7 Original and SEA model of the air handler with an opening

The connections between the plates are modeled as junctions and the coupling loss factor of the two connected plates were automatically determined by VA-One.

Additionally, 0.1% damping is assumed in each plate of the air handler. Furthermore, the sound source to the air handler is modeled as a diffuse acoustic field and the exterior sound field is modeled as semi-infinite fluid. The semi-infinite fluid is analogous to an anechoic room surrounding the air handler. Four test cases are considered for the validation study. These include a

- Fully sealed air handler with fiber.
- Fully sealed air handler without fiber.
- Air handler with an opening and with fiber.
- Air handler with an opening and without fiber.

Figures 4.8-4.11 show the results for the four test cases. Both the measurement and the simulation results are recorded in one-third octave bands. From Figures 4.8-4.11, the following observations can be made:

- The measured insertion loss of the air handler fully sealed with fiberglass has an excellent agreement with SEA over the entire frequency spectrum (Figure 4.7). The deviation between the measurement and the simulation is less than 3 dB over the entire frequency range measured.
- For the air handler fully sealed without fiberglass, it is apparent from Figure 4.8 that the simulation over predicts the measurement. The lack of agreement below 2000 Hz between the SEA prediction and the measurement is due to the absorption in the enclosure and the damping in the walls being estimated.

Furthermore, modal behavior in the walls of the air handler is not considered in the SEA analysis.

- Figures 4.9 and 4.10 compare the insertion loss an air handler with an opening, with and without the fiberglass respectively. The SEA agrees well with the measurement except for a few dips and peaks in measurement data at certain frequency bands. This is because the sound source used in the measurement is a loudspeaker which is not a monopole. Thus the location or the placement of the loudspeaker inside the air handler also influences the sound power radiating outside the air handler if the air handler has an opening. Additionally, the damping in the walls of the air handler also influences the SEA prediction unless determined experimentally.

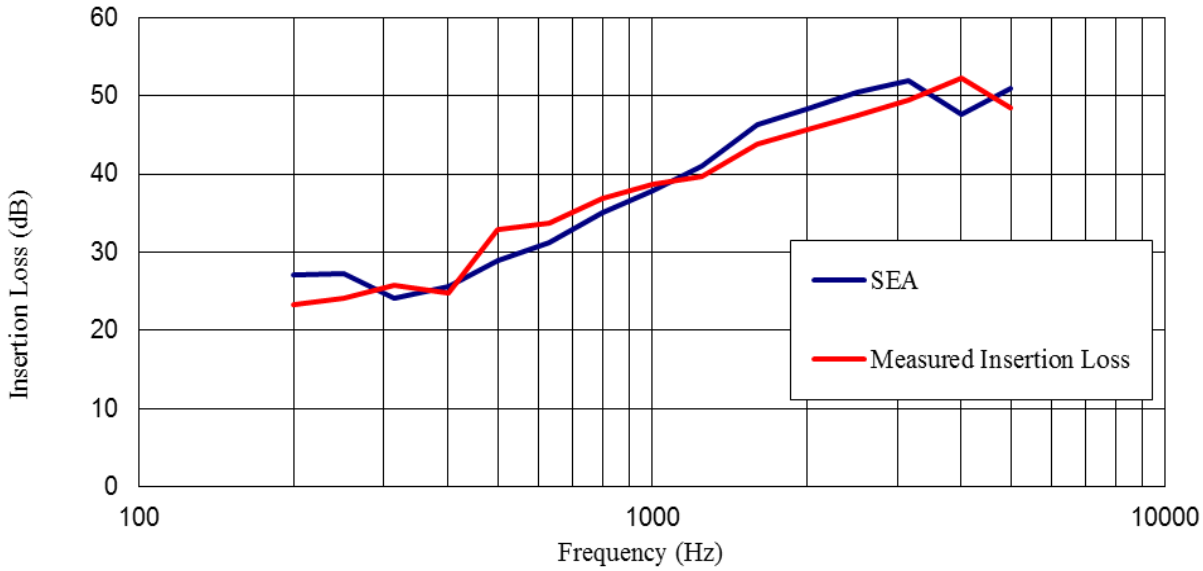

Figure 4.8 Enclosure fully sealed with fiberglass

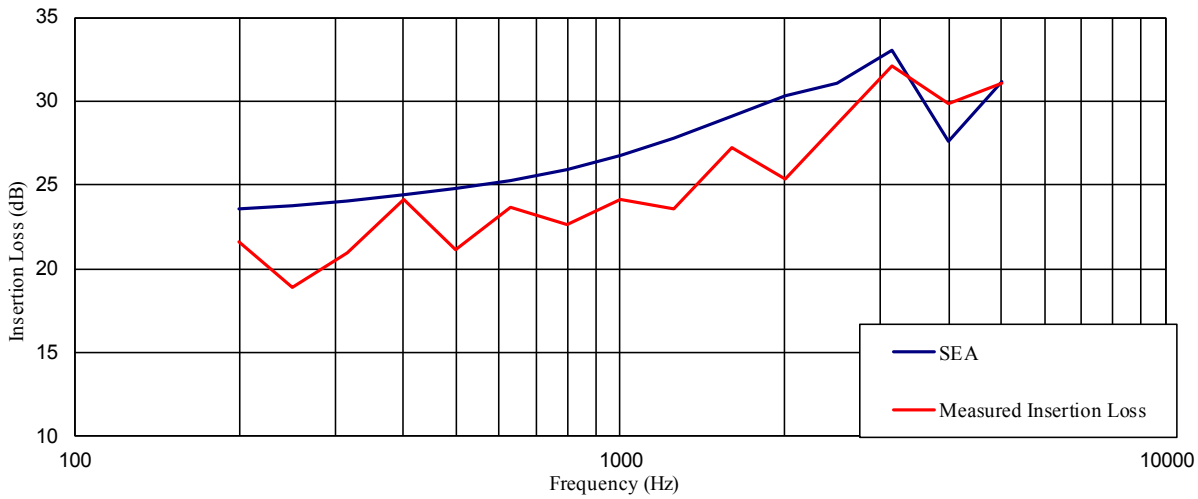

Figure 4.9 Enclosure fully sealed without fiberglass

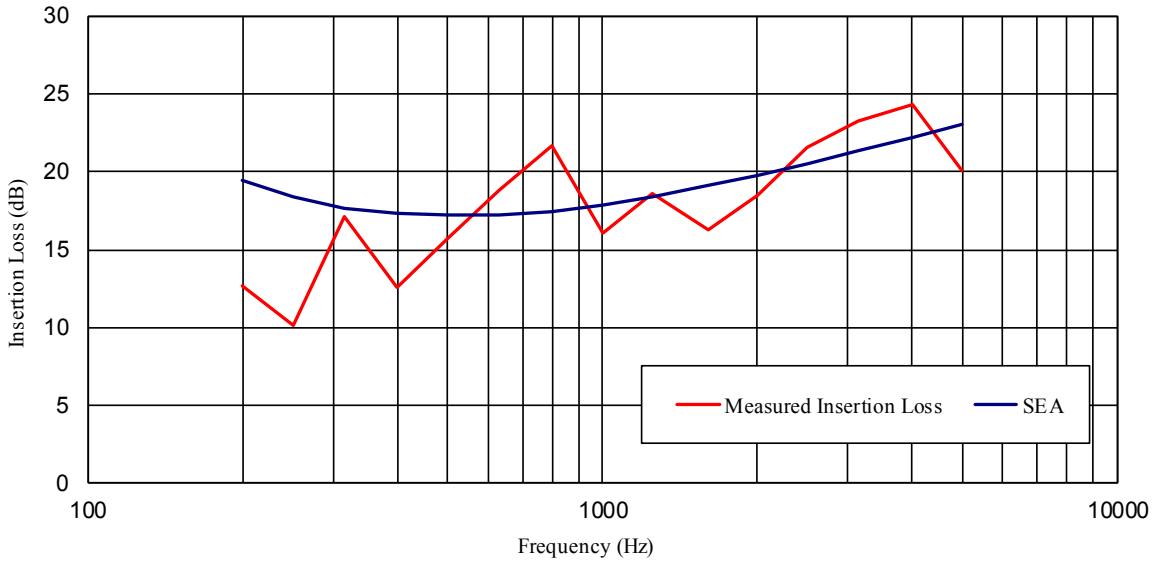

Figure 4.10 Enclosure with an opening with fiberglass

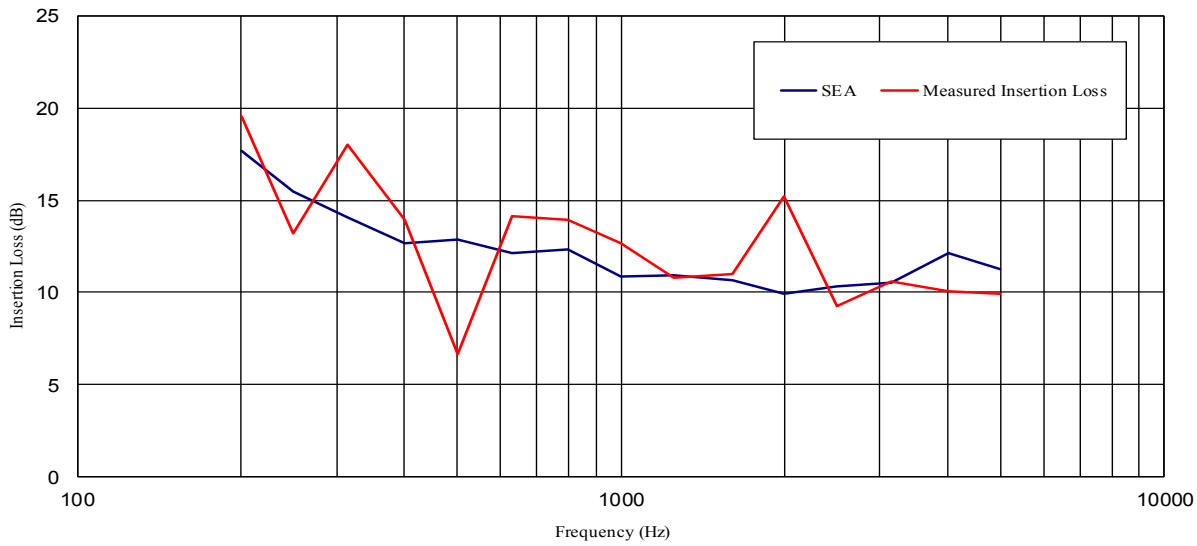

Figure 4.11 Enclosure with an opening without fiberglass

4.4 Summary

Prior work on breakout noise has been summarized in this chapter. In the research presented, energy methods are used to determine the wall transmission loss, which is the primary metric to assess the breakout noise. The power balance equations for a single subsystem and two subsystem cases are derived based on energy methods. Furthermore, the insertion loss of the air handler considered for this study was determined using energy methods (SEA) and compared experimentally.

The SEA prediction and the measured insertion loss are in good agreement with each other for each case. Results are not quite as good when there is very little absorption in the air handler. Moreover, the insertion loss of the air handler predicted using SEA could be improved by determining the SEA parameters experimentally. The aforementioned claim is validated by comparing the SEA model and measured machinery noise in the air handler, which will be discussed in Chapter 5.

CHAPTER 5

MACHINERY NOISE

5.1 Background

Rotating machinery such as compressors, fans, and power generating equipment in HVAC systems produce dynamic loads, which lead to structure-borne noise in the building spaces (ASHRAE Handbook (2007)[2]). Isolation or damping is normally used to treat structure-borne noise.

Several studies have documented the use of statistical energy analysis (SEA) to model structure-borne noise transmission due to the machinery. For building applications, Craik (1982)[74] modeled the energy propagation through the walls and floor. The coupling loss factors between the rooms and the walls were measured and compared with mathematical models. Additionally, different types of sound sources such as an electromagnetic shaker, impact machine and an airborne sound source (loud speaker) were used to check the applicability of SEA to determine the vibration velocity of the walls and the sound power level.

In addition to building applications, SEA has been used extensively in the automobile and ship industries. Cimerman et al. (1997)[36] determined the structure-borne noise paths in an automobile. An impact hammer and a loudspeaker were used as sources for the structural and the acoustic subsystems respectively. Further, Cimerman et al (1997) [36] used SEA to determine the interior cabin noise of a truck operating at 55 mph. Additionally, SEA was utilized to determine the contributions inside the truck cabin.

In similar work, Steel (1996)[75] and Yamazaki (2003)[37] applied SEA to predict the structure borne noise transmission in automobiles by determining the appropriate loss factors experimentally. Steel (1996) [75] determined the structure-borne sound transmission at the plate joints of a car body by exciting the plates with a plastic head hammer. Additionally, he determined the sound transmission at the rubber seals and the effect of coupling at the door hinges. Similarly, Yamazaki (2003) [37] applied experimental SEA on a V-6 automotive engine to determine the structure-borne noise transmission determining the coupling loss factors and the damping loss factors experimentally. Lalor (1989)[33] used a two subsystem method to determine the coupling loss factors and the decay test to determine the damping loss factors. Finally, in doing so good agreement between the measured and the estimated vibration velocity of the engine was achieved.

Hynna et al. (1995) [76] applied SEA to the machinery noise transmission in large ship structures. Hynaa et al determined the sound pressure level and the vibration velocity in the compartment spaces using analytical SEA. The sound pressure levels were calculated by using diffuse field approximation in octave bands.

5.2 Statistical Energy Analysis Background

Systems consisting of a number of components are most easily modeled using energy methods instead of deterministic approaches. For built-up systems, deterministic models will be large and computationally expensive. Furthermore, the response results from an ensemble of modes at high frequencies. Modes are closely spaced and results are typically averaged in one-third octave bands. In such cases, SEA will be preferred (Oldham and Hillarby (1991)[39]). SEA requires less detail about the model and

considers only resonant modes of the structure. SEA is generally more accurate when the modal density is high which normally occurs at high frequencies.

SEA predicts the acoustic behavior based on the energy flow in the system. The energy flow in the system is influenced by factors such as the coupling loss factor, damping loss factor and modal density. In order to improve the SEA predictions the aforementioned factors should be measured (Langley (1989)[30]; Lyon and DeJong, (1995)[29]).

SEA has been well documented by Fahy (1994)[32], Burroughs et al (1997)[28], Woodhouse (1981)[31], Langley (1989) [30], Lyon and DeJong (1995) [29], and Oldham and Hillarby (1991)[38, 39]. Fahy (1994) [32] reviewed the underlying assumptions of SEA. Burroughs et al. (1997)[28] illustrated SEA with two coupled oscillators and derived the SEA power balance equation. Burroughs et al. (1997) [28] also illustrated the difference between weak and strong coupling considering the damping and mass of the coupled oscillators.

SEA is a lumped parameter approach. By lumped parameter approach, it is assumed that the system has sufficient modal density to treat it in statistical sense. SEA assumes that the total energy in each subsystem, which is the sum of the energies of each mode in the subsystem, resides only in the resonant frequencies, and that those resonant frequencies are uniformly distributed over an analysis frequency band. The spatially and frequency averaged energy densities for subsystems are the degrees of freedom for an SEA model. Accordingly, SEA is computationally fast since the total number of degrees of freedom is much less than for a deterministic analyses even for large systems.

The chief assumptions of SEA are as follows (Lyon and DeJong (1995)[29]; Burroughs et al (1997)[28]).

- The power flow between two coupled subsystems is proportional to the difference between the modal energies of the subsystems.

- A power balance is maintained as the power transmitted to the subsystem is either dissipated by the subsystem itself due to damping or is transmitted to other subsystems through coupling.

- The input power spectrum is assumed to be broadband. Thus, there should be no strong pure tone in the input power spectra.

- Energy is dissipated from the subsystems through connections. Energy may not be created or added to the subsystem at junctions

- The damping loss factor remains constant irrespective of the modes in the subsystem and the frequency band.

- The modes within the subsystem interact to share an equipartition of energy and the modal responses are incoherent.

5.2.1 Statistical Energy Analysis of Two Coupled Subsystems

A two-subsystem system is shown in Figure 5.1. The energy dissipated from a subsystem is proportional to the energy in the system. Thus, the power dissipated from subsystem 1 ($\Pi_{1,\ diss}$) is

$$\Pi_{1,\ diss} = \omega E_1 \eta_1, \tag{5.1}$$

where ω is the angular frequency, E_1 is the energy in subsystem 1 due to the input power Π_1, and η_1 is the damping loss factor of subsystem 1. The net power flow (Π_{12}) between the two subsystems can be expressed as

$$\Pi_{12,} = \omega E_1 \eta_{12} - \omega E_2 \eta_{21} \tag{5.2}$$

where E_1 and E_2 are the energies in subsystems 1 and 2, respectively. η_{12} is the coupling loss factor between the two subsystems. The coupling loss factors from system 1 to 2 (η_{12}), and from 2 to 1 (η_{21}) can be related to each other by

$$\eta_{12} n_1 = \eta_{21} n_2 \tag{5.3}$$

where n_1 and n_2 are the modal densities in subsystems 1 and 2, respectively. Substituting Eqn. 5.3 into Eqn. 5.2, one obtains

$$\Pi_{12} = \omega \eta_{12} n_1 \left(\frac{E_1}{n_1} - \frac{E_2}{n_2} \right) \tag{5.4}$$

From Eqn. 5.4, it is evident that the power flows from the subsystem with higher modal energy to the subsystem with lower modal energy.

Using Eqns 5.1 and 5.2, a simple power balance equation for the two-subsystem case (Fig. 5.1) can be derived. The net power flow into a subsystem is equal to the power flow between the coupled subsystems and the power dissipated from the subsystem itself.

For subsystem 1 and 2,

$$\Pi_{net1} = \Pi_{diss1} + \Pi_{12} = \omega E_1 \eta_1 + \omega E_1 \eta_{12} - \omega E_2 \eta_{21} \tag{5.5}$$

and

$$\Pi_{net2} = \omega E_2 \eta_2 + \omega E_2 \eta_{21} - \omega E_1 \eta_{12} \tag{5.6}$$

The power input, coupling loss factor and the damping loss factors in Eqns. 5.5 and 5.6 can be determined experimentally. Once the loss factors and the input power are known, the energy flow in the subsystems can be determined by solving the two simultaneous equations with energies in the two subsystems as two unknowns. Once the energy in each subsystem is calculated the vibration velocity and the sound pressure level can be determined using the expressions

$$\left\langle v^2 \right\rangle = \frac{E_1}{M_1} \tag{5.7}$$

$$\left\langle p_1^{\,2} \right\rangle = \frac{E_1 \rho c^2}{V} \tag{5.8}$$

where v is the time and spatially averaged vibration velocity, p is the time and spatially averaged sound pressure level, ρ is the density of air, c is the speed of sound, M is the equivalent mass of the panel, and V is the total volume of the subsystem.

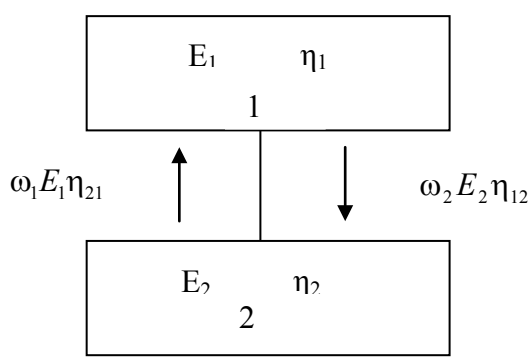

Figure 5.1 Two Subsystem SEA model

5.3 Application of Experimental SEA to an Air Handler to determine the Structure-Borne Noise

In this research work, the applicability of the experimental SEA in determining the structure-borne noise in HVAC plenums is studied. The air handler discussed in Chapter 4 is considered. Figure 5.2 shows the air handler of volume 0.72771 x 0.6095 x 0.6095 m^3. The air handler in the Figure 5.2 is a fairly complex structure assembled using panels made of galvanized steel. The panels are fastened to a well assembled framework which is also made of galvanized steel. Figure 5.3 shows how the panels are fastened and connected to each other by the frames. Two inch fiber is used to treat each panel of the air handler. The fiberglass is embedded into a perforated panel and is attached to each panel of the air handler.

The air handler is an excellent candidate for SEA because the thickness of the panels of the air handler is mm. Therefore the panels possess enough structural modes even at frequencies less than 100Hz. Hence, SEA was applied to the air handler from 100 Hz up, since most of the structure-borne noise problems are above 100 Hz.

Hence, the vibration velocity and the sound power radiated from the panels of the air handler are determined experimentally. The SEA parameters such as the damping and coupling loss factors were measured, and input into the SEA model of the air handler. Then, the measured vibration velocity and the sound power radiated from the panels of the air handler were compared to SEA prediction. The technique used to determine the loss factors experimentally is discussed extensively in Chapter 6.

Figure 5.2 Air handler used in this research work

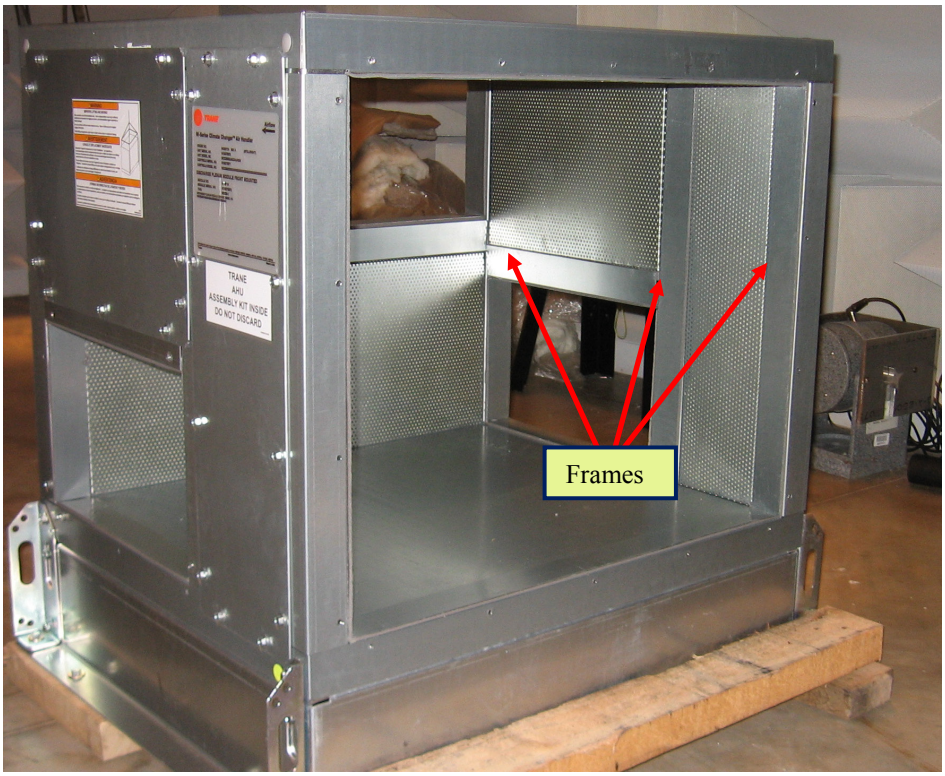

Figure 5.3 Panels of the air handler fastened to the frames

5.3.1 Procedure to determine the input power at the point of excitation

The SEA prediction is highly influenced by the input power that is used to excite the structure. The power input can either be measured experimentally or predicted using a numerical procedure by first determining the driving point impedance. In this research work, the input power is measured experimentally and averaged over one-third octave band. Figure 5.4 shows a pictorial representation of the power input measurement setup. For a structural excitation, the power input is expressed as

$$\Pi = \mathrm{Re}\left(FV^*\right) = F^2\,\mathrm{Re}\left[Y\right] \tag{5.9}$$

$$Y = \frac{A}{F} \tag{5.10}$$

where Π is the input power, F is the force at the point of excitation, V^* is the RMS amplitude of the vibration velocity of the structure, Y is the mobility and A is acceleration of the structure at the point of excitation

In order to measure the input power, a load cell and an accelerometer are used. Firstly, the transfer function between the acceleration and the force at the point of excitation i.e. the mobility is measured. The force is measured by the load cell and the acceleration is measured by the accelerometer. Then by substituting Eqn. 5.10 in Eqn. 5.9, the input power can be determined experimentally.

Additionally, as the loss factors are independent of the position of the excitation, it is important to normalize the power input by calculating the average power per unit force squared in order to avoid unequal forces affecting the measurement. Moreover, it is essential to maintain the phase relationship between the force transducer and the

accelerometer in order to avoid errors. The aforementioned problem can be overcome by using an impedance head where the force transducer and the accelerometers are phase calibrated. In this research work, a load cell and anaccelerometer are maintained was placed in close proximity to each other during the power input measurement.

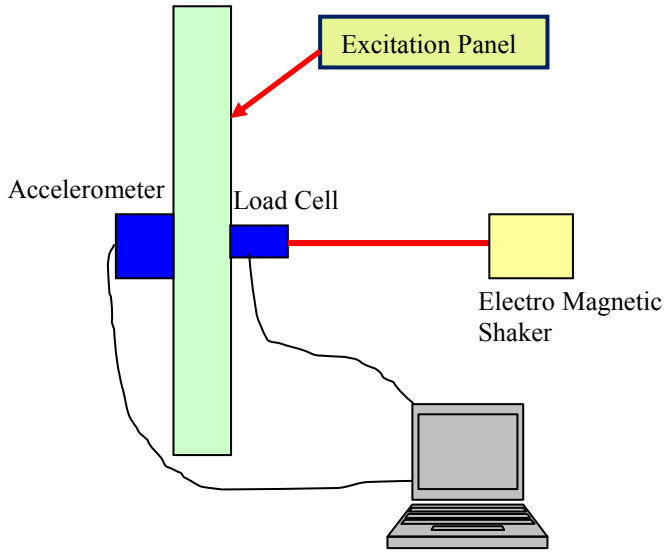

Figure 5.4 Power input measurement setup

5.3.2 Procedure to determine the Vibration Velocity and Sound Power

The vibration velocity of each panel of the air handler was measured using an accelerometer. An electromagnetic shaker was used to excite the panels of the air handler and the corresponding vibration velocity in each panel is measured. Additionally, the measured panel velocities are spatially averaged i.e. velocities are measured at 9 discrete points on each panel of the air handler and then averaged. The velocities are averaged over one-third octave bands. Figure 5.5 shows the experimental setup to determine the vibration velocity. The vibration velocity is expressed as

$$v = \frac{a}{\omega} \tag{5.11}$$

where v is the spatially averaged vibration velocity, a is the spatially averaged measured acceleration and ω is the angular frequency.

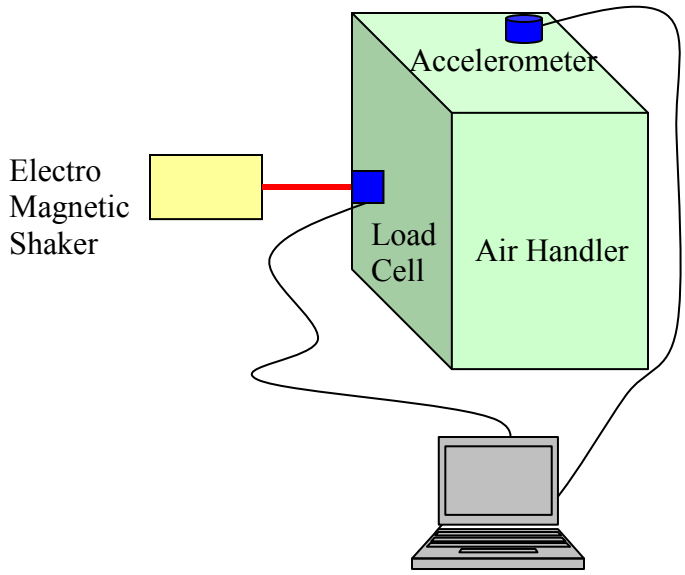

Figure 5.5 Setup to determine the vibration velocity

Similarly, the sound power radiated from each panel of the air handler was measured using a two-microphone sound intensity probe. The sound intensity measurement is made in accordance with ISO 9614-2[62]. Then, the sound power radiated from the panel due to the structural excitation is calculated from the measured sound intensity. The sound intensity and the sound power are expressed as

$$I = \frac{1}{2}\mathrm{Re}\left\langle \tilde{p}\tilde{u}_n^{\,*} \right\rangle \tag{5.12}$$

and

$$L_W = I * S \tag{5.13}$$

where I is the sound intensity, $\tilde{p}$ is the sound pressure, $\tilde{u}_n$ is the normal velocity, S is the surface area of the panel and L_W is the sound power radiated from the panel. The experimental setup to determine the sound intensity is shown in Figure 5.3.

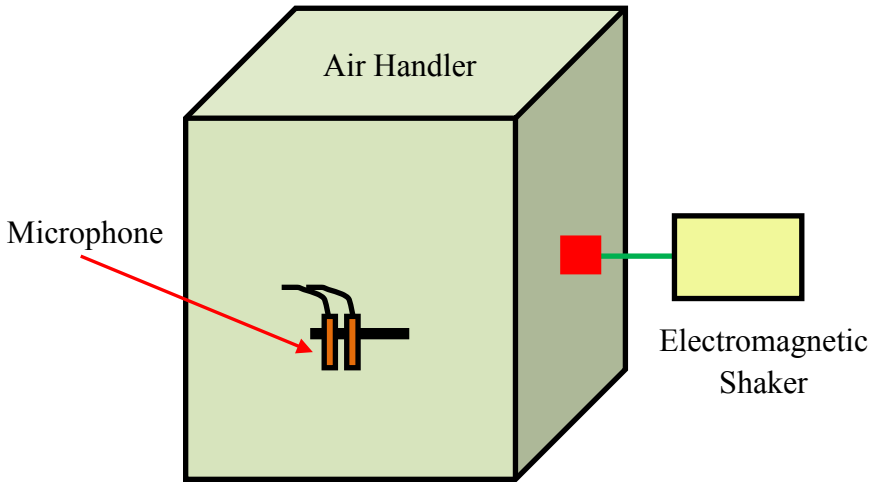

Figure 5.6 Sound power measurement setup

5.4 Validation Study

The validation study was performed to check the accuracy of experimental SEA in determining the structure-borne sound transmission in HVAC Plenums. The validation study compared the measured vibration velocity and the sound power radiated from the panels of an air handler (HVAC Plenum) with a SEA model. The air handler discussed in Section 5.3 is considered for the validation study.

The vibration velocity and the sound power radiated from the panels of the air handler was measured by exciting the air handler using an electromagnetic shaker. The measurement procedure is discussed in Section 5.3.2. Additionally the input power at the point of excitation is also measured based on the measurement procedure documented in section 5.3.1.

The SEA model of the air handler is created using VA-One(2010)[63] and is shown in Figure 5.7. Further the loss factors of the air handler were determined experimentally and input into the SEA model. The measured input power was used as the power source.

The validation study also considered the applicability of experimental SEA to determine the structure-borne noise for a HVAC plenum with multiple structural sources. Hence, for the validation study, two cases were considered

- Air handler with single structural source
- Air handler with two structural sources

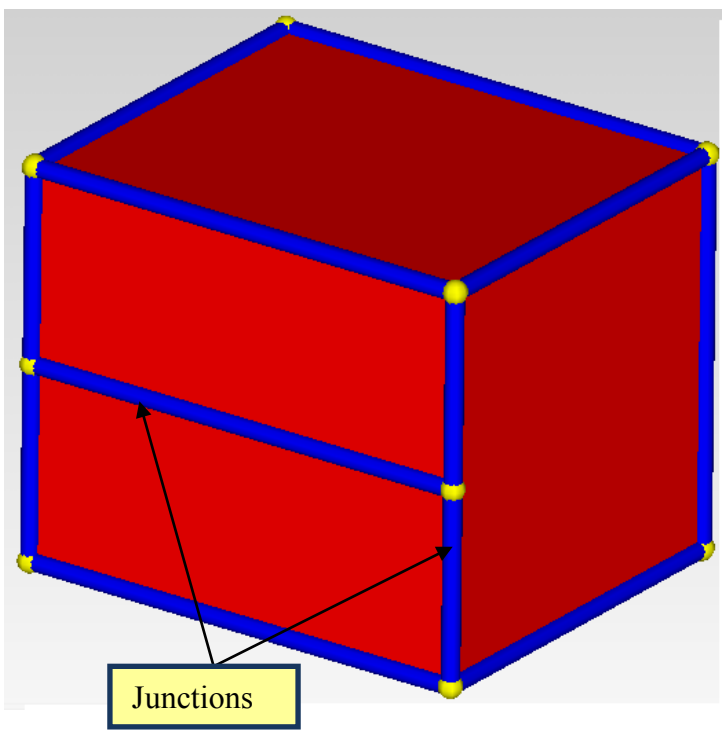

Figure 5.7 SEA model of the Air Handler.

5.4.1 Single Structural Source

The air handler is excited using an electromagnetic shaker which was used as the single structural source. The electromagnetic shaker excited the rear panel of the air handler as shown in Figure 5.8. As the shaker excites the air handler, the vibration velocity of the excitation (rear) panel and the opposite (front) panel were measured at 9 discrete points on the panel. Then the velocities were spatially averaged and in one-third octave bands. Additionally, the sound power radiating from the left side panel of the air handler was measured as the rear panel was excited.

The measured vibration velocity of the rear and the front panel and the sound radiation measured from the left side panel are compared to the SEA model in Figures 5.9 to 5.11 respectively. In Figures 5.9 to 5.11, experimental SEA refers to the SEA model of the air handler with the loss factors being measured. Measurement refers to the measured sound power and vibration velocity and software default refers to the SEA model that uses the default loss factors value specified in the software for the analysis. VA-One assumes 1% as the default damping loss factors for the plates. The software default case is chosen for comparison because engineers often use the default loss factors in commercial software if measured data is not available, in order to predict the structure-borne noise

The vibration velocity predicted using the experimental SEA agrees well with the measurement. Both the measurement and the experimental SEA predictions are averaged over the third octave band. However, the software default parameters do not provide good agreement with measurement and overestimate the measured vibration velocity (especially in Figure 5.10).

Figure 5.11 compares the radiated sound power from the left side panel. Experimental SEA agrees well with measurement above 300 Hz. In this case, low modal density in the panel below 300 Hz might influence the sound power radiated

Additionally, it is noted from figure 5.11 that using the software default parameters will lead to erroneous prediction for the entire frequency range. Thus, it can be concluded that SEA prediction will be more accurate, if loss factors are measured

.

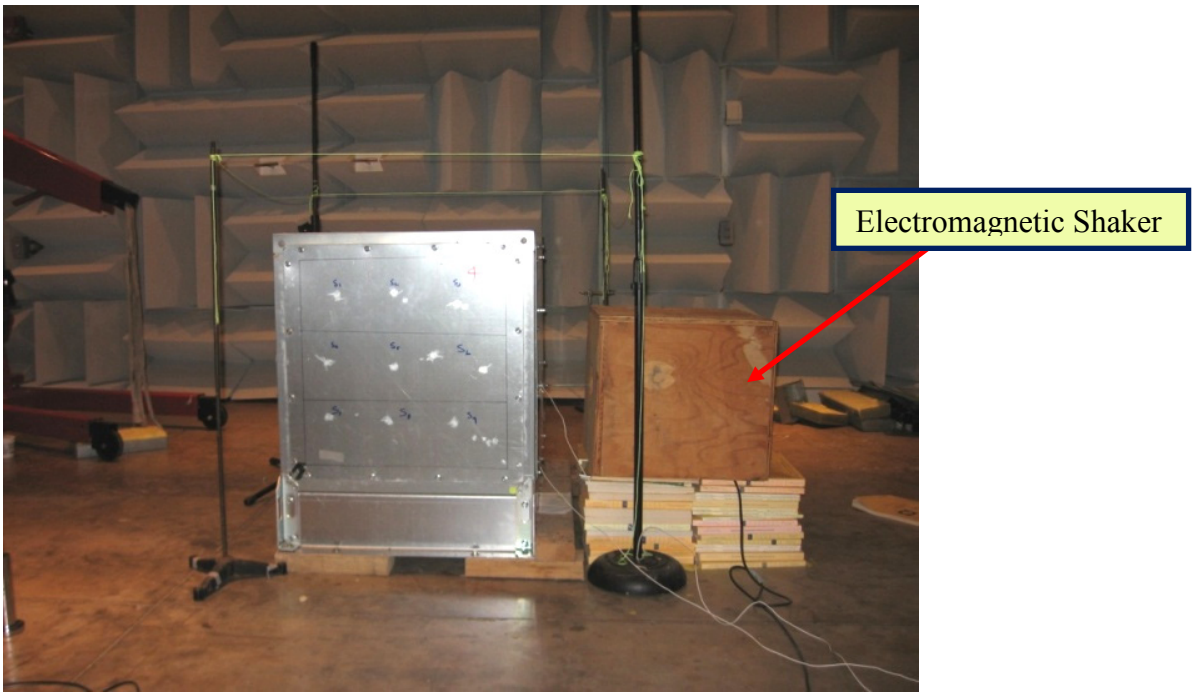

Figure 5.8 Air handler excited by single source (electromagnetic shaker)

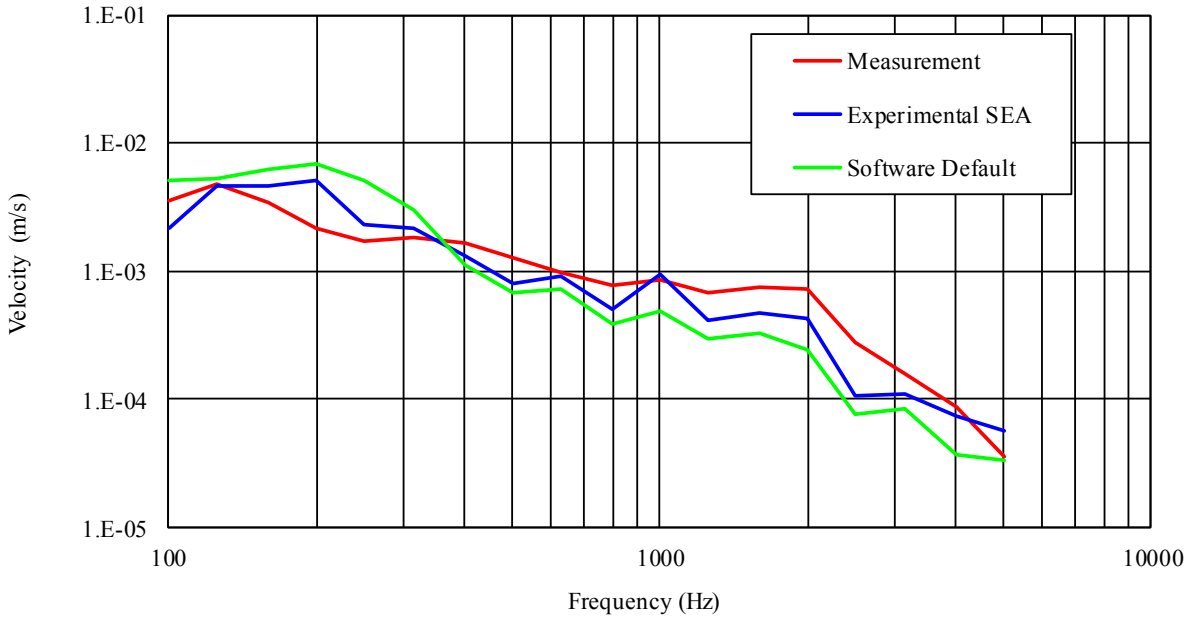

Figure 5.9 Excitation (rear) panel velocity

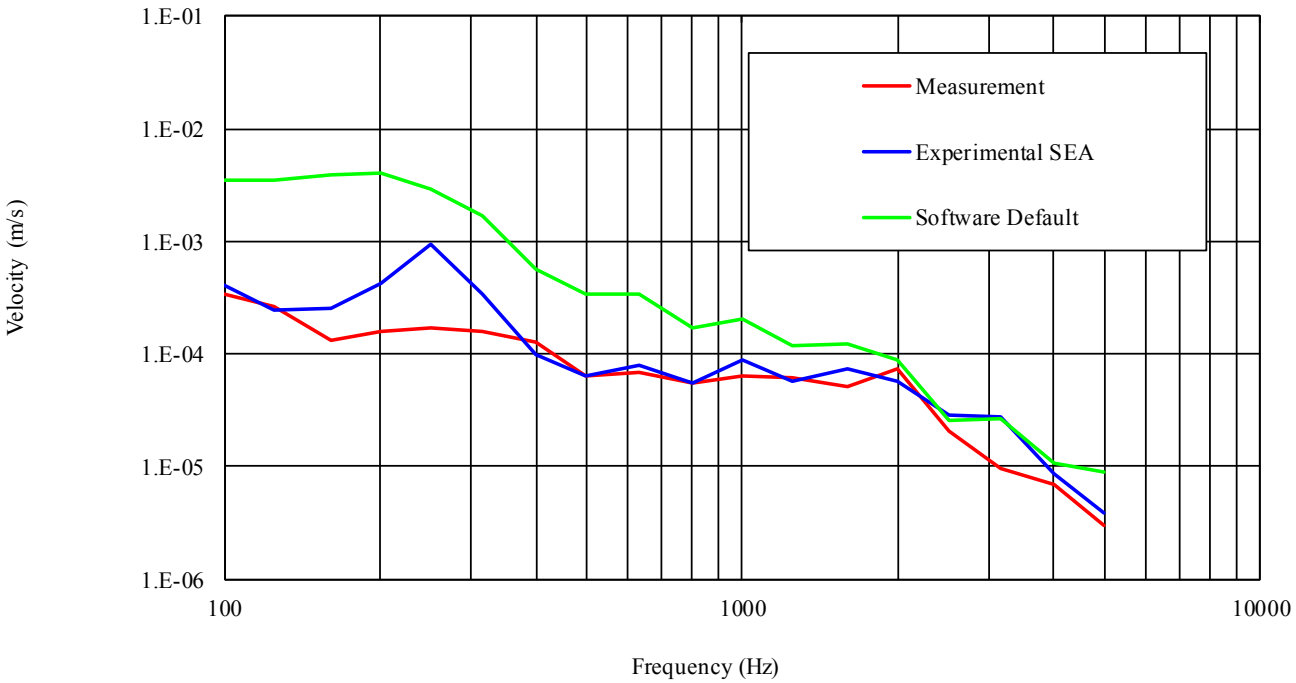

Figure 5.10 Opposite (front) panel velocity

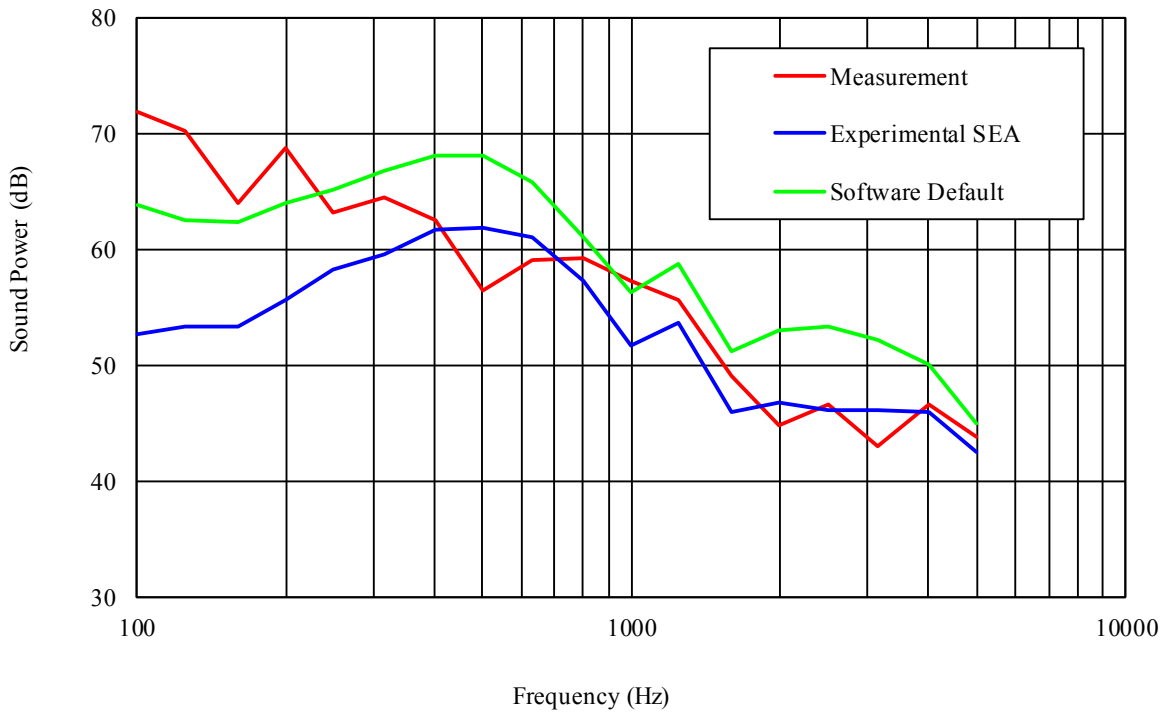

Figure 5.11 Sound power radiated from the adjacent (left side) panel

5.4.2 Multiple Structural Sources

Another case was considered in which the air handler was excited using two electromagnetic shakers as shown in Figure 5.12. From the figure, it can be noted that the rear and the right side panels of the air handler were excited using the electromagnetic shakers. The spatially averaged vibration velocity and the sound power radiated from the front and the top panels of the air handler were measured and compared with the SEA model. Again, all the comparisons are made in third-octave bands. Figure 5.13 compares the input power from the two electromagnetic shakers that are used to excite the air handler. It can be seen that the input power from the two electromagnetic shakers was similar over the entire frequency range.

Figures 5.14 and 5.15 compare measured and SEA predicted front panel and top panel vibration velocities, respectively. Again, the velocities were measured at 9 discrete points on the front and top panels and were spatially averaged. Figures 5.16 and 5.17 show the sound power radiated from the front and the top panels of the air handler. In the graphs, the experimental SEA refers to the SEA model of the air handler, which used measured damping and coupling loss factors. Additionally, measurement refers to the measured vibration velocities and radiated sound power.

From the Figures 5.14 to 5.17, it can be noted that, experimental SEA agrees well with measured vibration velocity as well as the sound power radiated from the panels except at very low frequencies. It is evident that experimental SEA can be used to accurately predict the structure borne noise for HVAC plenums (air handler), even if multiple sound sources excite the plenum.

Figure 5.12 Air handler excited by two shakers

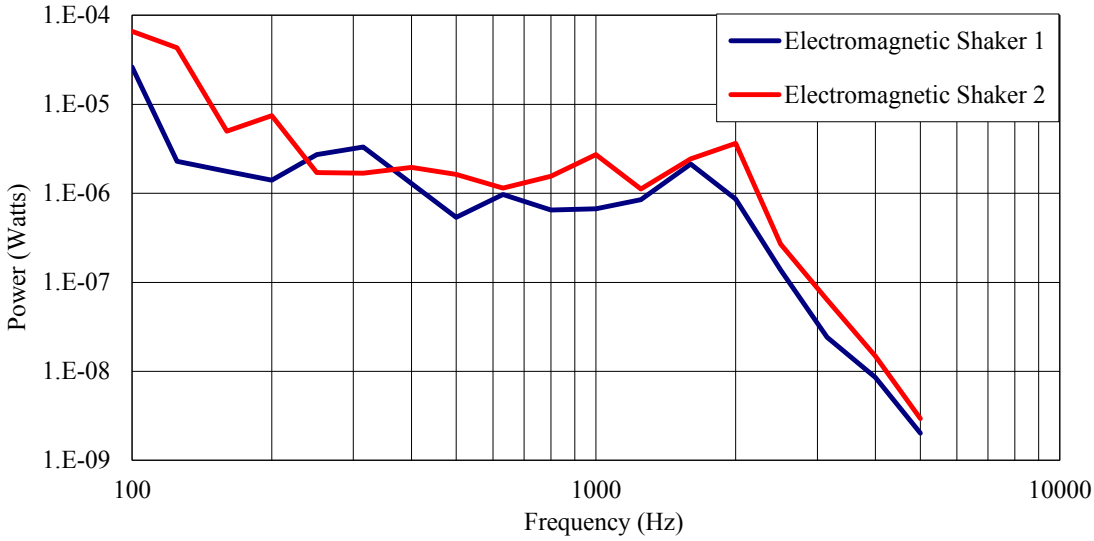

Figure 5.13 Power input from the two electromagnetic shakers shown in figure 5.9

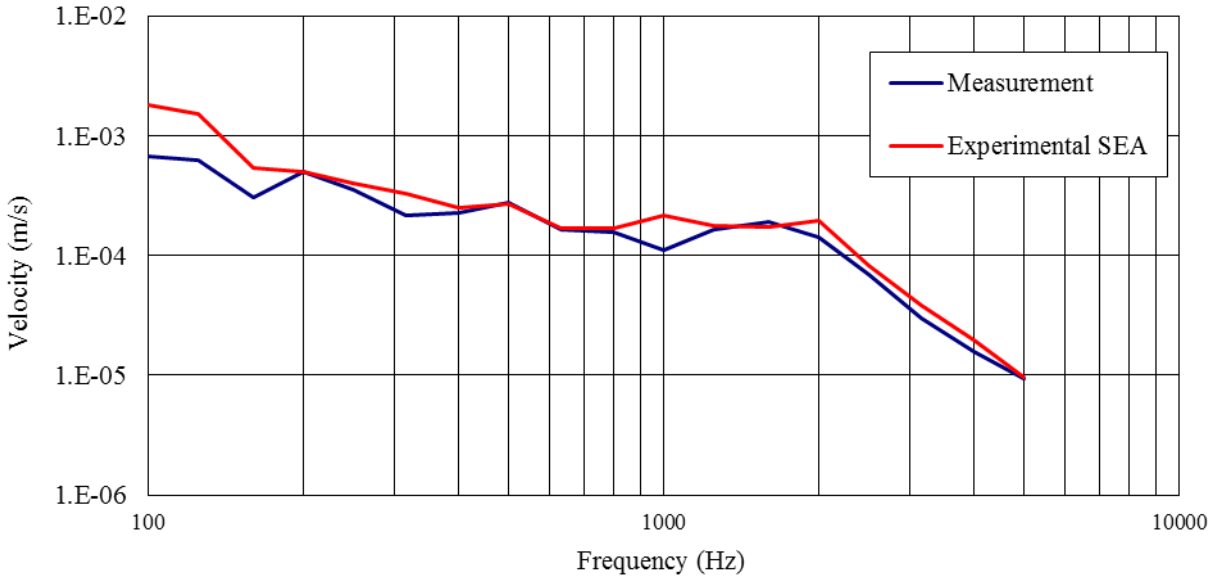

Figure 5.14 Comparison of measured and predicted front panel velocity

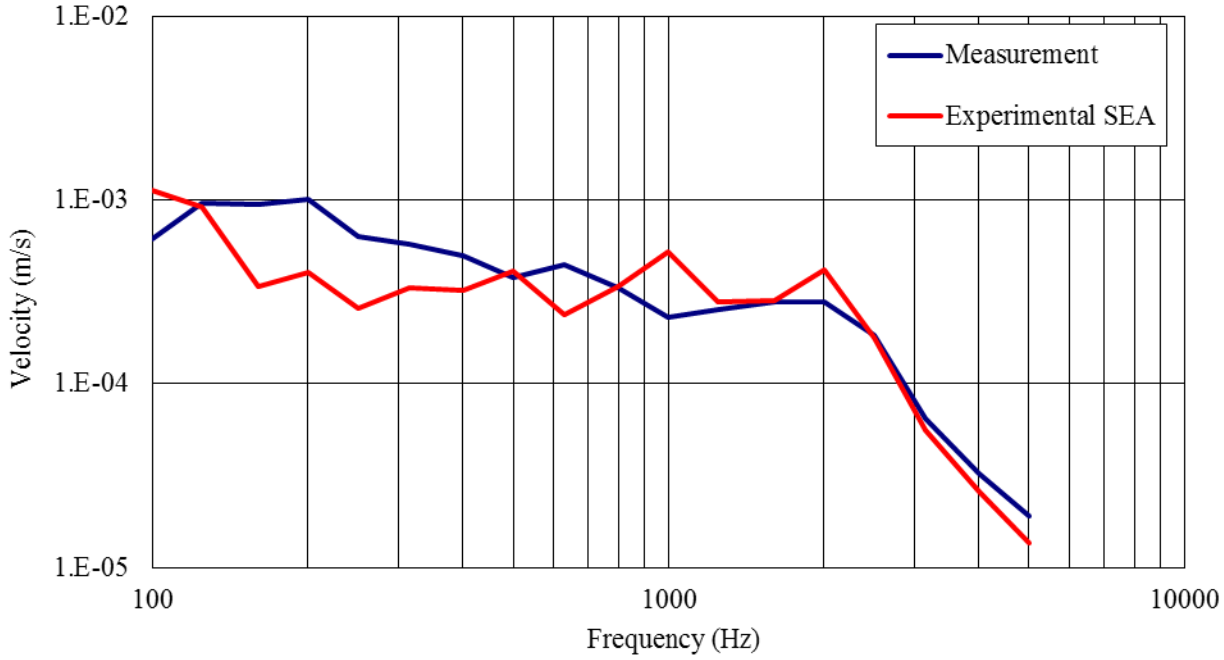

Figure 5.15 Comparison of measured and predicted top panel velocity

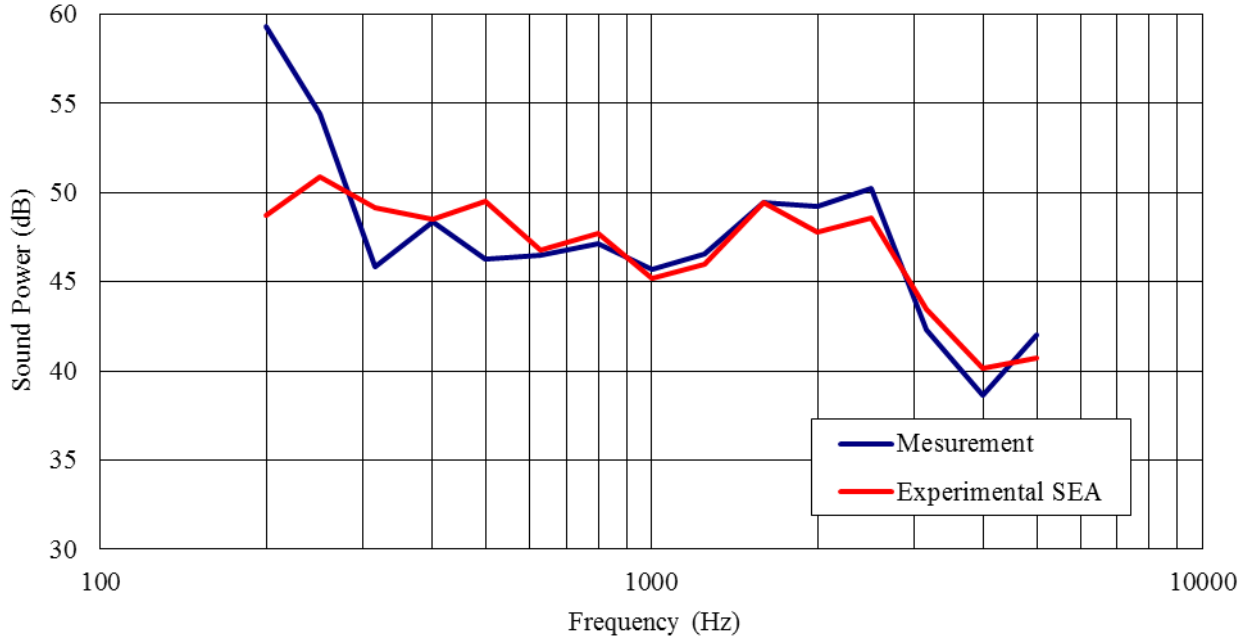

Figure 5.16 Comparison of measured and predicted sound power radiated from the front panel

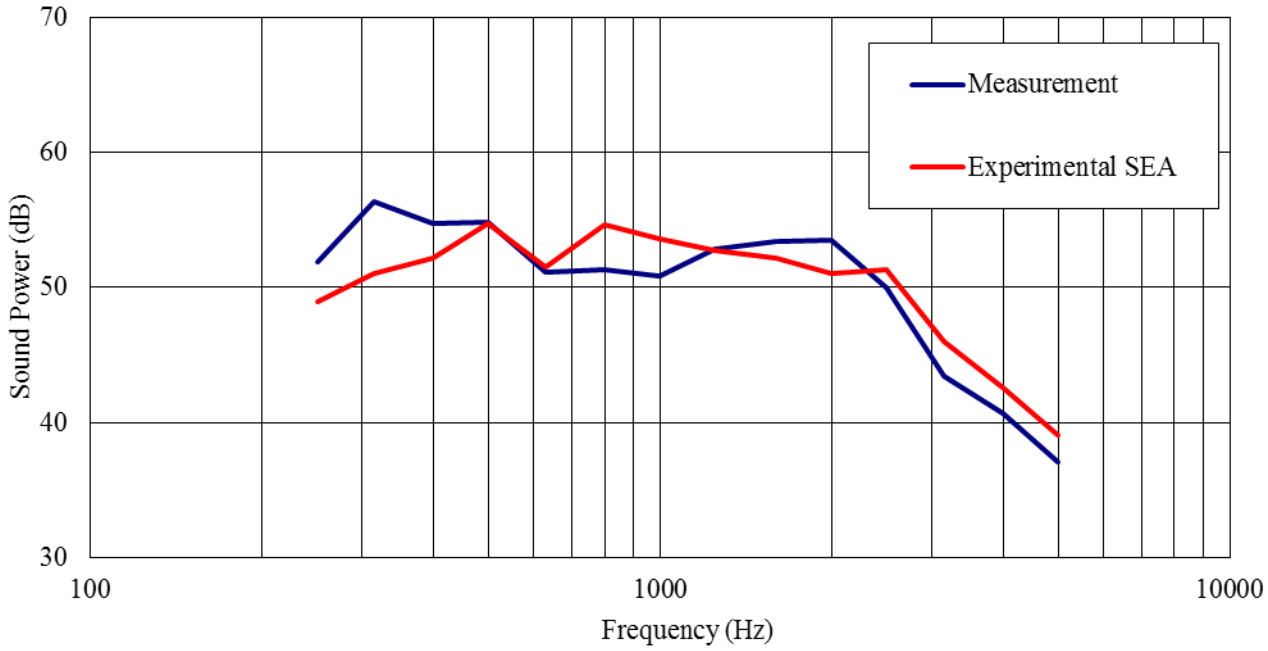

Figure 5.17 Comparison of measured and predicted sound power radiated from the top panel

5.5 Summary

The theoretical background on machinery noise and the statistical energy analysis (SEA) was documented. The power balance equation for a two subsystem system is derived based on modal densities, loss factors and input power. Loss factors were determined experimentally to determine the structure-borne noise transmission for an air handler. The vibration velocity and the sound power radiated from the panels were measured and validated analytically using SEA.

The experimental SEA predictions agree very well with the measurement above 250 Hz. It is observed that the SEA agreed well with measurement irrespective of the number of sound sources that excited the air handler. Moreover, experimental SEA proved to be significantly more accurate than a similar SEA model which utilized the default loss factors from the commercial software. It can be concluded that the coupling loss factors and damping loss factors used in the SEA model should be determined experimentally. The detailed discussion on the determination of the loss factors experimentally is documented in Chapter 6.

CHAPTER 6

NOTES ON EXPERIMENTAL SEA

6.1 Experimental SEA Background

The techniques to determine important SEA parameters experimentally are discussed in this chapter. Specifically, approaches for determining coupling and damping loss factors are examined. The determination of the SEA parameters will significantly influence the accuracy of the structural energy prediction, which will correspondingly improve predictions for the sound radiated from structures. It was demonstrated in Section 5.4.1 that determining the SEA coupling loss factors experimentally improved the results.

The coupling loss factor accounts for the energy flow between the two connected subsystems. On the other hand, the damping loss factor is the rate of energy flowing out of the subsystem through a dissipation mechanism (Lyon and Dejong (1995))[29]. It is well known that dissipation mechanisms are difficult to model. Accordingly, these loss factors are best determined experimentally

Prior to determining the loss factors, parameters such as the modal energy and the input power are determined, as the loss factor calculation includes all the aforementioned parameters. Measurement of input power is discussed in Section 5.3.1 and the details about the modal energy measurement are reviewed in the next section.

6.2 Modal Energy

The acoustic response of each subsystem can be obtained from measuring the spatially averaged energy level .The spatially averaged energy level of a structural subsystem depends on the equivalent mass of the subsystem and the spatially averaged

velocity. The methodology to determine the equivalent mass of a subsystem is discussed in Section 6.3. The spatially averaged energy level of an acoustic subsystem depends on the sound pressure level of the subsystem at the near field and the volume of the acoustic cavity. The spatially averaged energy level (E) of a structural subsystem can be expressed as

$$E = m\left\langle v^2 \right\rangle \tag{6.1}$$

where m is the equivalent mass of the subsystem and v is the spatially averaged vibration velocity of the subsystem. The spatially averaged vibration can be estimated experimentally by measuring acceleration at a number of points and averaging. For the investigation detailed here, 9 points were averaged on each panel.

Likewise, the spatially averaged energy level for an acoustic subsystem can be expressed as

$$E = \frac{V}{\rho c^2}\left\langle p^2 \right\rangle \tag{6.2}$$

where V is the volume of the airspace, c and ρ are the respective speed of sound and air density, and p is the spatially averaged sound pressure level. The spatially averaged sound pressure level can be estimated experimentally by averaging at a number of points or by roving a microphone. For this investigation, sound pressure results were averaged at 9 points.

6.3 Equivalent Mass

The concept of equivalent mass was developed by Lalor (1989)[33]. Similarly Wu et al. (1996)[77] and Gelat and Lalor (2001)[78] suggested that the estimation of the equivalent mass of a subsystem depends on the complexity of the structure, structural modes, and the homogeneity of the structure. In addition, the spatial sampling of the velocity will also affect the prediction of the mass of the subsystem, which can be explained from the Eqn.6.1.

At first glance, Eqn. 6.1 appears to offer a straightforward relationship between the energy and the velocity. In practice, deriving the subsystem energy from the measurement of a set of velocities presents some difficulties because the spatial sampling of the velocity is made at discrete locations that may not yield an accurate representation of the subsystem space averaged velocity. Moreover, only the normal velocity is measured. Thus, the energy stored by longitudinal and in-plane waves is overlooked.

Secondly, it is evident from Eqn. 6.1 that the total energy in the subsystem is equal to twice the kinetic energy. This implies that the energy is stored in resonant modes since the kinetic and potential energy are equal to each other at a mode. However this SEA assumption is not always validated during measurement.

Wu et al. (1996)[77] concluded that, at low frequencies, the equivalent mass of a subsystem would be greater than the actual mass. As frequency increases, the agreement between the actual mass and equivalent mass of the subsystem should improve and will be similar.

In this study, the equivalent mass of the subsystem was determined experimentally. The equivalent mass is determined using the decay rate method. The

decay rate method depends on the transient response of a resonant mode with linear damping (Lyon and DeJong, 1995[29]). In order to determine the transient response, the modes in the subsystem are initially excited and then the excitation is stopped. After terminating the excitations of the modes, the energy of the mode E at its resonant frequency f will decay in time at a rate proportional to

$$E \propto e^{-2\pi f \eta t} \tag{6.3}$$

where η is the damping in the subsystem, t is the decay time.

Moreover, the energy of the mode E is proportional to the square of the peak response amplitude C. The peak response amplitude refers to the amplitude of the displacements, pressure, etc. Hence,

$$E \propto C \tag{6.4}$$

Since the energy in the mode is proportional to the square of the peak response amplitude, the peak response amplitude will decay at the rate of $e^{-\pi f \eta t}$ .Therefore from Eqn. 6.4,

$$C \approx e^{-\pi f \eta t} \tag{6.5}$$

Hence, at two successive times t_1 and t_2, the amplitude decays and can be expressed as

$$20\log_{10}\left(\frac{C_1}{C_2}\right) = 20\log_{10}\left(\frac{e^{-\pi f \eta t_1}}{e^{-\pi f \eta t_2}}\right) \tag{6.6}$$

where $C_1$and C_2 are the response peak amplitudes at time t_1 and t_2 respectively.

Eqn.6.6 can be written as

$$20\log_{10}\left(\frac{C_1}{C_2}\right) = 20\log_{10}\left(e^{\pi f \eta (t_2 - t_1)}\right) = 20\pi f \eta (t_2 - t_1)\log_{10}(e) \tag{6.7}$$

Further simplifying Eqn.6.7, one obtains

$$20\log_{10}\left(\frac{C_1}{C_2}\right) = 20\pi f\eta(t_2 - t_1)(0.4313) = 27.3 f\eta(t_2 - t_1) \tag{6.8}$$

Finally, the decay rate is defined as the slope of the decay in dB/sec. From Eqn.6.8,

$$\gamma = \frac{20\log_{10}\left(\frac{C_1}{C_2}\right)}{(t_2 - t_1)} = 27.3 f\eta \tag{6.9}$$

and therefore

$$\eta = \frac{\gamma}{27.3 f} \tag{6.10}$$

where η is the damping loss factor of the subsystem, γ is decay rate in dB/sec and f is the center frequency.

For an isolated subsystem, the input power to the subsystem is defined as the power absorbed by the subsystem (Gelat and Lalor, 2002 [78]). The input power to the isolated subsystem is expressed as

$$\Pi_i = \omega E_i \eta_i \tag{6.11}$$

where Π_i is the input power, ω is the angular frequency, E_i is the total energy, and η_i is the damping loss factor for the subsystem *i*.

From the Eqn.6.1, the total energy in the subsystem can be expressed as

$$E_i = M_i^{eq} \langle V_{ii} \rangle^2 \tag{6.12}$$

Substituting Eqn.6.12 into Eqn. 6.11,

$$\Pi_i = \omega M_i^{eq} \langle V_{ii} \rangle^2 \eta_i \tag{6.13}$$

Eqn.6.13 can be expressed in terms of M_i^{eq} as

$$M_i^{eq} = \frac{\Pi_i}{\omega \langle V_{ii} \rangle^2 \eta_i} \tag{6.14}$$

Substituting Eqn.6.10 into Eqn.6.14 one obtains

$$M_i^{eq} = \frac{\Pi_i}{2\pi f \langle V_{ii} \rangle^2 \frac{\gamma}{27.3 f}} \tag{6.15}$$

which can be simplified as

$$M_i^{eq} = \frac{\Pi_i}{0.23 \gamma_i \langle V_{ii}^2 \rangle} \tag{6.16}$$

where M_i^{eq} is the equivalent mass , Π_i is the input power, V_{ii} is the spactially averaged velocity, and γ_i is the initial decay rate coefficient for the subsystem *i*.

It is evident from Eqn. 6.16 that the initial decay rate coefficient is required to determine the equivalent mass. The initial decay rate coefficient can be obtained from a decay test. The initial slope of the transient response of the subsystem for an impulse excitation is obtained by impacting the subsystem using an impact hammer. Figure 6.1 shows the top panel of the air handler being tapped using an impact hammer and the corresponding transient response is measured using an accelerometer. Figure 6.2 represents the transient response of the top panel of the air handler, from which the slope of the initial decay is determined. A filter, which is an inbuilt module in the LabVIEW based data acquisition system, is used to filter the transient response of the panel in one third octave bands.

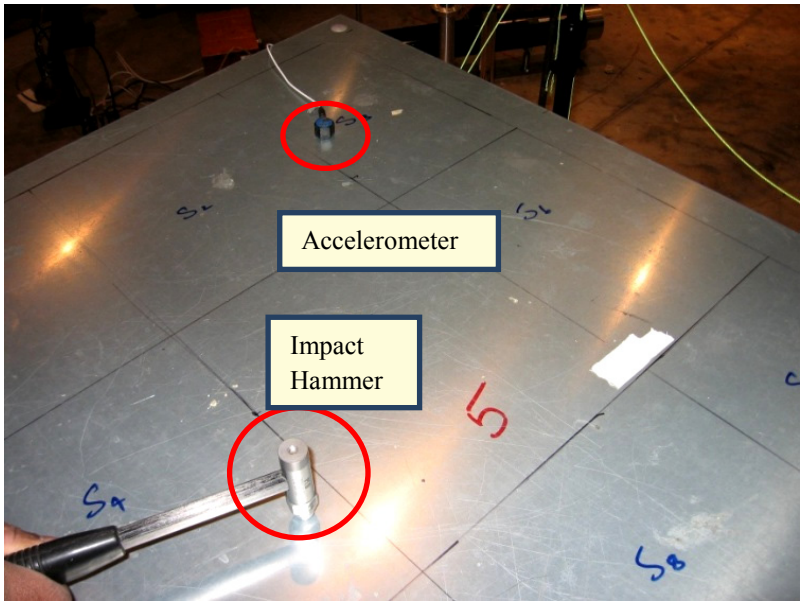

Figure 6.1 Decay Test conducted on the top panel of the air handler

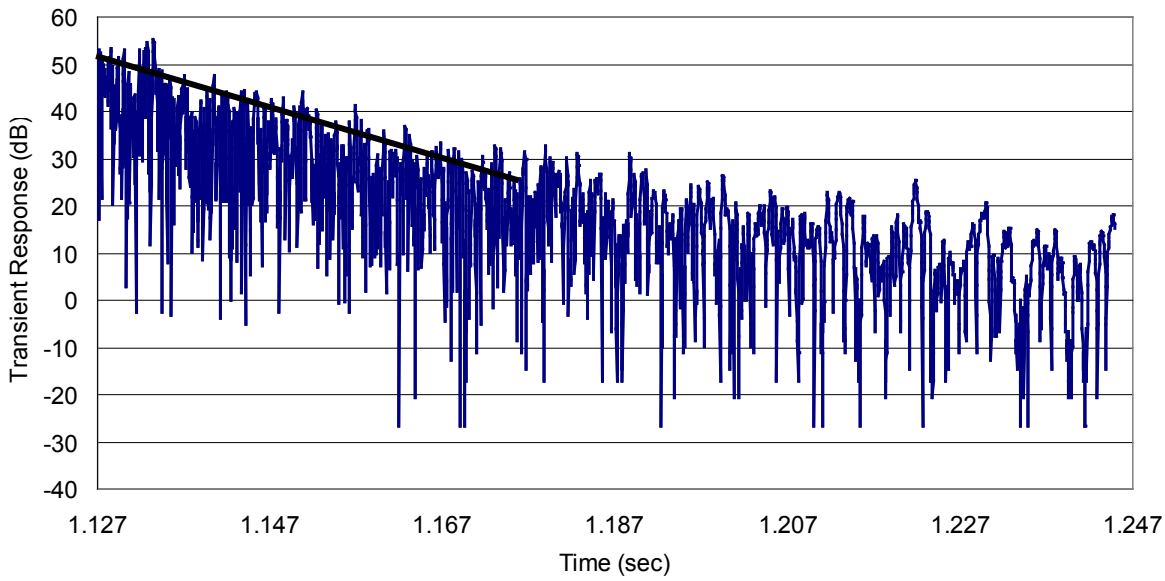

Figure 6.2 Transient response of the top panel

6.4 Coupling Loss Factor

The coupling loss factor is the rate of energy flow out of a subsystem through coupling to another subsystem. In other words, the coupling loss factor between two subsystems is defined as the ratio of the average power flow between the coupled mode groups (subsystems) to the difference between the dynamic modal energies of the coupled mode groups. (Lyon and DeJong, 1995[29]) Thus the net power between the systems can be expressed as

$$\Pi_{net} = \omega \eta_{ij} n_i \left(\frac{E_i}{n_i} - \frac{E_j}{n_j} \right) \tag{6.17}$$

where η_{ij} is the coupling loss factors and ω is the angular frequency, E_i and E_j are the energy, and n_i and n_j are the modal densities of subsystems *i* and *j* respectively.

The results in Sections 5.4.1 and 5.4.2 demonstrated, that SEA predictions are more accurate if the coupling loss factors are measured since it is very hard to model dissipation mechanisms and connections between subsystems in a complex structure.

The coupling loss factors in a mechanical structure can be measured by using:

- The Inverse Matrix Method
- The Two Subsystem Method

Both approaches will be discussed in the sections that follow.

6.4.1 Inverse Matrix Method

The inverse matrix method was directly derived from the SEA power balance equation and was developed by Lalor (1989)[33]. He proposed that, for a system with N subsystems, *N* matrix equations of order (*N*-1) x (*N*-1) can be formulated, from which the coupling loss factors of the subsystems may be calculated. For example, the air handler

that is presented in Chapter 5 consists of 6 subsystems. By using Lalor's approach, 6 sets of energy matrices of order 5 x 5 are formulated which can be used to determine the coupling loss factors. The matrix equation of order (N-1) x (N-1) can be expressed as

$$\begin{bmatrix} \eta_{1i} \\ \cdots\cdots \\ \cdots\cdots \\ \eta_{Ni} \end{bmatrix}_{j \neq i} = \frac{\Pi_i}{\omega E_{ii}} \begin{bmatrix} \left(\frac{E_{11}}{E_{i1}}\right) - \left(\frac{E_{1i}}{E_{ii}}\right) & \cdots\cdots & \left(\frac{E_{N1}}{E_{i1}}\right) - \left(\frac{E_{Ni}}{E_{ii}}\right) \\ \cdots\cdots & \cdots\cdots & \cdots\cdots \\ \left(\frac{E_{1N}}{E_{iN}}\right) - \left(\frac{E_{1i}}{E_{ii}}\right). & \cdots\cdots & \left(\frac{E_{NN}}{E_{iN}}\right) - \left(\frac{E_{Ni}}{E_{ii}}\right) \end{bmatrix}^{-1} \begin{Bmatrix} 1 \\ \cdots\cdots \\ 1 \end{Bmatrix} \tag{6.18}$$

where E_{ji} is the energy of response panel j with respect to the excitation panel i, Π_i is the input power to the excitation panel i, ω is the angular frequency and η_{ij} is the coupling loss factor between the subsystems i and j.

The coupling loss factors of the air handler shown in Figure 6.3 are determined experimentally using Eqn. 6.18. According to Lalor (1989)[33], the coupling loss factors of the air handler are measured by exciting each panel separately. For each panel excitation, the corresponding energy level in each of the six panels is measured. Therefore, an energy matrix of order 5 x 5 can be formed for each input power location. Hence, six energy matrices of order 5 x 5 can be wrote for the air handler.

Figure 6.3 Air handler used for coupling loss factors measurement

Additionally, the inverse matrix expressed in Eqn. 6.18 is a well-conditioned matrix since the diagonal terms in the matrix are much larger than the off-diagonal terms. This can be verified by calculating the condition number of the inverse matrix. Figure 6.4 compares the condition numbers of the inverse matrix formed from the front, top and rear panel excitation of the air handler.

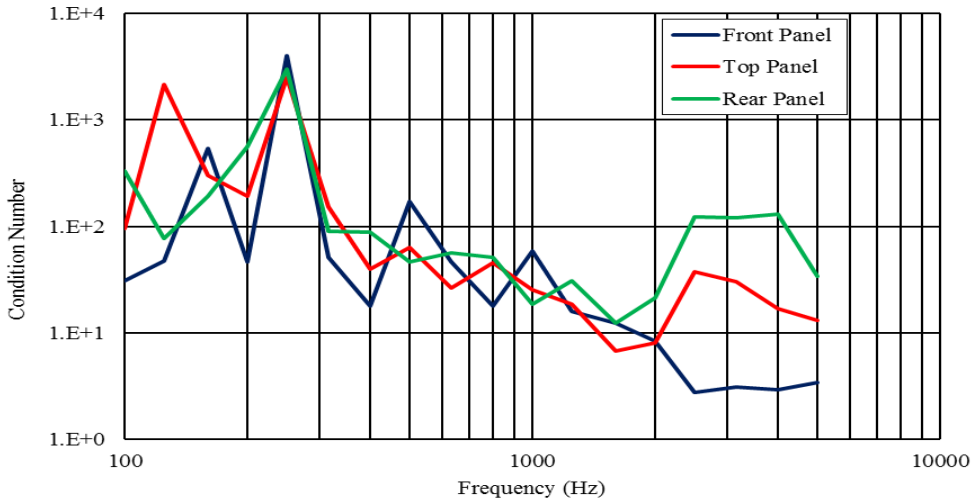

Figure 6.4 Condition number of the inverse matrix.

Golub and Van Loan (1996)[79] commented that a matrix of order 5x5 will be well conditioned provided that the condition number doesn't exceed 10^5. Accordingly, it is apparent that, for the inverse energy matrix of order 5 x 5, the condition number will not exceed 10^4 over the entire frequency band. It can be concluded that the matrices which are inverted should be well conditioned. Therefore, once the energy matrix is formed, the coupling loss factor between the subsystems is calculated. Figure 6.5 shows the coupling loss factors of the rear and the top panel as the front panel of the air handler is excited. Note that the coupling loss factors will be much higher for connected panels. Figure 6.6 shows the setup for the measurement.

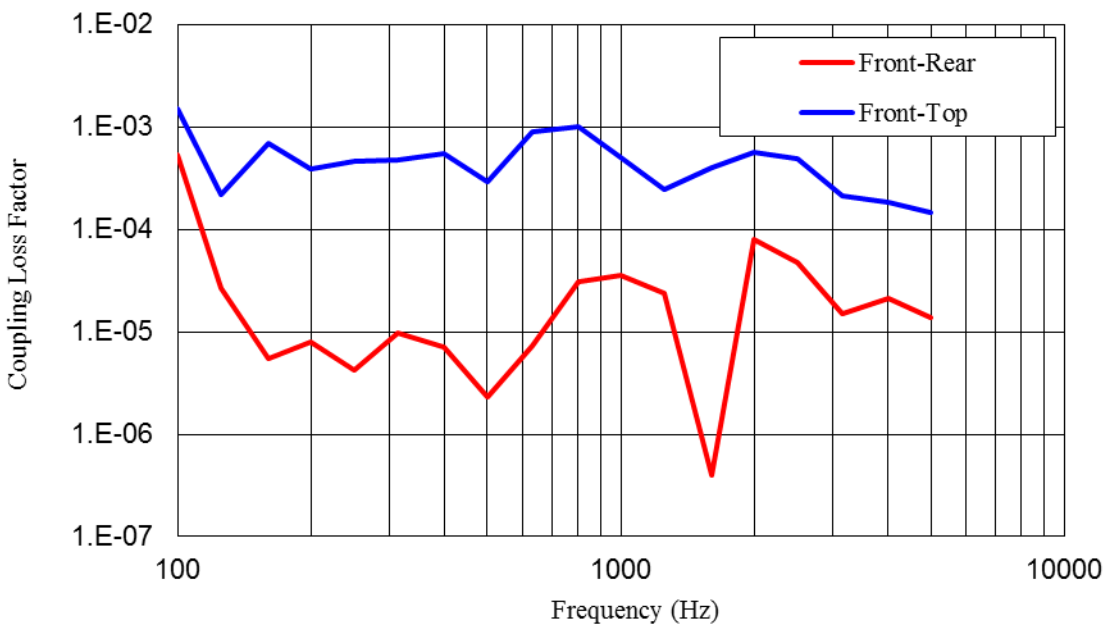

Figure 6.5 Comparison of the coupling loss factors

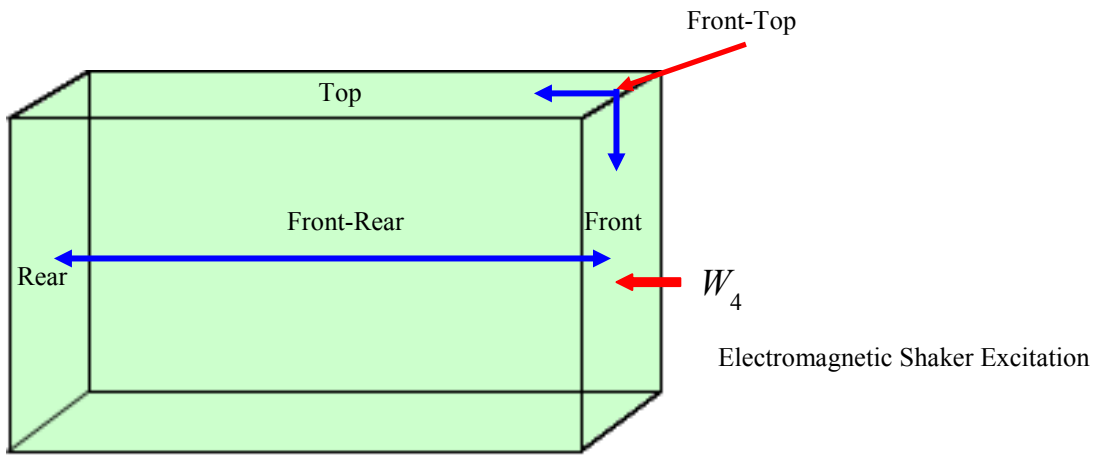

Figure 6.6 Representation of the coupling loss factors between the panels

It is evident from Figure 6.5 that the coupling loss factor between the front and top panel is much higher than the coupling loss factor between the front and the rear panel. This is because the front and the top panel are directly connected to each other as indicated in Figure 6.6. On the other hand, the front and the rear panel are opposite to each other and there is no direct coupling between the two panels. Thus, the energy transfer from the front to the rear panel is mainly through the frames, which are used to fasten the panels.

Furthermore, Figures 6.7-6.9 show the coupling loss factors between all the panels of the air handler as the top panel, left side panel and the front panel are excited respectively. Notice that the panels that are directly connected to the excitation panel have high coupling loss factors when compared to the panels that are not directly connected. In other words, the coupling loss factors are high for subsystems (panels) with direct coupling when compared to the subsystems with indirect coupling. This implies that more energy should go through the connections.Moreover, the coupling loss factors are sometimes negative at low frequencies for subsystems that are not directly connected.

This is likely a result of measurement error since the energy transmitted to the indirectly connected panel is so low.

Notice that the inverse matrix method requires measurement for each subsystem in order to determine the loss factors irrespective of the coupling between the subsystems. Accordingly, the inverse matrix method will only be feasible for systems having a reasonable number of subsystems. If the system is complex with more subsystems, then the resulting order of the inverse matrix will be higher and the level of effort for the measurement will be too high. These limitations can be overcome by utilizing the two-subsystem method to determine the coupling loss factors.

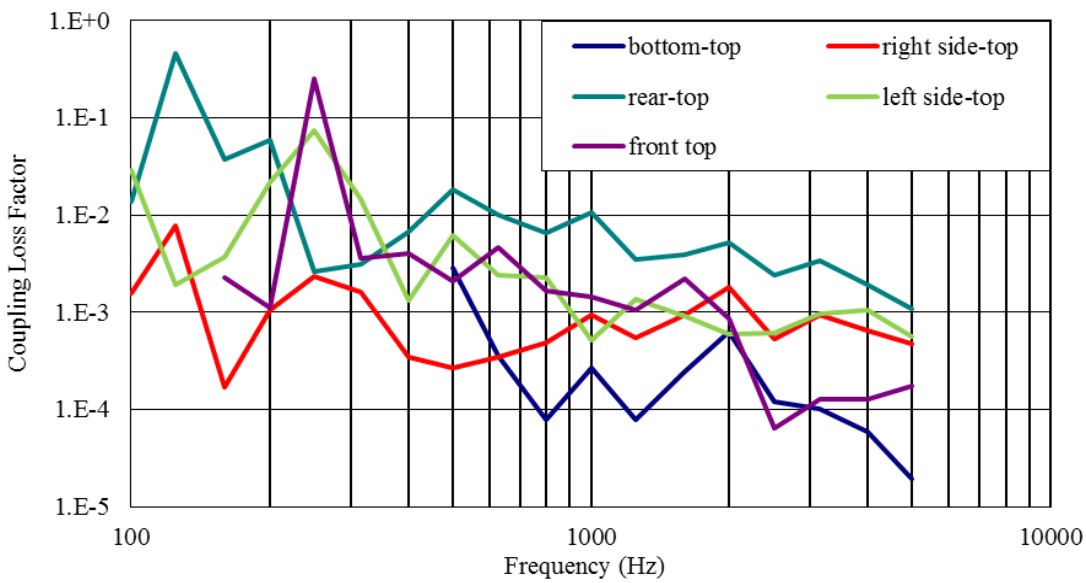

Figure 6.7 Comparison between the coupling loss factors between all the panels of the air handler as the top panel is excited.

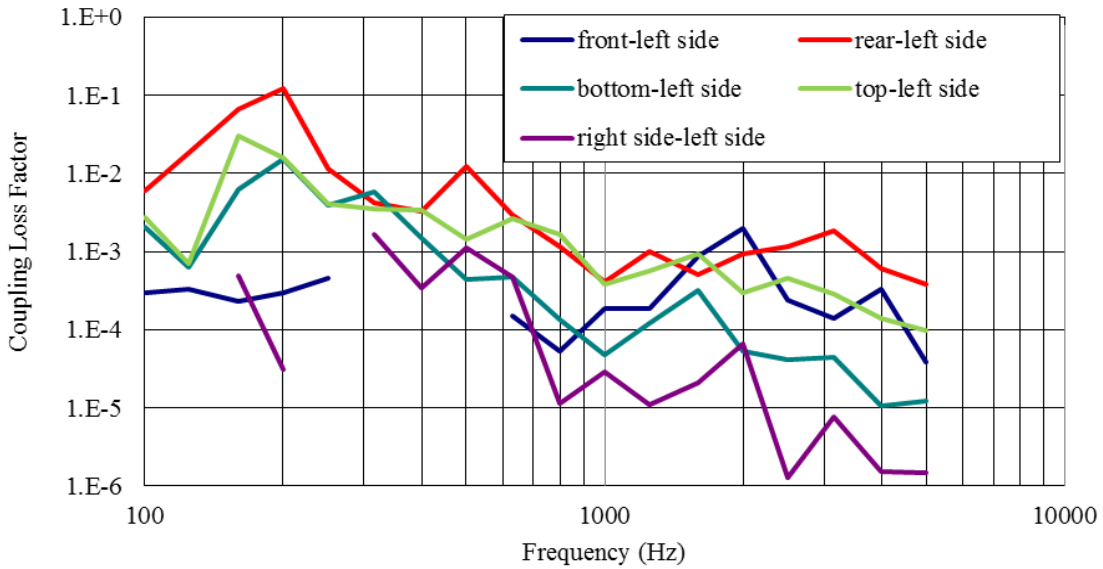

Figure 6.8 Comparison between the coupling loss factors between all the panels of the air handler as the left side panel is excited.

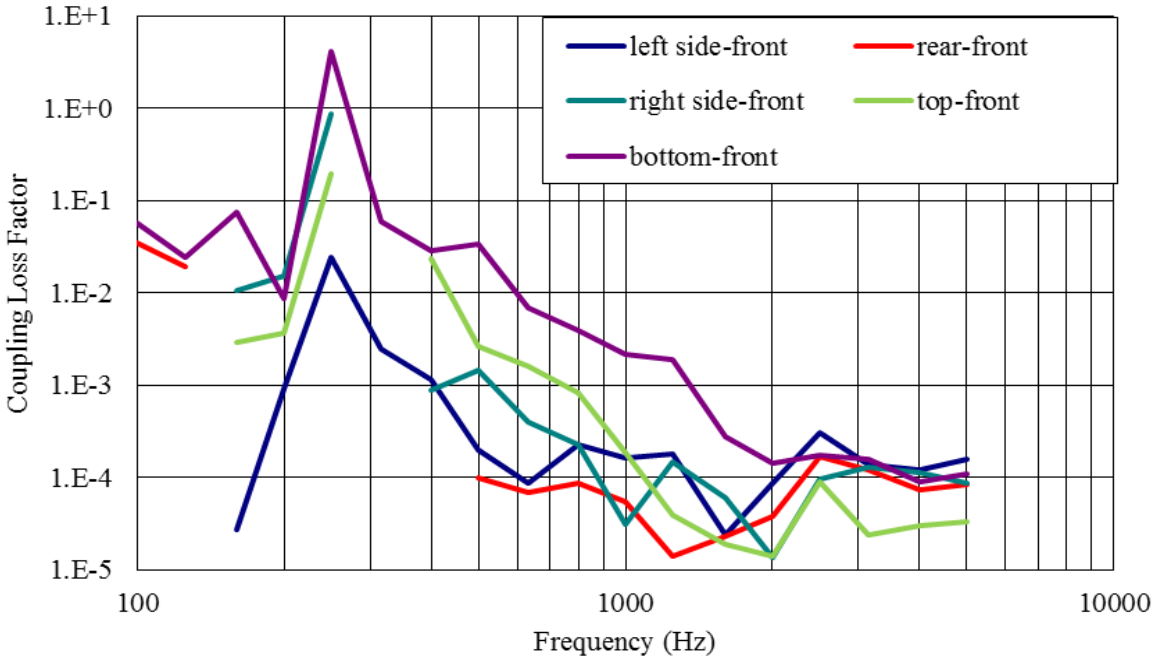

Figure 6.9 Comparison between the coupling loss factors between all the panels of the air handler as the front panel is excited.

6.4.2 Two-Subsystem Method

The two-subsystem method is a simpler approach to determine the coupling loss factors. Using this approach, only two subsystems, which have direct coupling with each other, are measured. Thus, the two-subsystem method doesn't consider the entire system to determine the coupling loss factors. Rather, it considers a pair of subsystems that are directly coupled. Figure 6.10 shows a schematic illustrating the two-subsystem approach.

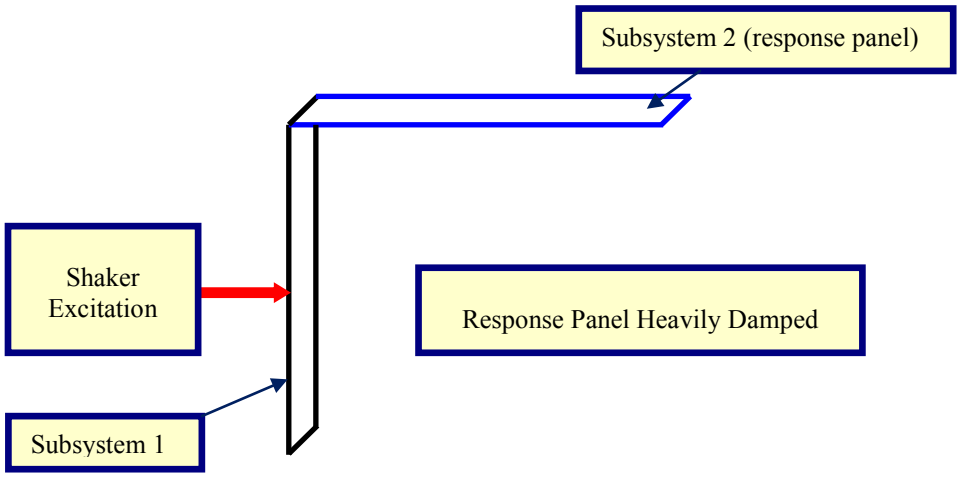

Figure 6.10 Two Subsystem Method

The two subsystem method (Lalor (1990)[80]) assumes that coupling between the subsystems should be weak. In other words the modal energy of the excited subsystem must be greater than that of the modal energy of the passive subsystem connected to it. This is achieved by increasing the damping of the response subsystem. In the case of the air handler, which is used in this research, the response panel was heavily damped using sand bags. By increasing the damping of the response panel, it is assumed that the power flows directly from the excited subsystem, to the response subsystem, even if there is a

secondary energy path i.e. even if a third panel is attached to the excitation and the response panel.

Figure 6.11 shows an SEA model of a three panel system with the response panel being heavily damped (5% damping) and the excitation panel and the third panel, which is the secondary path, assumed to have a damping of 1% each. Figure 6.12 shows the comparison of the energy flow in the response panel with and without the secondary energy path. It is evident from the Figure 6.12 that the presence of the secondary path doesn't affect the energy flow into the response panel if the response panel is heavily damped. Further, the effect of measurement error is minimized by making the response panel energy sink.

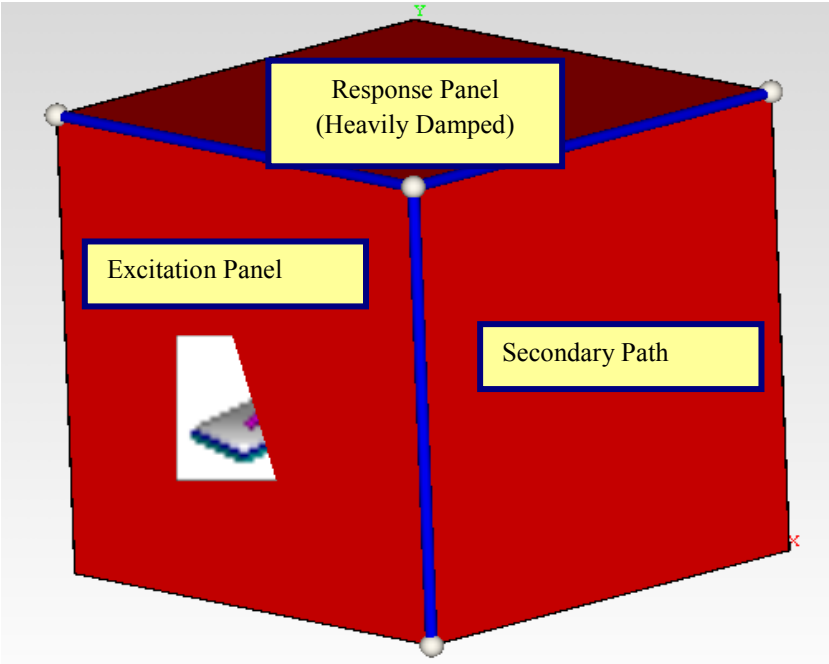

Figure 6.11 SEA model of a two subsystem system with a secondary path

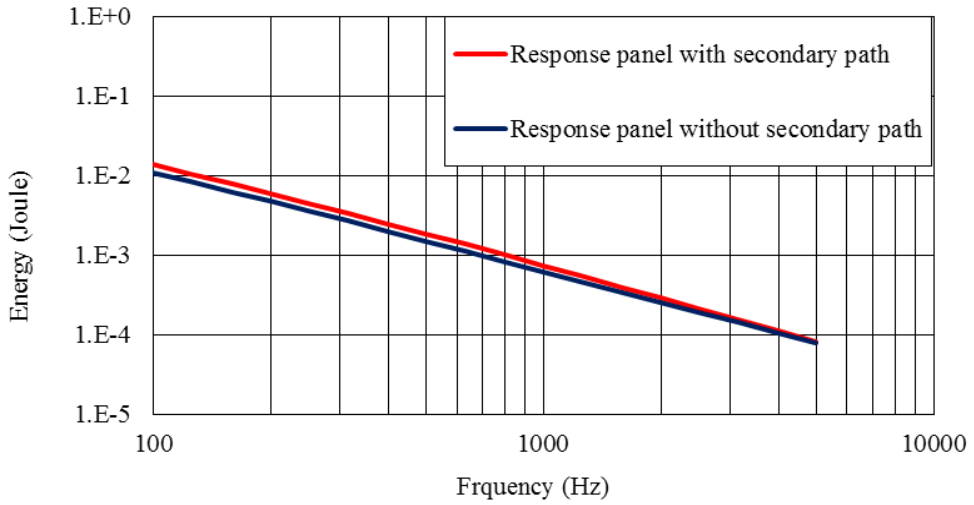

Figure 6.12 Comparison of the energy flow in the response panel

Figure 6.13 shows the panels of the air handler with sand bags attached. Additionally, Figures 6.14 and 6.15 compare damping loss factors of the right side panel and left side panel of the air handler respectively. It is evident from Figures 6.14 and 6.15 that the damping loss factor of the panels is increased by nearly an order of magnitude when sand bags are attached. The methods to determine the damping loss factors are extensively discussed in Section 6.5

Figure 6.13 Panels heavily damped using sand bags

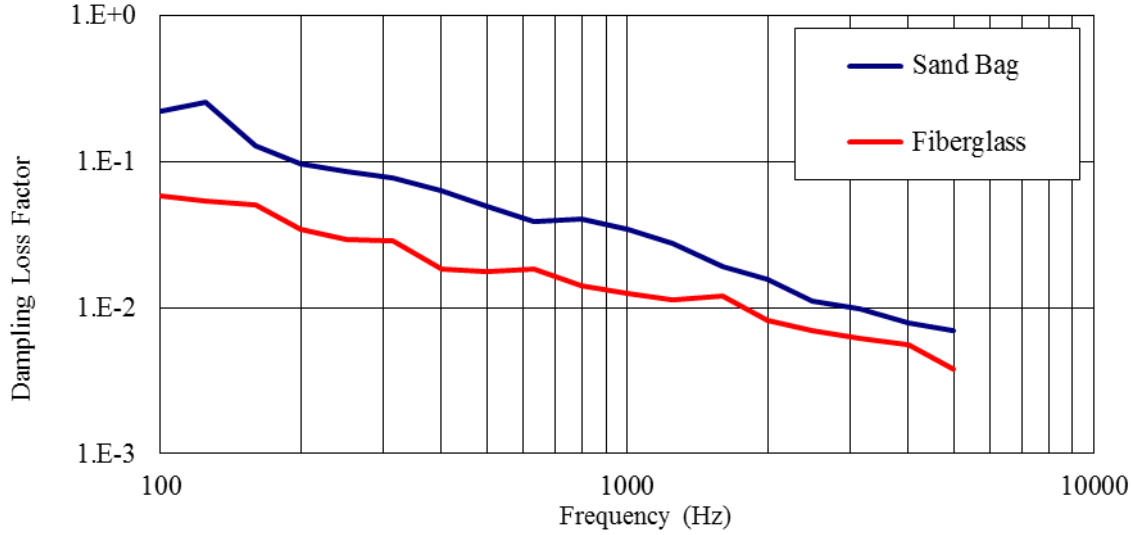

Figure 6.14 Damping Loss Factor of the right side panel of the air handler

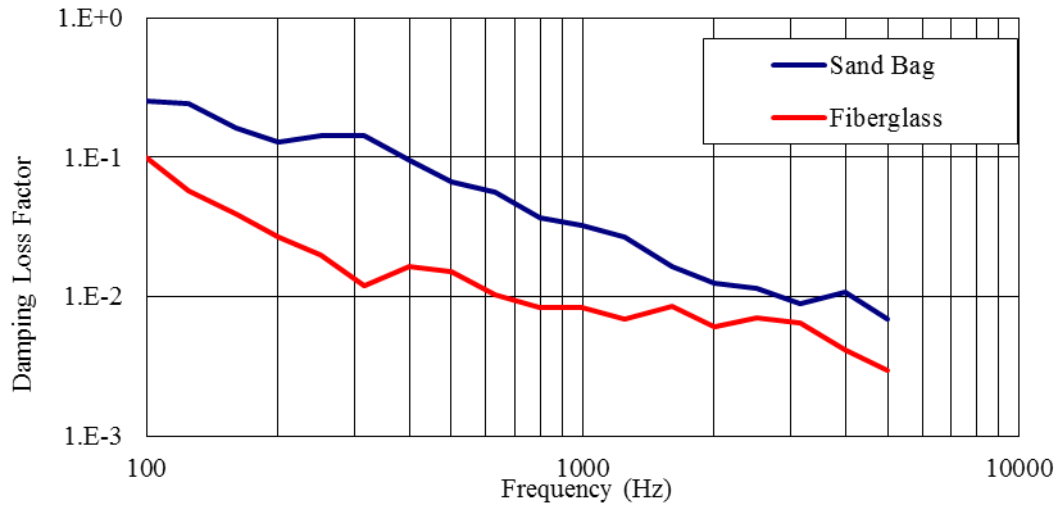

Figure 6.15 Damping Loss Factor of the left side panel of the air handler

Thus coupling loss factor for subsystems with direct coupling can be determined using

$$\eta_{12} = \frac{\Pi_2}{\omega E_{22}} \left[\frac{E_{11}}{E_{21}} - \frac{E_{12}}{E_{22}} \right]^{-1} \tag{6.19}$$

It is assumed that the energy in the directly driven subsystem is greater than the subsystem connected to it. Therefore

$$\frac{E_{12}}{E_{22}} \cong 0 \tag{6.20}$$

Substituting Eqn. 6.20 into Eqn. 6.19 gives

$$\eta_{12} = \frac{\Pi_2}{\omega E_{22}} \left[\frac{E_{11}}{E_{21}} \right]^{-1} \tag{6.21}$$

which can be rewritten as

$$\eta_{12} = \frac{1}{\omega} \left(\frac{\Pi_2}{E_{22}} \right) \left(\frac{E_{21}}{E_{11}} \right) \tag{6.22}$$

The coupling loss factor (η_{ij} is the coupling loss factor between the subsystems i and j) in Eqn. 6.22 is generalized as

$$\eta_{ij} = \frac{1}{\omega} \left(\frac{E_{ji}}{E_{ii}} \right) \left(\frac{\Pi_j}{E_{jj}} \right) \tag{6.23}$$

where Π_j is the input power to the excitation panel j, E_{ii} is the energy in the excitation panel i , E_{jj} is the energy in the excitation panel j, and E_{ji} is the energy in the response panel j for an excitation panel i.

Figures 6.16 to 6.18 compare the coupling loss factor of the left side panel and the rear panel, the rear panel and the top panel, and the right side panel and the top panel of the air handler, respectively. In each case, coupling loss factors are compared between the inverse matrix method and the two-subsystem method.

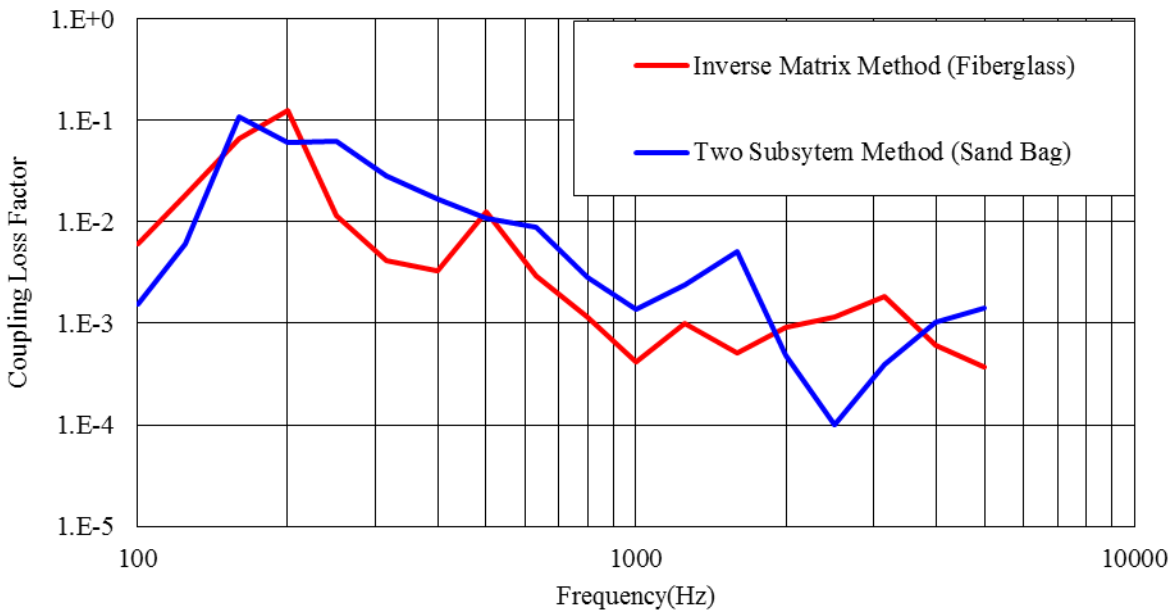

Figure 6.16 Comparison of the coupling loss factors between the left side panel and the rear panel of the air handler.

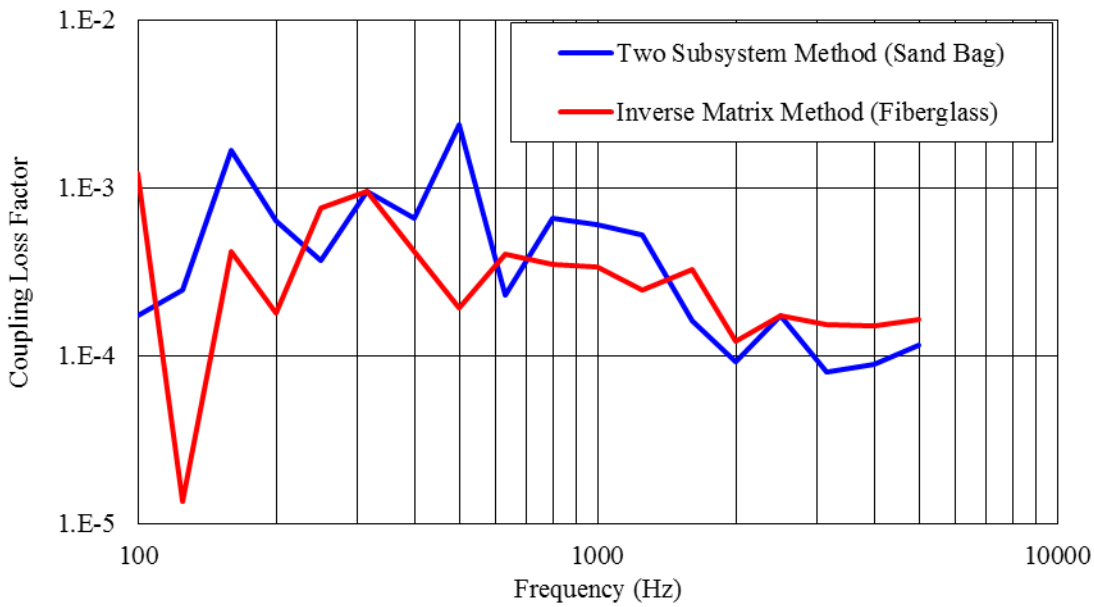

Figure 6.17 Comparison of the coupling loss factors between the rear panel and the top panel of the air handler.

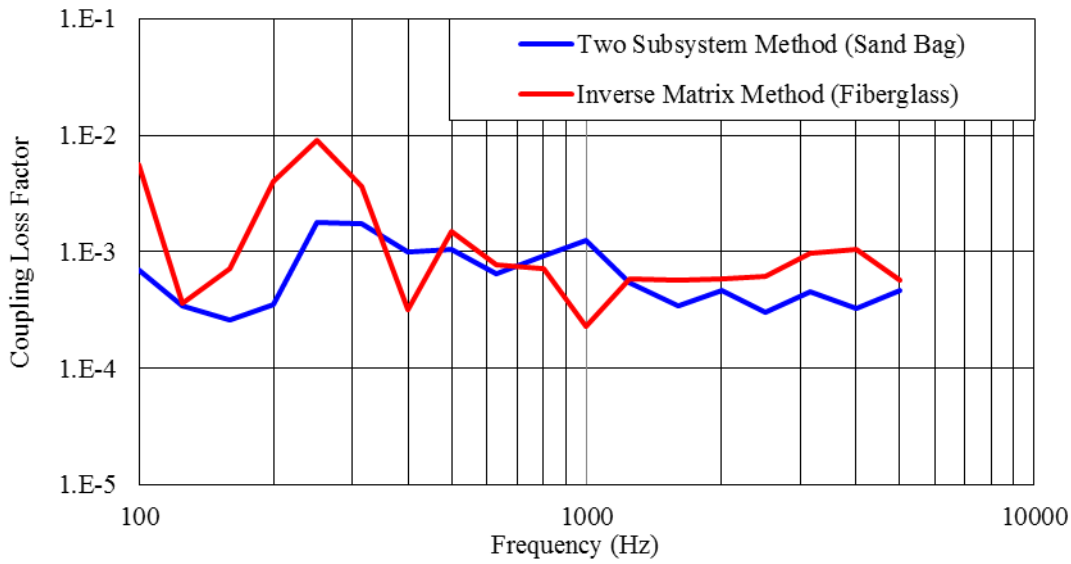

Figure 6.18 Comparison of the coupling loss factors between the right side panel and the top panel of the air handler.

From Figures 6.16 to 6.18, the following observations can be made. The coupling loss factors obtained using either approach agrees well except in low frequency bands. For air handlers, it can be concluded that the two subsystem method can be utilized instead of the inverse matrix because

- The measurement time and the computational time are much less since only two subsystems are considered for measurement
- The two-subsystem method doesn't involve inverse matrices and hence the coupling loss factor predictions are less prone to ill conditioning.
- The results presented demonstrate that coupling is unimportant between indirectly connected panels for air handlers

6.5 Damping Loss Factor

The damping loss factor is defined as the amount of power dissipated by the subsystem to the maximum potential energy of the subsystem (Lyon and DeJong (1995)[29]). Generally, damping is due to various factors such as friction and viscosity, and will depend on how subsystems are connected to each other. The two most common methods of determining the damping loss factors are

- The Decay Rate Method
- The Energy Matrix Method

6.5.1 Decay Rate Method

The response of the subsystem is measured in the time domain by exciting the subsystem using an impulse. The modal energy at resonance frequencies decays as shown in the Figure 6.2, and the initial slope of the transient response is determined using a band pass filter in particular frequency bands and is called the decay rate (DR). Accordingly, the damping loss factor (η) is expressed from Eqn. 6.10 as

$$\eta = \frac{DR}{27.3f} \tag{6.24}$$

where f is the center frequency of the third octave band.

6.5.2 Energy Matrix Method

Alternatively, the loss factors can also be found using the energy matrix approach described earlier. From the power balance equation of an isolated subsystem (Lalor (1989)[33]), the damping loss factor η can be expressed as

$$\eta = \frac{1}{\omega} E_{tot}^{-1} \Pi_{in} \tag{6.25}$$

where E_{tot} is the total energy in the subsystem, and Π_{in} is the input power to the subsystem

For a system with *N* subsystems, the damping loss factor expression involves an inverse energy matrix of order *N* x *N*. Hence, the damping loss factors (η_i) for a system consisting of *N* subsystems is expressed as

$$\begin{bmatrix} \eta_1 \\ \dots \\ \eta_N \end{bmatrix} = \frac{1}{\omega} \begin{bmatrix} E_{11} & \dots & E_{N1} \\ \dots & \dots & \dots \\ E_{1N} & \dots & E_{NN} \end{bmatrix}^{-1} \begin{bmatrix} \Pi_1 \\ \dots \\ \Pi_N \end{bmatrix} \tag{6.26}$$

where Π_i is the power input to the subsystem *i*, and E_{ij} is the measured energy in subsystem *i* due to an excitation in subsystem *j*.

In this research work, the aforementioned methods to determine the damping loss factors are applied to the air handler. Figures 6.19 to 6.24 compares the damping loss factors measured using the decay rate method and the energy matrix method for the front panel, right side panel, rear panel, left side panel, top panel and the bottom panel of the air handler, respectively.

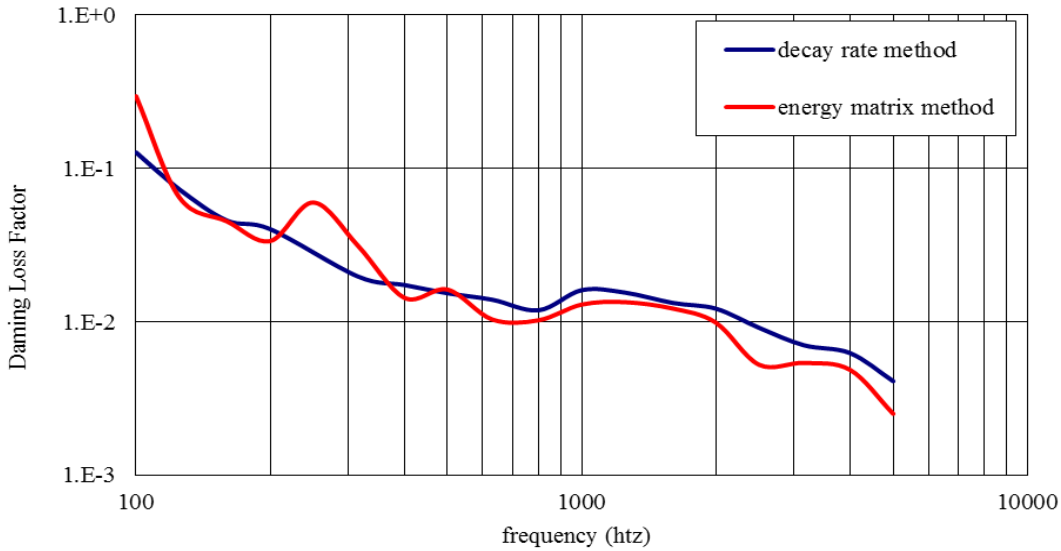

Figure 6.19 Damping loss factor of the front panel of the air handler.

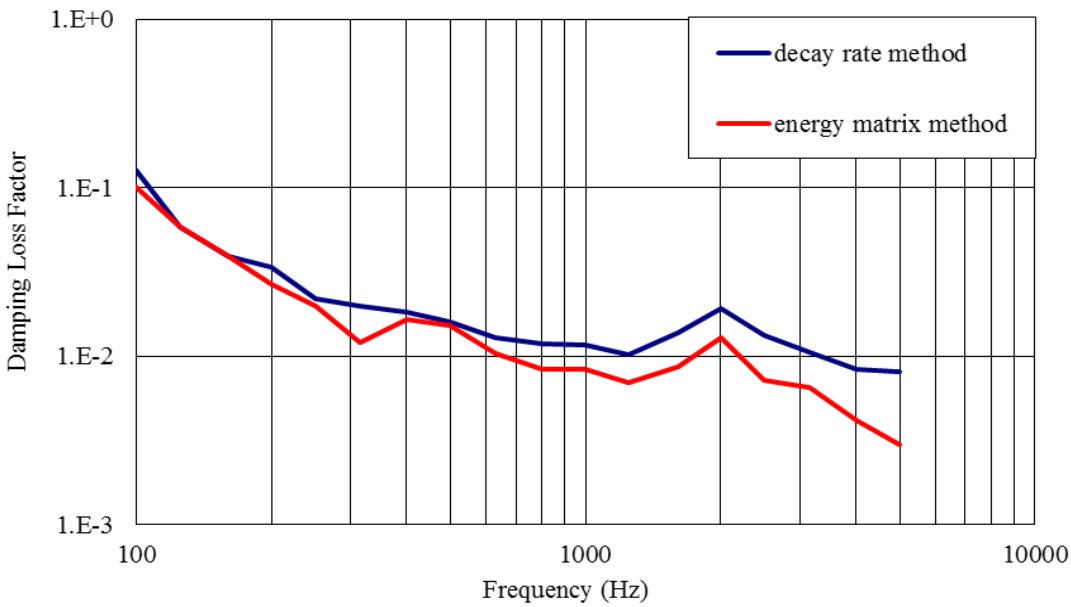

Figure 6.20 Damping loss factor of the right side panel of the air handler.

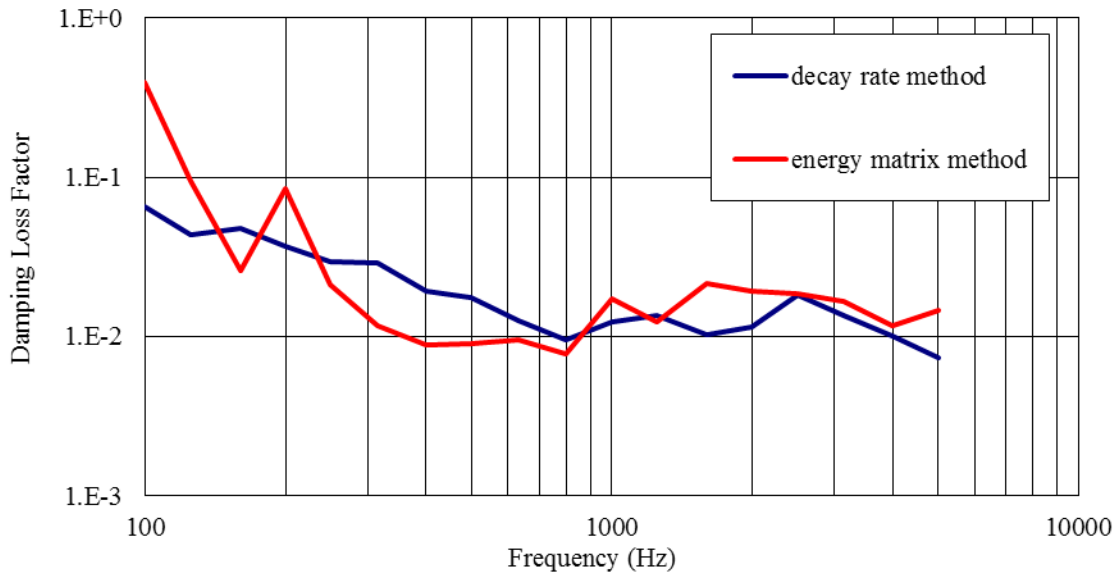

Figure 6.21 Damping loss factor of the rear panel of the air handler.

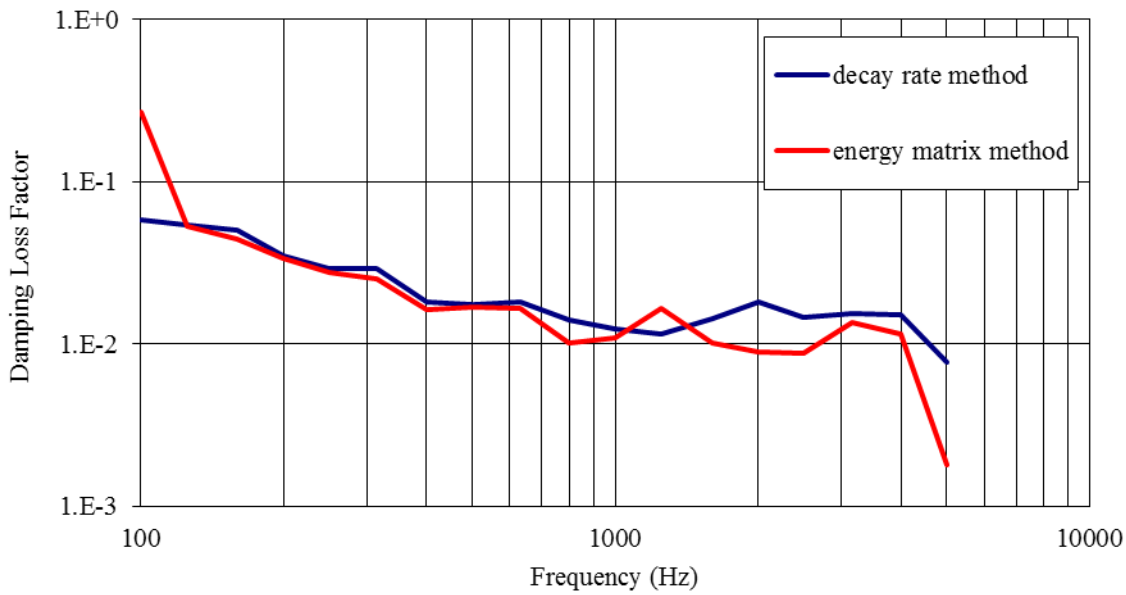

Figure 6.22 Damping loss factor of the left side panel of the air handler.

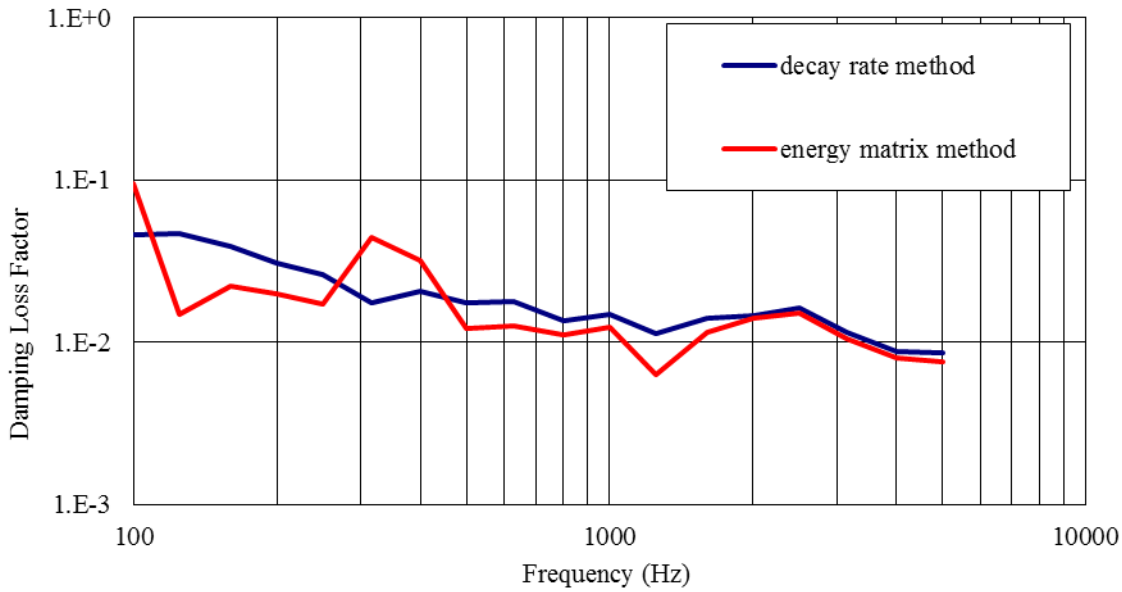

Figure 6.23 Damping loss factor of the top panel of the air handler.

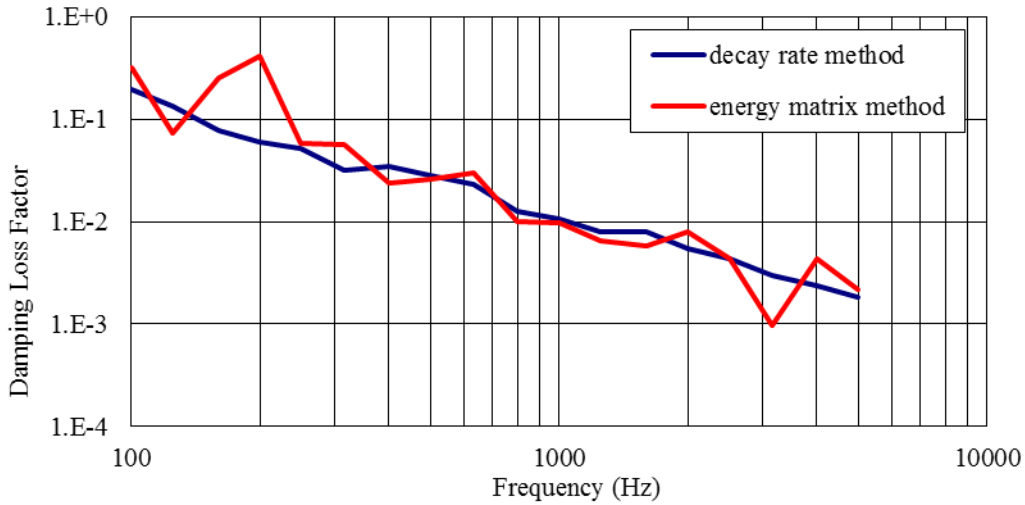

Figure 6.24 Damping loss factor of the bottom panel of the air handler.

From Figures 6.19-6.24, the following observations can be made. The damping loss factors calculated using the decay rate method and the energy matrix method have a good agreement with each other over the entire frequency range. Furthermore, in the case

of a complex system, which involves more than 6 subsystems, the decay rate method is preferred because the energy matrix method involves an inverse matrix. Furthermore, the order of the inverse matrix increases as the number of subsystems increases. Moreover, it is likely that method will be more prone to error as the order of the matrix increases.

6.6 Summary

The methods to determine the coupling and damping loss factors have been discussed extensively in this chapter. Furthermore, the importance of measuring the loss factors and their influence on the SEA predictions are also documented. Specifically, the methods to determine the modal energy and the equivalent mass, which are used in determining the loss factor, have been detailed.

Secondly, the determination of the coupling loss factors based on the inverse matrix and the two-subsystem method has been discussed. A good agreement is seen between the coupling loss factors predicted using each approach. The two-subsystem method is recommended for air handlers because the measurements are easier to make, and the method does not entail a matrix inversion.

Finally, the determination of the damping loss factors using the decay rate method and the energy matrix method has been surveyed. The damping loss factors predicted by the aforementioned methods have good agreement over the entire frequency band. Further, the decay rate method is recommended over the energy matrix method, as the energy matrix method requires a matrix inversion.

CHAPTER 7

CONCLUSIONS

7.1 Summary and Conclusions

Noise problems in building spaces are primarily induced by HVAC power generating equipment including fans, compressors, chillers, pumps, and boilers. For the most part, the noise generated by the power generating equipment is propagated either structurally or acoustically through the duct systems.

Generally, the sound energy propagated through the duct air space is called airborne noise and the sound transmission through the duct structure itself is termed structure-borne noise. The structure-borne noise in the HVAC system can be categorized as two types: (i) duct breakout or (ii) machinery noise. The duct breakout, which is an indirect airborne path, propagates energy from the duct air space to the surrounding duct walls, which in turn radiate energy into building spaces. On the other hand, rotating machinery transmits sound energy to other parts of the building by exciting the floor, wall, or ceiling of a source room. The focus of this thesis was to assess different ways to model each of the three energy transmission paths.

7.2 Airborne Attenuation in Plenums

The first energy path investigated was the airborne path through the duct systems. Insertion loss is normally used instead of transmission loss as the metric to characterize the attenuation in HVAC plenums since it is easier to measure. Furthermore, it is an appropriate metric above the plane wave cutoff frequency.

The acoustic FEM with special boundary condition was used to determine the insertion loss. A diffuse acoustic field input was used along with a baffled termination.

The acoustic FEM was compared to published measured results (Mouratidis and Becker, 2003[9]), the ASHRAE Handbook (2007)[2] model developed by Wells (1958)[5], SEA, and an empirical model developed by Mouratidis and Becker (2003) [9]. Eight different duct configurations were considered including cases with inlet/outlet ducts inline or at right angles, and lined and unlined with fiber.

It was concluded that the acoustic FEM with special boundary condition agreed well with the measured insertion loss over the entire frequency spectrum except at low frequencies. Comparisons were made in one third-octave bands and were within 3 dB except for a few isolated frequency bands. It was notable that plane wave behavior was not assumed in the plenum or even in the inlet/outlet ducts.

The ASHRAE Handbook (2007) [2] model agreed well with the measured insertion loss above the plane wave cutoff frequency for inline ducts. For plenums with inlet/outlet ducts offset by 90 degrees, the Handbook did not compare well with the measured noise reduction above the plane wave cutoff frequency. Below the plane wave cutoff, the Handbook is off by as much as 10 dB since insertion loss will be sensitive to the individual plenum modes. The Handbook does not account for the modal character of the duct cavities since it is an energy approach. SEA was similar to the ASHRAE Handbook (2007) as both techniques are based on energy principles.

The empirical model developed by Mouratidis and Becker (2003) [9] appeared to be superior to the ASHRAE Handbook (2007) at low frequencies though results were mixed at high frequencies. However, the empirical model has limited in application since it was only developed for plenums with inlet and outlet ducts configured inline with each other.

7.3 Breakout Noise in Duct Systems

The insertion loss of an enclosure was used as the primary metric to assess the airborne indirect path, which is often referred to as breakout noise. An air handler (HVAC plenum) was used as a test case and the insertion loss was measured and results were compared with SEA predictions. The SEA model of the air handler was modeled and analyzed using VA-One in narrowband, and results were later summed in third-octave bands. Four different air handler configurations were examined. These included a:

- Full enclosure with fiber lining.
- Full enclosure with no fiber lining.
- Partial enclosure with fiber lining.
- Partial enclosure with no fiber lining.

SEA agreed well with the measured insertion loss for the full enclosure with fiber lining over the entire frequency spectrum. For unlined cases, the SEA under predicted the insertion loss of the air handler by 5 dB. In that case, the absorption and damping of the walls were assumed. Accordingly, one would anticipate that the result would improve significantly if damping was measured instead. For the partially enclosed air handler, SEA agreed well with the measurement except at the enclosure resonances.

7.4 Machinery Noise in HVAC Plenums

In this research work, the structure-borne noise path due to vibrations caused by the machinery in HVAC plenums was examined using SEA. SEA was used since the air handler walls are thin and should be modally dense. In order to test the applicability of SEA, the air handler was excited with an electromagnetic shaker(s) at a single location and at two locations.

Damping and coupling loss factors were determined experimentally and the measured loss factors were then incorporated into the SEA model of the air handler. The spatially averaged vibration velocity of the panels and the sound power radiated from individual panels of the air handler were measured and compared with the SEA model. It was concluded that experimental SEA agreed well with measurement over the entire frequency spectrum. It was observed that the SEA model was very sensitive to the selection of loss factors and assumed loss factors were not sufficient. Accordingly, it was concluded that he loss factors used in the SEA model should be determined experimentally. Furthermore, SEA was used successfully to determine the response irrespective of the number of energy sources exciting the plenum. However, it was crucial to measure the input power of the source.

7.4.1 Determination of Loss Factors

Experimental SEA was used to determine the coupling and damping loss factors. Though experimental SEA is utilized heavily in the automotive industry, the approach is novel to the HVAC industry to our knowledge. Coupling loss factors were determined between the panels of the air handler using the energy matrix and two-subsystem methods. Both methods agreed well. However, the two-subsystem method was preferred because of ease and the fact that the energy matrix approach is prone to errors particularly for a high number of subsystems since the matrix must be inverted. The two-subsystem method can only be used to find loss factors between directly coupled subsystems. However, the results suggest that direct coupling is most important for air handlers and ducts.

Loss factors were determined using the (i) decay rate and (ii) energy matrix methods. The damping loss factors of the panels of the air handler determined by the aforementioned methods were in good agreement with one another. However, the decay rate method was preferred over the energy matrix method in order to avoid the necessity of performing a matrix inversion.

7.5 Future Work

The research documented in this thesis, demonstrates various techniques to assess the airborne direct, airborne indirect and the structure borne noise paths in the HVAC plenums. In the aforementioned sections, the viability of the approaches used by the ASHRAE community is documented. In this section the possible follow-on work is outlined.

Firstly, it is recommended to the ASHRAE community to utilize the modeling approach (acoustic FEM with special boundary conditions) to determine the airborne path in an assortment of HVAC plenum and duct configurations. Then, an empirical equation can be devised based on the simulation results similar to the empirical model developed by Mouratidis and Becker (2003) [9]. Thus an improved empirical model to predict the airborne direct path in HVAC plenums can be developed. The ASHRAE community can utilize the newly developed model instead of the existing models like the ASHRAE Handbook model (2007)[2] or the Mouratidis and Becker model (2003) [9]) which have limited application for some plenum configurations and are problematic at low frequencies.

Secondly, the experimental SEA can be used to determine the damping loss factors and coupling loss factors of the HVAC plenums. The advantage of using

experimental SEA is that once the damping loss factors and the coupling loss factors of a plenum are determined, the data can be used to model similar plenums and ducts. Therefore, a database on the damping loss factors and the coupling loss factors of plenums with a particular design configuration can be formed.

REFERENCES

1. *Technology for a Quieter America*. 2010: National Academy of Engineering.
2. *ASHRAE Handbook - HVAC Applications (SI): Heating, Ventilating, and Air-Conditioning Applications/SI Edition*. 2007: ASHRAE, 2007. 1039
3. *Ashrae Handbook 2011: Heating, Ventilating, and Air-Conditioning Applications: SI Edition*. 2011: Amer Society of Heating, 2011.
4. J.Crocker, M., *Handbook of Noise and Vibration Control*. 2007, Canada: John Wiley & Sons, Inc., Hoboken, New Jersey.
5. Wells, *Acoustical plenum chambers.* Noise Control Engineering Journal, 1958. **4**: p. 9–15.
6. M.L.Munjal, *Acoustics of ducts and mufflers*. 1982, New York: Wiley-Interscience.
7. L.J.Ericksson, *Higher order mode effects in circular ducts and expansionchambers.* J Acoust Soc Am, 1980. **68**(2): p. 545-550.
8. Cummings, A., *Attenuation of Lined Plenum Chambers in Ducts .1. Theoretical-Models.* Journal of Sound and Vibration, 1978. **61**(3): p. 347-373.
9. E. Mouratidis , J.B., *The aero-acoustic properties of common HVAC plena.ASHRAE TRP-1026.* 2003.
10. Ih, J.G. and B.H. Lee, *Analysis of Higher-Order Mode Effects in the Circular Expansion Chamber with Mean Flow.* Journal of the Acoustical Society of America, 1985. **77**(4): p. 1377-1388.
11. Ih, J.G. and B.H. Lee, *Theoretical Prediction of the Transmission Loss of Circular Reversing Chamber Mufflers.* Journal of Sound and Vibration, 1987. **112**(2): p. 261-272.
12. Lee, B.H., S. Hache, and R.E. Simard, *A Rapid Method for Differentiation of Dairy Lactic-Acid Bacteria by Enzyme-Systems.* Journal of Industrial Microbiology, 1986. **1**(4): p. 209-217.

13. Lee, B.H. and J.M. Thibaud, *A Critical-Review of the Taxonomy of Gulgastrura-Reticulosa (Collembola, Hypogastruridae), a Cave Springtail from Korea.* Systematic Entomology, 1987. **12**(1): p. 73-79.

14. Ih, J.G., *The Reactive Attenuation of Rectangular Plenum Chambers.* Journal of Sound and Vibration, 1992. **157**(1): p. 93-122.

15. Munjal, M.L., *A Simple Numerical-Method for 3-Dimensional Analysis of Simple Expansion Chamber Mufflers of Rectangular as Well as Circular Cross-Section with a Stationary Medium.* Journal of Sound and Vibration, 1987. **116**(1): p. 71-88.

16. Selamet, A. and P.M. Radavich, *The effect of length on the acoustic attenuation performance of concentric expansion chambers: An analytical, computational and experimental investigation.* Journal of Sound and Vibration, 1997. **201**(4): p. 407-426.

17. Selamet, A. and Z.L. Ji, *Acoustic attenuation performance of circular expansion chambers with offset inlet/outlet: I. Analytical approach.* Journal of Sound and Vibration, 1998. **213**(4): p. 601-617.

18. Munjal, M.L., *Plane wave analysis of side inlet/outlet chamber mufflers with mean flow.* Applied Acoustics, 1997. **52**(2): p. 165-175.

19. Venkatesham, B., M. Tiwari, and M.L. Munjal, *Transmission loss analysis of rectangular expansion chamber with arbitrary location of inlet/outlet by means of Green's functions.* Journal of Sound and Vibration, 2009. **323**(3-5): p. 1032-1044.

20. Craggs, A., *Finite-Element Method for Damped Acoustic Systems - Application to Evaluate Performance of Reactive Mufflers.* Journal of Sound and Vibration, 1976. **48**(3): p. 377-392.

21. Craggs, A., *Finite-Element Method for Modeling Dissipative Mufflers with a Locally Reactive Lining.* Journal of Sound and Vibration, 1977. **54**(2): p. 285-296.

22. Peat, K.S., *Evaluation of 4-Pole Parameters for Ducts with Flow by the Finite-Element Method.* Journal of Sound and Vibration, 1982. **84**(3): p. 389-395.

23. Sahasrabudhe, A.D., S.A. Ramu, and M.L. Munjal, *Matrix Condensation and Transfer-Matrix Techniques in the 3-D Analysis of Expansion Chamber Mufflers.* Journal of Sound and Vibration, 1991. **147**(3): p. 371-394.

24. Wu, T.W. and P. Zhang, *Boundary element analysis of mufflers with an improved method for deriving the four-pole parameters.* Journal of Sound and Vibration, 1998. **217**(4): p. 767-779.

25. Barbieri, R., N. Barbieri, and K.F. de Lima, *Application of the Galerkin-FEM and the improved four-pole parameter method to predict acoustic performance of expansion chambers.* Journal of Sound and Vibration, 2004. **276**(3-5): p. 1101-1107.

26. Herrin DW, T.Z., Scalf EL, Allen SA, Seybert AF, *Using numerical acoustics topredict the attenuation of HVAC plenums.* ASHRAE Trans 2007, 2007. **113**(1).

27. Wang, C.N., C.C. Tse, and Y.N. Chen, *Analysis of 3-Dimensional Muffler with Boundary-Element Method.* Applied Acoustics, 1993. **40**(2): p. 91-106.

28. Burroughs, C.B., R.W. Fischer, and F.R. Kern, *An introduction to statistical energy analysis.* Journal of the Acoustical Society of America, 1997. **101**(4): p. 1779-1789.

29. Lyon RH, D.R., *Theory and application of statistical energy analysis*. 2, illustrated ed. 1995: Butterworth-Heinemann, 1995.

30. Langley, R.S., *A General Derivation of the Statistical Energy Analysis Equations for Coupled Dynamic-Systems.* Journal of Sound and Vibration, 1989. **135**(3): p. 499-508.

31. Woodhouse, J., *An Approach to the Theoretical Background of Statistical Energy Analysis Applied to Structural Vibration.* Journal of the Acoustical Society of America, 1981. **69**(6): p. 1695-1709.

32. Fahy, F.J., *Statistical Energy Analysis - a Critical Overview.* Philosophical Transactions of the Royal Society of London Series a-Mathematical Physical and Engineering Sciences, 1994. **346**(1681): p. 431-447.

33. Lalor N, *The Experimental Determination ofVibrational Energy Balance in Complex Structures*, in *SIRA Conf. on Stress andVibration*1989: London. p. 108429.

34. DeLanghe, K. and P. Sas, *Statistical analysis of the power injection method.* Journal of the Acoustical Society of America, 1996. **100**(1): p. 294-303.

35. Stimpson, G.J., J.C. Sun, and E.J. Richards, *Predicting Sound Power Radiation from Built-up Structures Using Statistical Energy Analysis.* Journal of Sound and Vibration, 1986. **107**(1): p. 107-120.

36. Cimerman B., B.T., Borello G., *Overview of the Experimental Approachto Statistical Energy Analysis*, in *the Society of Automotive Engineers,Noise and Vibration* 1997.

37. Yamazaki, T., K. Masahiko, and Y. Asahara, *Applicability of experimental statistical energy analysis to an engine structure.* Jsae Review, 2003. **24**(3): p. 263-267.

38. Oldham, D.J. and S.N. Hillarby, *The Acoustical Performance of Small Close Fitting Enclosures .1. Theoretical-Models.* Journal of Sound and Vibration, 1991. **150**(2): p. 261-281.

39. Oldham, D.J. and S.N. Hillarby, *The Acoustical Performance of Small Close Fitting Enclosures .2. Experimental Investigation.* Journal of Sound and Vibration, 1991. **150**(2): p. 283-300.

40. Seybert, A.F., et al., *An Advanced Computational Method for Radiation and Scattering of Acoustic-Waves in 3 Dimensions.* Journal of the Acoustical Society of America, 1985. **77**(2): p. 362-368.

41. Seybert, A.F.a.W.T.W., *Acoustical Modelling: Boundary Element Methods*, in *Encyclopedia of Acoustics* M.J. Crocker, Editor 1997, John Wiley and Sons, Inc: New York. p. 173-184.

42. Selamet, A. and Z.L. Ji, *Acoustic attenuation performance of circular expansion chambers with extended inlet outlet.* Journal of Sound and Vibration, 1999. **223**(2): p. 197-212.

43. Zhang, Z.D., N. Vlahopoulos, and S.T. Raveendra, *Formulation of a numerical process for acoustic impedance sensitivity analysis based on the indirect boundary element method.* Engineering Analysis with Boundary Elements, 2003. **27**(7): p. 671-681.

44. Ji, Z.L., *Boundary element acoustic analysis of hybrid expansion chamber silencers with perforated facing.* Engineering Analysis with Boundary Elements, 2010. **34**(7): p. 690-696.

45. Bernhard, R.J., et al., *Prediction of Sound Fields in Cavities Using Boundary-Element Methods.* Aiaa Journal, 1987. **25**(9): p. 1176-1183.

46. Suzuki, S., S. Maruyama, and H. Ido, *Boundary Element Analysis of Cavity Noise Problems with Complicated Boundary-Conditions.* Journal of Sound and Vibration, 1989. **130**(1): p. 79-96.

47. Utsuno, H., et al., *Prediction of Sound Fields in Cavities with Sound Absorbing Materials.* Aiaa Journal, 1990. **28**(11): p. 1870-1876.

48. Demkowicz, L., et al., *Solution of Elastic-Scattering Problems in Linear Acoustics Using H-P Boundary Element Methods.* Journal of Computational and Applied Mathematics, 1991. **36**(1): p. 29-63.

49. DeSanto, J.A., *Exact boundary integral equations for scattering of scalar waves from infinite rough interfaces.* Wave Motion, 2010. **47**(3): p. 139-145.

50. Muhammad Mushtaq, N.A.S., Ghulam Muhammad, *Advantages and Disadvantages of Boundary Element Methods For Compressible Fluid Flow Problems.* Journal of American Science, 2010. **6(1)**.

51. Felippa, C.A., *Interfacing Finite-Element and Boundary Element Discretizations.* Applied Mathematical Modelling, 1981. **5**(5): p. 383-386.

52. Vlahopoulos, N., et al., *Numerical implementation and applications of a coupling algorithm for structural-acoustic models with unequal discretization and partially interfacing surfaces.* Finite Elements in Analysis and Design, 1999. **32**(4): p. 257-277.

53. Cook, R.D., Malkus,D.S.,and Plesha, M.E. *Concepts and Applications of Finite Element Analysis*. 1989. New York: John Wiley &Sons.

54. Nefske, D.J., J.A. Wolf, and L.J. Howell, *Structural-Acoustic Finite-Element Analysis of the Automobile Passenger Compartment - a Review of Current Practice.* Journal of Sound and Vibration, 1982. **80**(2): p. 247-266.

55. Davis D.D. Jr., H.C.M., *Acoustical filters and mufflers*, in *Handbook of Noise Control*. 1975, McGraw-Hill Book Company, Inc: New York.

56. Shorter, P.J. and R.S. Langley, *On the reciprocity relationship between direct field radiation and diffuse reverberant loading.* Journal of the Acoustical Society of America, 2005. **117**(1): p. 85-95.

57. Shorter, P.J. and R.S. Langley, *Vibro-acoustic analysis of complex systems.* Journal of Sound and Vibration, 2005. **288**(3): p. 669-699.

58. Langley, R.S., *On the diffuse field reciprocity relationship and vibrational energy variance in a random subsystem at high frequencies.* Journal of the Acoustical Society of America, 2007. **121**(2): p. 913-921.

59. Langley, R.S., *Numerical evaluation of the acoustic radiation from planar structures with general baffle conditions using wavelets.* Journal of the Acoustical Society of America, 2007. **121**(2): p. 766-777.

60. Shorter P, M.S. *Modeling the mid-frequency response of poro-elastic materials in vibro-acoustics application.* in *Symposium on the acoustics of poro-elastic materials*. 2008. Bradford, United Kingdom.

61. International, A., *ASTM E 477-06a*, in *Standard Test Method for Measuring Acoustical and Airflow Performance of Duct Liner Materials and Prefabricated Silencers*2006.

62. ISO, *ISO 9614-2*, in *Acoustics -- Determination of sound power levels of noise sources using sound intensity -- Part 2: Measurement by scanning*2006.

63. *VA-One*, 2010, ESI Group

64. Cummings, A., *Higher-Order Mode Acoustic Transmission through the Walls of Rectangular Ducts.* Journal of Sound and Vibration, 1983. **90**(2): p. 193-209.

65. Astley, R.J. and A. Cummings, *A Finite-Element Scheme for Acoustic Transmission through the Walls of Rectangular Ducts - Comparison with Experiment.* Journal of Sound and Vibration, 1984. **92**(3): p. 387-409.

66. Cummings, A. and I.J. Chang, *Noise Breakout from Flat-Oval Ducts.* Journal of Sound and Vibration, 1986. **106**(1): p. 17-33.

67. Cummings, A., *Sound transmission through duct walls.* Journal of Sound and Vibration, 2001. **239**(4): p. 731-765.

68. Venkatesham, B., M. Tiwari, and M.L. Munjal, *Analytical prediction of the breakout noise from a rectangular cavity with one compliant wall.* Journal of the Acoustical Society of America, 2008. **124**(5): p. 2952-2962.

69. Venkatesham, B., M. Tiwari, and M.L. Munjal, *Analytical prediction of break-out noise from a reactive rectangular plenum with four flexible walls.* Journal of the Acoustical Society of America, 2010. **128**(4): p. 1789-1799.

70. Venkatesham, B., M. Tiwari, and M.L. Munjal, *Prediction of Breakout Noise from a Rectangular Duct with Compliant Walls.* International Journal of Acoustics and Vibration, 2011. **16**(4): p. 180-190.

71. H P Wallin, U.C., M Abom, H Boden and R Glav, *Sound and Vibration*. second ed. 2011.

72. Beranek, I.V.a.L., *Noise and Vibration Control Engineering Princples and Application*. second ed. 2006: John Wiley &Sons,Inc.

73. Lawrence E. Kinsler, A.R.F., *Fundamentals of acoustics*. fourth ed. 2000: John Wiley & Sons,Inc.

74. Craik, R.J.M., *The Prediction of Sound-Transmission through Buildings Using Statistical Energy Analysis.* Journal of Sound and Vibration, 1982. **82**(4): p. 505-516.

75. Steel, J.A., *The prediction of structural vibration transmission through a motor vehicle using statistical energy analysis.* Journal of Sound and Vibration, 1996. **193**(3): p. 691-703.

76. Hynna, P., P. Klinge, and J. Vuoksinen, *Prediction of Structure-Borne Sound-Transmission in Large Welded Ship Structures Using Statistical Energy Analysis.* Journal of Sound and Vibration, 1995. **180**(4): p. 583-607.

77. Wu L., A.A. *Analysis of Initial Decay Rate in Relation to Estimates of Loss FActor and Equivalent Mass in Experimental SEA*. in *ISMA* 1996. Leuven, Belgium.

78. Gelat, P. and N. Lalor, *The role and experimental determination of equivalent mass in complex sea models.* Journal of Sound and Vibration, 2002. **255**(1): p. 97-110.

79. Gene Howard Golub, C.F.V.L., *Matrix Computations*. 3, annotated ed. 1996: JHU Press.

80. Lalor, *ISVR Technical Report*, 1990.

VITA

Srinivasan Ramalingam was born in 19th July, 1988 in Pondicherry, India. He received the degree of Bachelor of Technology in Mechanical Engineering from Pondicherry University, India in May 2009. In January 2010, he enrolled in the graduate school at the University of Kentucky for MS in Mechanical Engineering. During his graduate years at the University of Kentucky, he published a journal article in Applied Acoustics. He also received graduate scholarship award from fall 2010 to spring 2012 from the University of Kentucky.

Srinivasan Ramalingam